Planet Formation Across the Stellar Mass Spectrum

Grant Malcolm Kennedy

A thesis submitted for the degree of

Doctor of Philosophy

of The Australian National University

THE AUSTRALIAN NATIONAL UNIVERSITY

Research School of Astronomy and Astrophysics
The Australian National University
Canberra ACT 0200
Australia

February 2009

Disclaimer

The work contained in this thesis has been entirely carried out by the candidate, Grant M. Kennedy, with the exception of general supervision by principal supervisor Dr. Scott J. Kenyon. The contribution of Dr. Kenyon to each Chapter generally comprises advice regarding the style and content of each. In a few cases sentences and/or paragraphs were contributed. Dr. Ben C. Bromley contributed to numerical simulations, which were in part motivation for the study undertaken in Chapter 2.

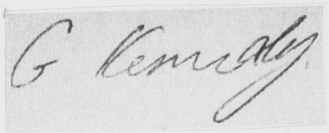

Grant Kennedy

Acknowledgements

Though it can be hard work at times, the PhD process need not be a long arduous journey one needs to make a big deal of. I feel the same way about acknowledgements.

I am indebted to my supervisor, Scott Kenyon, who has guided me academically the last few years. His ability to let me pursue the things I found interesting have made it an absolute pleasure. I am also grateful for the opportunity to spend a year in Boston.

I have many colleagues, friends, and family spread across New Zealand, Australia, the United States, and more recently the UK, who have supported me with love, friendship, money, advice, and occasionally a place to stay. Thank you all.

Abstract

This thesis considers several aspects of planet formation across a range of stellar masses. Starting with the idea of a moving "snow line" and its application to planet formation, I show how icy super Earth-mass planets can form around low-mass stars. I then develop the snow line model further, including the contribution of energy liberated by viscous disk evolution. This improved snow line model is applied to gas giant formation over a range of stellar masses. The main result of this second study is an increase in gas giant frequency with stellar mass, consistent with recent discoveries of planets around low and intermediate-mass stars. The snow line model is also applied to the formation of super-Earth mass planets over a range of stellar masses. I show that low-mass planets need not follow the increase in frequency with stellar metallicity found for gas giants, in line with preliminary observational results. This third study finds that short-period super-Earths should be most common around low mass stars. Finally, I investigate whether disk dispersal times vary consistently with stellar mass. Intermediate-mass stars lose their disks earlier than solar-mass stars with marginal statistical significance, due to small sample numbers. I compare the results to a simple photoevaporation model and suggest the larger orbits of planets around intermediate-mass stars may result from shorter disk lifetimes. The photoevaporation model explains the results much better than the null hypothesis—that disk dispersal is independent of stellar mass. The results of this fourth and final study suggest future directions for observational and theoretical work. Larger and more complete cluster samples are needed to strengthen the statistical significance of stellar mass dependent disk dispersal. Theoretical planet formation models should include stellar mass dependent disk dispersal times. In the medium to long term, discoveries of lower mass planets will test hot super-Earth models. The most promising short term directions suggested by this thesis involve larger scale studies of disk dispersal and the implications for gas giant formation across the stellar mass spectrum.

CONTENTS

LIST OF FIGURES

LIST OF TABLES

The purpose of any cosmogonic theory is to seek out ideally simple conditions which could have resulted in the world, and from which, by the play of recognised forces, that world, in all its complexity, may be resulted.

Lemaître, Primeval Atom: An Essay on Cosmogony, 1950

CHAPTER 1

INTRODUCTION

1.1 Overview

Long before planets were known to exist around other stars, the study of our solar system suggested possible cosmogonies (e.g. Kant, 1755; Laplace, 1796). In his *Exposition du système du monde*, Laplace writes

> However arbitrary the system of the planets may be, there exists between them some very remarkable relations, which may throw light on their origin.

While making the point that the solar system (circa 1796) might lead to detailed formation theories, this statement also highlights the general nature of astronomical science: that theory is always constrained, and commonly led, by observation.

Though Laplace's "nebular hypothesis" did not stand up to detailed scrutiny (e.g. Kirkwood, 1880), his conclusion that the solar system planets formed in a disk has remained. Over 200 years later, the near co-planar orbits of the solar system planets still provide the strongest constraint on planet formation models. In more recent times, confidence in this hypothesis has been strengthened by the discovery of disks around nearby young stars (e.g. McCaughrean & O'Dell, 1996). Their discovery is perhaps a rare example of a solid prediction preceding an observational discovery, in this case by hundreds of years.

Steps toward discovering the first extra-solar planets were suggested as early as 1952. Struve (1952) suggested that both radial velocity and transit were possible techniques, and that there was no reason not to expect planets to orbit at 1/50th of an AU, where these techniques are most sensitive.

The first extra-solar planets were found nearly 200 years after Laplace's *Exposition du système du monde.* However, these discoveries came from a far more precise and unexpected technique than suggested by Struve. Despite an initial discovery/retraction hiccup (Bailes et al., 1991; Lyne & Bailes, 1992), the first extra-solar planetary system was discovered in 1992 (Wolszczan & Frail, 1992). The three planets in this system seem relatively normal in a solar system context, with masses of $\sim$0.2–2 $M_{\oplus}$ (Earth masses) and orbits of 0.19–0.46 AU. However, this system orbits a rapidly rotating neutron star and thus clearly bears little resemblance to the solar system.

Three years later, the planet 51 Peg b was found to orbit a normal, main-sequence (MS), solar-type star (Mayor & Queloz, 1995).[†] This time however, the surprise lay with the planet. Though it probably has a mass comparable to Jupiter, this planet orbits at 0.05 AU, orbiting the star every 4 days. With little resemblance to the solar system, this planet provided a new and unusual constraint on models and required mechanisms with no obvious application in the case of our solar system (Rasio & Ford, 1996; Lin et al., 1996). The discovery of 51 Peg b was the first of many steps toward the current diversity extra-solar planets.

With improved techniques and a systematic search over the last ten years, hundreds of planets are now known to orbit stars other than our Sun.[‡] As with the first discovery, these planets have continued to surprise. The planets have a wide range in almost every imaginable parameter. They can have eccentric or circular orbits, be hot or cold, big or small, dense or not-dense, and be made of mixtures of rocky, icy, and gaseous material.

At a somewhat slower rate, the diversity of stellar hosts has also increased. For scientific (and perhaps anthropic) reasons, many of the first planets were discovered around solar-type stars. Low-mass stars are too faint, and intermediate-mass stars have fewer spectral lines, when compared to their solar-type counterparts. Thus many early (and ongoing) surveys focused on solar-type stars. With technological advances surveys have been able to look at fainter stars. Now, many planets are known to orbit low-mass stars. The problems associated with intermediate-mass stars have been side-stepped with the help of stellar evolution. As stars run out of hydrogen in their cores, their envelopes expand and they become cooler. Spectroscopy is possible for these "retired" A-type stars, with a handful of planet discoveries since the first in 2002 (Frink et al., 2002).

The veritable zoo of known planetary systems provides a challenge for theories. To produce such a diversity of planets from a single, overall model with plausible, physically motivated boundary conditions is a formidable task.

This thesis explores one potential way to a greater understanding, provided by the range of stellar host masses. Crucial parameters such as luminosity, temperature,

[†]Throughout this thesis, I generally refer to extra-solar planets as those orbiting normal, MS stars, thus excluding the pulsar planets from this definition.

[‡]See http://exoplanet.eu and http://exoplanets.org

orbital period, disk mass, and disk lifetime change with stellar mass. When used within the current planet formation paradigm, these changes make specific predictions of current and future trends that appear among extra-solar planets.

In this Chapter, I outline the current paradigm of disk evolution and planet formation. These ideas are the basis for the studies in the remaining Chapters of this work. I first cover the current observational knowledge of young stars, circumstellar disks, and the extra-solar planets they form. I then move on to outline the theoretical framework used to model disk evolution and planet formation. Where appropriate, I note aspects of each that are directly related to parts of this thesis.

1.2 Disks and their Planets: Observations

From the perspective of this thesis, observations provide both beginning and end points for theoretical models. In a field as uncertain as star and planet formation, models must make many assumptions about uncertain or unknown initial conditions. Thus, obtaining useful estimates and constraints on as many of these as possible makes a model more physically plausible. Observations also provide the end point for models, because any useful model needs to make predictions of observable quantities.

The current observational knowledge pertaining to these models can be neatly split in two: the disks planets are thought to form in and the planets themselves. The ability to make such a neat division is a reflection of observational limitations; planets are most easily discovered around billion year old MS stars, not while embedded in million year old circumstellar disks. New high resolution facilities such as the Giant Magellan Telescope (GMT) and Atacama Large Millimetre Array (ALMA) in the next decade may allow direct detection of (proto)planets within young disks, but for now the prospects for finding planets in circumstellar disks are minimal.

1.2.1 Circumstellar Disks

There are few direct observational links between primordial disks and planets. However, Occam's razor suggests they are inextricably connected. The solar system planets have co-planar orbits, and young stars posses disks of gas and dust with masses sufficient to form solar systems. Infra-red spectra of stars with circumstellar disks also show remarkable similarity to those of solar system comets (Lisse et al., 2006). In this section I first cover the methods used to infer disks and then discuss what these observations imply for their structure and evolution.

Looking ahead, observations suggest that a young star passes though several stages on the path from cloud collapse to becoming a bona fide hydrogen burning star. Stars in these different stages are assigned "classes," moving through a logical sequence of Class 0 cores, embedded Class I objects, Class II star + disk systems, and finally Class III stars without disks (Lada, 1987; Andre et al., 1993). These classes are generally assigned on the basis of photometry in a number of near-mid infra-red (IR) bands. For individual stars, the relatively small number of objects "caught" in the act of dispersing their disks suggests the transition between the Class II and III stages occurs rapidly; in $\sim 10^5$ years. For clusters of stars, this sequence occurs gradually and takes the bulk population ~5–10 million years, suggesting a wide range of Class II disk lifetimes.

This evolution has been inferred from a multitude of observations of many objects in nearby star forming regions. Because disks are observed to span a wide range of spatial scales, from tens to thousands of AU (e.g. McCaughrean & O'Dell, 1996), the physical conditions in the disk vary widely, from tens to thousands of Kelvin. Simple disk models derived from observations suggest densities ranging from $\sim 10^{-4}$ to $\lesssim 10^{-14}$ g cm^{-3}, depending on radial and vertical location. The wide range of temperatures and densities therefore dictate the type of observations used to search for gas and dust in different regions. Each method yields an independent estimate of particular disk characteristics.

Unfortunately the main disk component, H_2, is hard to detect, particularly at large distances from the star. Beyond the ~10 AU planet forming region, gas is therefore detected by the presence of trace molecular species such as CO. Dust is generally detected from thermal emission in far-IR to millimetre bands.

At AU scales, where planets form and are found, dust temperatures correspond to near and mid-IR wavelengths. The presence of dust is therefore inferred from an IR excess above the stellar photosphere. Gas is ionised by shocking and heating as it accretes onto the star and is visible through excess UV emission (Calvet & Gullbring, 1998). The ionisation of hydrogen also means the presence of the Hα line, whose equivalent width (EW[Hα]) is typically greater than any chromospheric emission for an accreting object (White & Basri, 2003).

With a number of measurements in different bands, the Spectral Energy Distribution (SED) of an object is obtained. The observed SED is then compared with a stellar model. For a star with no disk, the two are the same. When a star has a disk, the IR and UV excesses cause a departure from the stellar model, which is commonly quantified in several different ways. The slope of the SED over some range, usually long-ward of ~1 μm, defined by $\alpha = \mathrm{d} \log \lambda F_\lambda / \mathrm{d} \log F_\lambda$ (e.g. Adams et al., 1987; Lada et al., 2006), gives a measure of whether a star possesses a disk or not. Stars with α above some threshold ($-2.5 \lesssim \alpha \lesssim -1.8$, Lada et al., 2006; Luhman et al., 2008) are classified as having disks.

The SED has been central to understanding the sequence of Classes mentioned above, illustrated by 2MASS and Spitzer IRAC SEDs of real stars in Figure 1.1

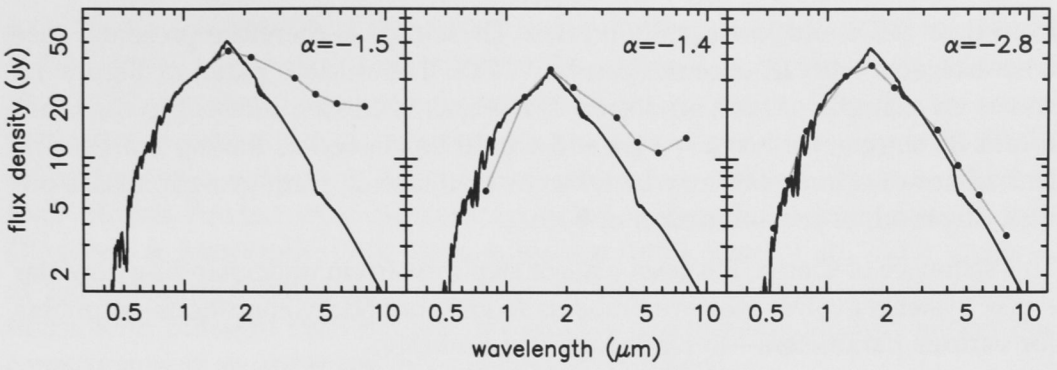

Figure 1.1 Example SEDs showing an evolutionary sequence from Class II, to a transition disk, to Class III. Each panel shows the flux density in various bands (*dots, solid grey lines*) compared to a stellar photosphere (*solid black lines*) for the appropriate spectral type (matched at J, Castelli & Kurucz, 2003). The spectral index α is derived from a linear fit to the four IRAC data points. Objects are taken from the cluster database used in Chapter 5.

(see also Lada et al., 2006). The left panel shows a typical star + disk system; a Class II object. After 1–10 million years, young stars lose their disks and become Class III objects, like the object in the right panel.

A separate, but closely related classification is based on the accretion signature. The star T Tauri, discovered in 1852 by Hind, is the prototype of accreting objects, thus commonly called "Classical T Tauri" stars, or CTTS. CTTS are defined as being lower-mass stars ($\lesssim 2\,M_\odot$). Higher mass analogues are known as Herbig Ae/Be objects, after their discovery and characterisation by Herbig (1960). With time, the accretion signature declines, until eventually the object becomes known as a "Naked" or "Weak lined" T Tauri stars, or WTTS. "Weak lined" refers to the weaker spectral emission lines (such as Hα) being more likely due to chromospheric activity than disk accretion processes. Generally, stars with disks inferred from IR excesses are CTTS, and stars without IR excesses are WTTS.

While this overall evolution provides a general picture of disk evolution and the timescales involved, there are further subtleties. For the youngest clusters, such as Taurus and Chamaeleon I, there is a marked separation between the spectral indices of objects with and without disks (Skrutskie et al., 1990; Kenyon & Hartmann, 1995). Because objects must evolve through intermediate indices as their disks disperse, this result suggests that the time for an individual star to disperse its disk is short; of the order 10^5 years. For older clusters this separation is less clear, because SED slopes tend to decrease over time (Hernández et al., 2007).

Though the short disk dispersal time for individual objects suggests using SED slopes is a relatively robust method of disk characterisation, some stars have been caught in the act of dispersing their disks. These objects are known as "transition disks," and appear to have inner holes in their dust disks, as inferred

from their SEDs and low accretion rates. These objects therefore present a case where objects with IR excesses can be WTTS. The middle panel of Figure 1.1 shows an example of such an object. This object is clearly different to the Class II and III objects, yet has $\alpha = -1.4$ and would be classed as having a disk. The lack of hot dust emission may be taken as evidence of grain growth, inside-out disk dispersal, or a combination of both.

This sequence of Classes has been a major step forward in understanding how star + disk systems evolve. However, models require boundary conditions—numbers for various parameters—to reproduce this evolution.

Measurement of excess UV or hydrogen recombination lines yield an estimate of the accretion rate (e.g. Hartmann, 1998; Gullbring et al., 1998). Observations of several different clusters find an interesting result; the accretion rate appears to scale as the square of stellar mass (Muzerolle et al., 2005; Natta et al., 2006). This strong scaling is something of a conundrum for theoretical models (Padoan et al., 2005; Hartmann et al., 2006; Throop & Bally, 2008), but may simply be the result of observational limits (Clarke & Pringle, 2006), with $\dot{M}_{\rm accr} \propto M_\star$ a more likely scaling. Assuming a power law decline of accretion, the accretion rate also yields an estimate of the mass remaining in the disk (Hartmann et al., 1998). These measurements typically find disk masses 0.01–0.1 times the mass of the star (e.g. Hartmann et al., 1998; Natta et al., 2006).

There are several other methods used to infer disk masses. Augmenting the masses of the solar system planet to solar abundance and spreading them out into a disk yields a "Minimum Mass solar Nebula" (MMSN), with a power law radial surface density profile (Weidenschilling, 1977b; Hayashi, 1981). This model represents the minimum amount of solar composition material needed to form the solar system, 0.01–0.1 solar masses.

Millimetre observations of circumstellar disks in regions such as Taurus and ρ Ophiuchi yield similar estimates of disk masses (Natta et al., 2000; Andrews & Williams, 2005, 2007). These observations find that disk mass tends to scale roughly linearly with stellar mass. With an assumed gas/dust ratio of 100 (e.g. Lilley, 1955), these observations find relatively low disk masses, with median disk/star mass ratios around 0.01. However, it is thought that these observations underestimate the disk mass, perhaps by an order of magnitude when compared to other measures (such as from accretion, Andrews & Williams, 2007). Millimetre observations are sensitive to millimetre size objects and cannot take into account the possible presence of invisible centimetre size or larger objects.

These observational techniques yield the main input for disk models and dictate the amount of mass for building planets, where the bulk of it is located, and its accretion rate onto the star. However, they are not the only important observational results; stars of different ages yield estimates of the typical disk lifetime. These lifetimes constrain models of disk evolution and gas giant formation.

As with most astronomical timescales, disk evolution proceeds much too slowly to be followed for individual objects. The solution is to observe a series of objects of different ages, with the reasonable assumption that the sequence presents a typical temporal sequence. In the case of pre–main-sequence (PMS) stellar evolution, estimating stellar ages is particularly difficult. Because different PMS models predict very different ages and masses for individual stars (e.g. D'Antona & Mazzitelli, 1994; Palla & Stahler, 1999; Siess et al., 2000), clusters of approximately coeval stars are used. Though the absolute age of a cluster varies with different PMS models, the relative age between clusters allows the construction of an approximate evolutionary sequence.

Observations of stars in young clusters yield several interesting bulk properties. The most commonly quoted and used is the fraction of stars with disks. Compiling the disk fraction for a series of clusters of different ages shows a decline with time. Figure 1.2 shows this evolution for EW[Hα] and Spitzer IR excess disk signatures. The disk fraction declines to ~10% in ~5 Myr, an estimate of the disk dispersal timescale. Studies of dust evolution at shorter and longer wavelengths find similar results (Haisch et al., 2001b; Mamajek et al., 2004), with somewhat longer disk lifetimes at longer wavelengths. This difference can be understood in terms of disk evolution and grain growth, which proceeds at a rate proportional to the local orbital period. Thus, evolution is slower at the greater distances probed by longer wavelengths. As suggested by evolution through the different SED classes, the average SED slope is also seen to systematically decline with cluster age (Hernández et al., 2007).

A recent trend emerging from the large scale studies made possible by Spitzer is the comparison of disk fractions for different spectral types (Hernández et al., 2005; Carpenter et al., 2006; Lada et al., 2006; Hernández et al., 2007; Dahm & Hillenbrand, 2007; Luhman et al., 2008). This comparison inevitably leads to differences, which, due to relatively small numbers, are only marginally convincing. However, most clusters show the same trend; a decreasing disk fraction with increasing stellar mass or earlier spectral type. Further investigation of the significance of this trend and its comparison to theoretical models is the basis of Chapter 5.

Though this thesis does not consider their evolution, no discussion of circumstellar disks is complete without mention of the "debris disks" observed around MS stars. Debris disks are a somewhat different phenomenon, defined by much lower levels of excess IR emission than their primordial counterparts and little or no gas content (e.g. Backman & Paresce, 1993; Meyer et al., 2007; Wyatt, 2008). Because the timescale for removal of the observed dust is shorter than the stellar lifetime, these disks are evidence of ongoing dust replenishment from collisions. These collisions are thought to arise from stirring by larger objects and cause the disk mass to decrease over hundreds of millions of years (Dominik & Decin, 2003; Kenyon & Bromley, 2004a; Wyatt et al., 2007).

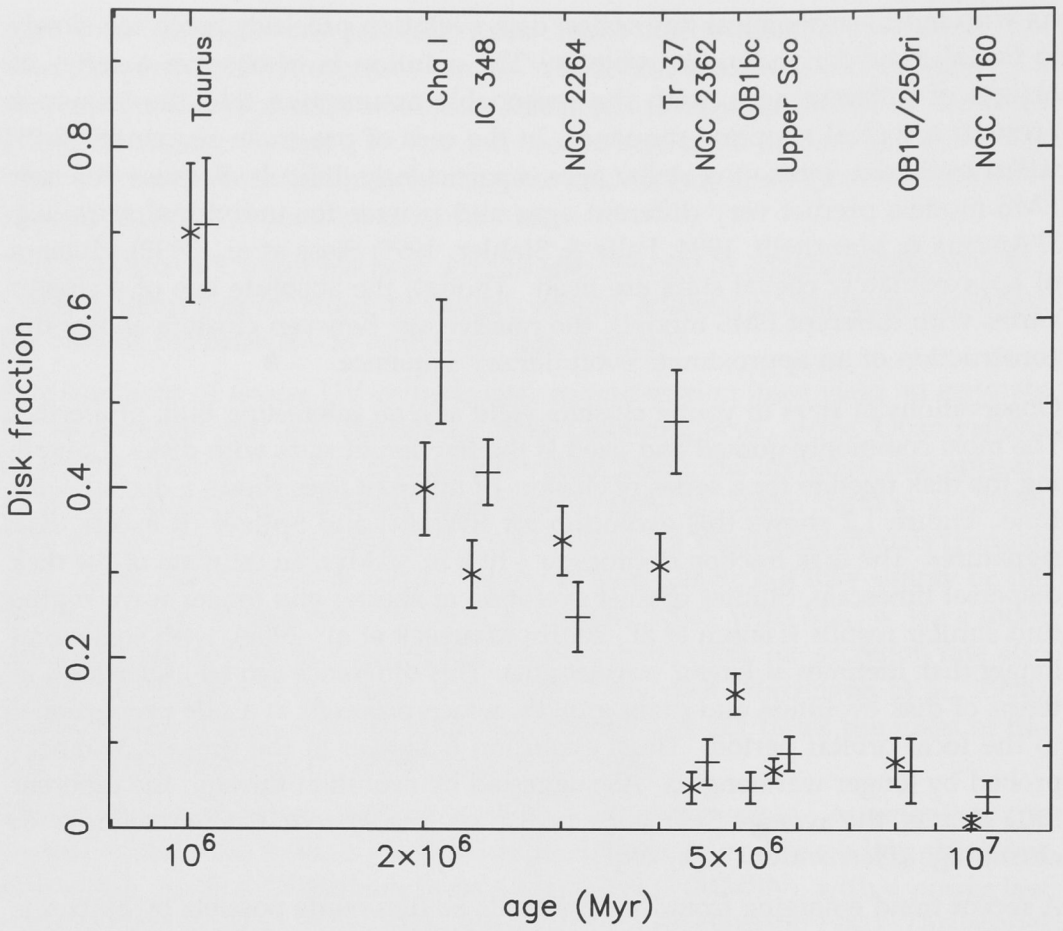

Figure 1.2 Overall cluster accretion (×) and IR fractions (+), as a function of cluster age. The disk fraction shows a systematic decline with cluster age and indicates a bulk disk dispersal timescale of ~5 Myr.

In summary, the observational results important to planet formation are:

- Disks are observed around nearly all young stars. By ~10 Myr, very few stars have primordial disks. Most disks are dispersed by ~5 Myr.
- Young stars have a wide range of disk masses; 0.01–0.1 stellar masses. Disk mass scales roughly linearly with stellar mass.
- Accretion rates depend on stellar mass, with observations suggesting $\dot{M}_{\rm accr} \propto M_\star^2$. However, an observational bias means the dependence is probably nearer to linear.
- There is evidence that the disk lifetime becomes shorter with earlier spectral type and increasing stellar mass.

1.2.2 Extra-solar Planets

There exist many different techniques for discovery and characterisation of extra-solar planets. Each has unique strengths, weaknesses, and biases, which have been influential in shaping our understanding of planet formation. Because the first planets orbiting MS stars were discovered by the radial velocity (RV) technique—most sensitive to planets with close orbits—we have something of an "inside-out" knowledge of planetary systems: it is only after ten years that discoveries are reaching the sensitivity to see solar system analogues. Had a technique with no bias towards close orbits been prevalent, perhaps the "typical" architecture of extra-solar systems would have been different.

In the solar system, planets are defined as those that orbit the Sun, have sufficient mass to be round in shape, and have cleared their orbits. While the requirement of a near spherical shape due to hydrostatic equilibrium defines a lower-mass limit, this definition lacks an upper limit to apply to extra-solar planets. This limit is usually defined by the onset of deuterium burning at $\sim 13\,M_{\rm Jupiter}$.

Planets appear to be fairly common. Cumming et al. (2008) find that 10.5% of solar-type stars have gas giants within ~3 AU. This frequency is a lower limit, because many stars probably have planets residing on larger orbits; extrapolation suggests ~20% frequency for gas giants within 20 AU. Given these frequencies and the inevitable increases from new low-mass planets, planet formation may be an inevitable consequence of star formation.

Figure 1.3 shows a mass vs. semi-major axis diagram of known planets.[†] This diagram is packed with information about the planets and the observational techniques used to discover them. Considering each technique individually allows insight into how this diagram is being filled.

RV surveys are most sensitive to close, massive planets; those that shift the system centre of mass furthest from the centre of the host star and make it move fastest. A disadvantage of this technique is that it only yields the *minimum-mass* of a planet, because the system inclination is unknown. With a large sample however, this deficiency is less of a problem. The average increase in planet mass for randomly inclined orbits is a factor of 1.3. Thus, some planets with minimum masses near $13\,M_{\rm Jupiter}$ will have larger true masses and be brown dwarfs. Sensitivity to lower-mass planets is attained by improved technology and more measurements. Thus the discovery space has shifted down the plot with technological development. Sensitivity to longer period planets is again attained with better technology and by observing a star for an extended period of time—of order the time taken for an orbit. Thus, the discovery space has shifted rightward in the plot with longer temporal baselines. On the whole, RV fills this diagram towards the lower right corner, as seen by the distribution of ○'s and ⊙'s.

[†]All planet diagrams in this thesis use planets reported in the exoplanet.eu database.

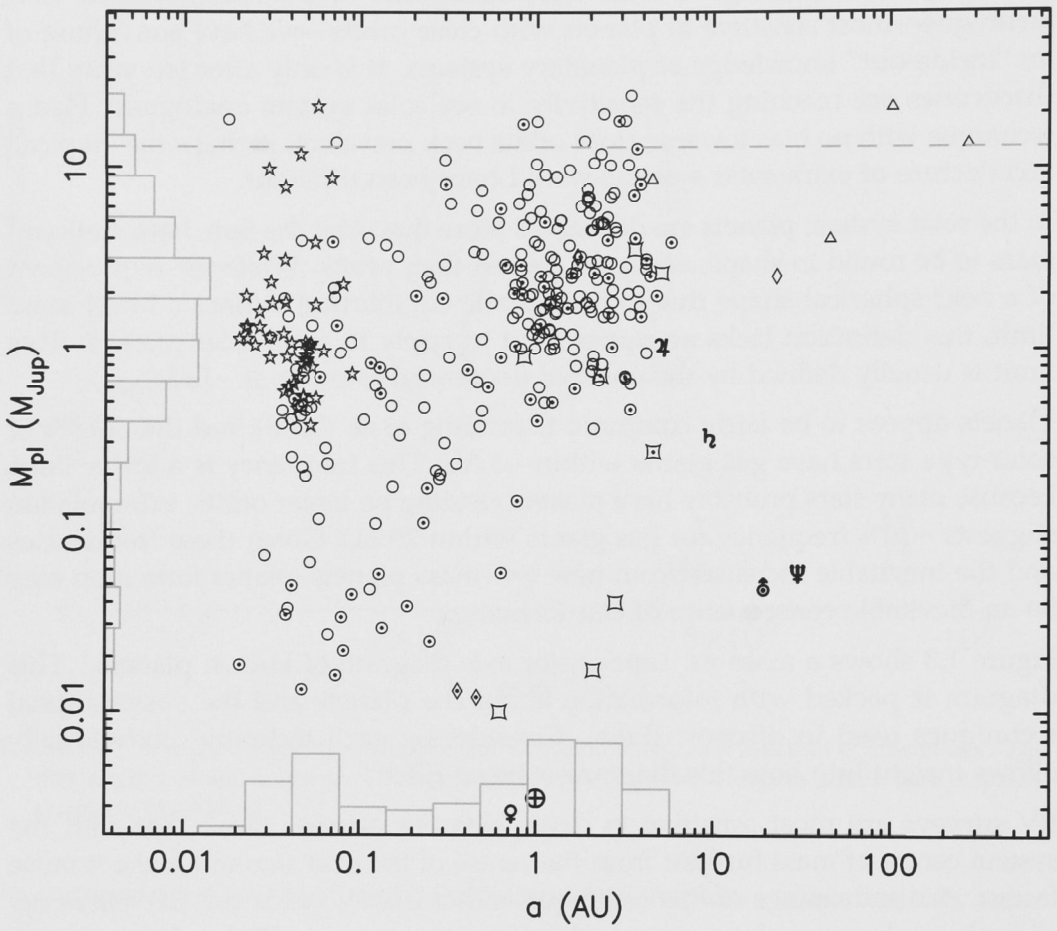

Figure 1.3 Mass vs. semi-major axis (a) of extra-solar planets. Symbols denote different detection methods: RV (minimum masses, *circles*), imaging (*triangles*), transits (*stars*), timing (pulsar and pulsation, *diamonds*), and microlensing (*pinched squares*). Multiple planet systems are marked with a small dot inside their symbol. The solar system planets are included, marked by their astronomical symbols. Histograms show the distribution of stars in both mass and semi-major axis. The dashed line shows the mass where planets start burning deuterium, entering the brown dwarf regime ($\sim 13\, M_{\rm Jupiter}$). RV discovered planets below this line may also be brown dwarfs due to inclined orbits.

The sensitivity of transit surveys—looking for planets repeatedly transiting their star from Earth's perspective—is a very strong function of planet semi-major axis (Sackett, 1999). Therefore all planets discovered by transit have orbits within 0.1 AU of the central star.[†] Because the transit signal depends on the relative area of the star and planet, this method is more sensitive for larger planets and smaller stars. A major advantage of this technique is that it yields the system inclination—essentially edge on—and thus the actual planet mass. With a known mass (from RV follow-up) and planet radius (estimated from the stellar radius and transit signal strength) the average density can be estimated. Other useful properties can be derived, such as the relative inclination of the stellar rotation and planet orbit (Rossiter, 1924; McLaughlin, 1924; Charbonneau et al., 2007).

These two methods have contributed the bulk of known extra-solar planets. With the ability to survey tens of thousands of stars in a single field, transit detections are rapidly catching up to the number of RV discoveries. The other methods, microlensing, timing, and direct imaging may have found far fewer planets, but still make useful and interesting statements about the general nature of planetary systems.

Imaging surveys for planets in wide orbits have found a few planets (Chauvin et al., 2004; Neuhäuser et al., 2005; Chauvin et al., 2005). However, these planets are generally much more massive than Jupiter and may be fusing deuterium. It is more common for imaging surveys to place limits on the mass of planetary companions (e.g. Luhman & Jayawardhana, 2002; Zinnecker et al., 2006; Kasper et al., 2007; Janson et al., 2008). With current technology, these limits are still many Jupiter-masses and barely in the regime well known to RV and transit techniques.

Though the first planets were discovered by pulsar timing (Wolszczan & Frail, 1992), only one more system has been discovered by this method since (Backer et al., 1993). This paucity perhaps reflects a lack of planets around these extreme objects. One other planet has been detected by timing. For V 391 Pegasi, a hot sub-dwarf B star, it was differences in pulsation periods that signaled the presence of a planet.

The final discovery technique, microlensing, has the unique capability of finding ~Earth-mass planets at ~AU scales around MS stars. Though only eight planets have been announced, these discoveries imply that planets with star/planet ratios $\sim 10^{-4}$—similar to Neptune in the case of the Sun—are common. Planets discovered by microlensing are interesting because they orbit further from their parent stars than most low-mass RV detections, perhaps in the regions where they form. I explore this possibility with reference to a particular planet—OGLE-2005-BLG-390Lb—in Chapter 2.

[†]The longest period transiting planet, HD 17156 b, orbits at 0.16 AU. It was discovered by RV and later found to transit (Barbieri et al., 2007).

Unfortunately, microlensing events are rare and yield limited information: the star/planet mass ratio. It takes many years before the planet hosting star can be characterised, yielding the true planet mass (Bennett et al., 2007). Planets are unlikely to be verified or studied further due to their large (kpc) distances (Figure 1.5).

Combined, these techniques cover much of the discovery space shown in Figure 1.3. However, finding Earth-mass planets at habitable distances from their stars—the ultimate goal of planet hunting—is difficult for all techniques. Further development is needed to push the discovery space down into this regime. The introduction of yet another technique, astrometry, may be used to search for Earth mass planets in the future (Bower et al., 2007; Beichman et al., 2008).

The first extra-solar planets inspired new theories for forming individual systems (e.g. Lin et al., 1996; Rasio & Ford, 1996). However, with hundreds of planets now known, attempts to explain individual systems are generally reserved for multiple systems with interesting configurations (e.g. Lee & Peale, 2002; Alibert et al., 2006). Instead, population synthesis is becoming useful as a tool for testing what particular mechanisms predict for the bulk population (e.g. Ida & Lin, 2004a,b, 2005; Chambers, 2006b; Ida & Lin, 2008; Miguel & Brunini, 2008). As the number of known planets has grown, certain trends have emerged, which provide focal points for this theoretical development.

The best example of an observational trend providing a convincing constraint on a theoretical model lies with the giant planet-metallicity relation (Gonzalez, 1997; Santos et al., 2001; Fischer & Valenti, 2005). There was initially doubt whether this trend was cause or effect; whether the process of forming close-in planets increased the stellar metallicity, or whether higher metallicity made it more likely that gas giants would form and migrate. The former case arises because any material interior to a migrating gas giant is probably accreted onto the star, thus increasing its metallicity. The latter case implies that giant planets are more likely to form when there is more solid material available. Initial studies considered both possibilities and concluded the former (e.g. Gonzalez, 1997). Later studies concluded that the result is more likely primordial, due to a lack of correlation between planetary orbital parameters and metallicity (Santos et al., 2001).[†]

As noted earlier, most planet discoveries have been around solar-type stars. Thus, some trends have only been discovered recently, made possible by the extension of planet hunting surveys to a wider range of stellar masses. Butler et al. (2006) found that GK-type stars were several times more likely to harbour giant planets

[†]There also exist trends among the subset of transiting planets. The period of transiting planets appears to decrease with increasing planet mass (Mazeh et al., 2005). Further, the residuals from a fit to this trend may depend on stellar metallicity (Torres et al., 2008). There may also be two separate classes of transiting giant planets (Hansen & Barman, 2007). This dichotomy requires further planet discoveries to be verified. Finally, there is evidence that higher metallicity leads to planets with greater heavy-element content (Guillot et al., 2006).

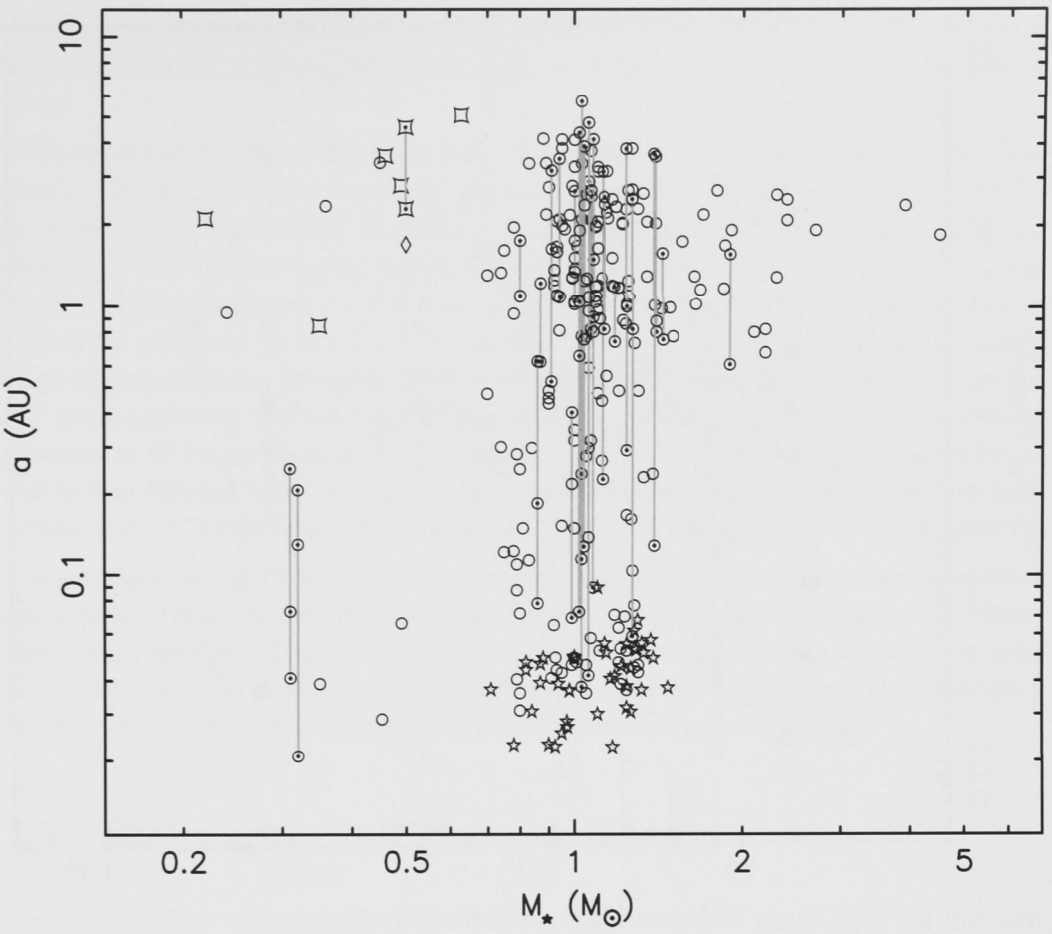

Figure 1.4 Semi-major axis vs. stellar host mass of extra-solar planets. Symbols as in Figure 1.3, with grey lines linking systems of planets. The most notable feature is a "step" in the orbits of planets around stars $>1.6\,M_{\odot}$.

than M-dwarfs. With the discovery of a number of planets orbiting intermediate-mass stars, Johnson et al. (2007a) noted that this trend also extended above solar-mass stars. Chapter 3 is in part concerned with prediction and explanation of this trend.

Another trend with stellar mass is shown in Figure 1.4, which shows planet semi-major axes vs. the mass of the host star. There is a curious "step" in semi-major axis for planets orbiting stars more massive than 1.6 solar masses. Because the sensitivity of RV surveys decreases with increasing planet semi-major axis, there cannot be giant planets in closer orbits in these systems.

However, there is a major caveat that goes with this feature: most of these stars are not on the MS. Main-sequence intermediate-mass stars are too hot to have many spectral lines, thus making them unsuitable for RV surveys. These stars can be targeted later, as they exhaust their hydrogen fuel supply and expand

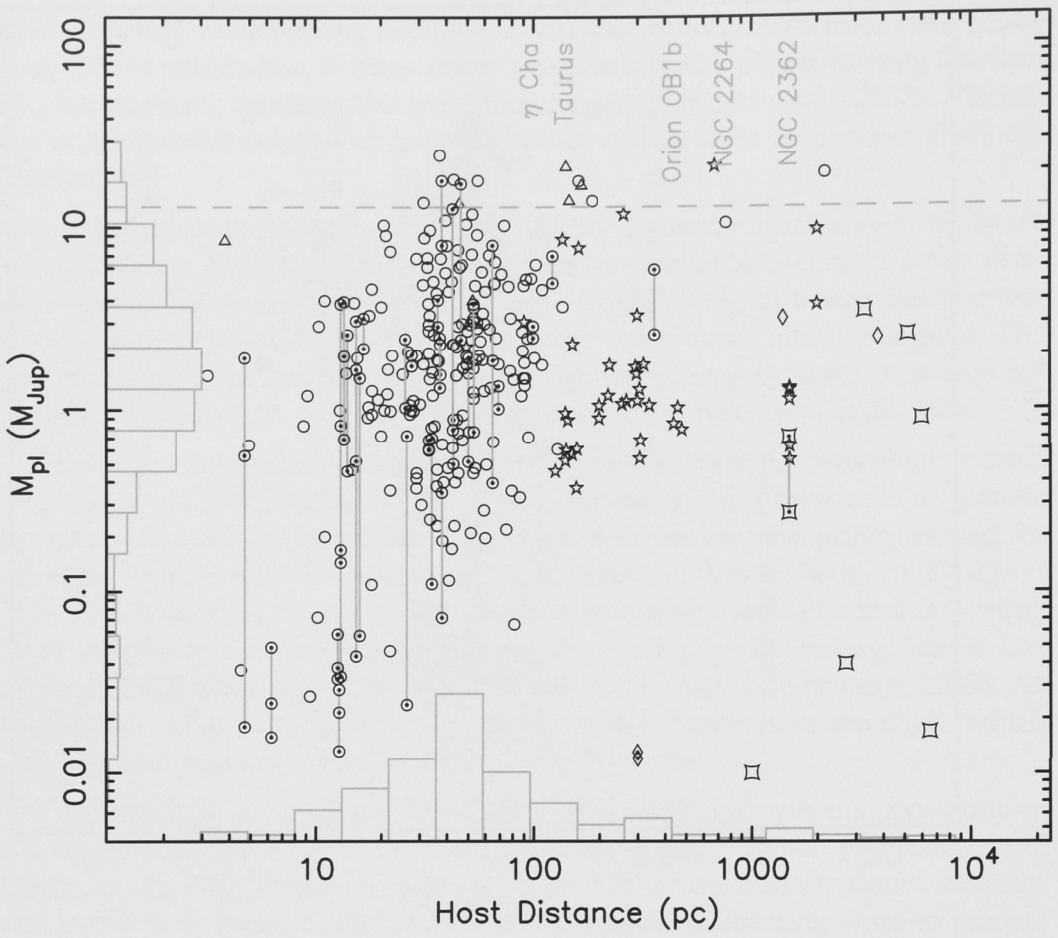

Figure 1.5 Planet masses vs. distance to host star. Symbols as in Figure 1.3. Histograms show the distribution of planet masses and stellar distances. Text labels show approximate distances to selected nearby star forming regions and associations.

to become (sub-)giants. The greater radii of these stars might then cause the trend to larger orbits, by engulfing closer planets or causing their orbits to decay through tidal interaction (Rasio et al., 1996). While engulfment and tidal decay may be plausible scenarios for post–helium-flash stars, more detailed investigation suggests they are unlikely for those yet to ignite their helium fuel supply (Johnson et al., 2007b; Sato et al., 2008a). In Chapter 5, I suggest this trend may arise from the shorter disk lifetimes around intermediate-mass stars.

To put extra-solar planets in the context of star formation, Figure 1.5 shows extra-solar planet masses vs. the distance to their host stars. The mass of planets increases with stellar distance for radial velocity detection; it is easier to find planets around brighter stars. The bulk of radial velocity discovered planets reside within 100 pc, with most around ~50 pc. Planets discovered around more distant stars are discovered by the transit, timing, and microlensing methods, or orbit intermediate-mass stars. The nearest young star forming regions—where

stars have circumstellar disks and are forming planets—are at comparable and larger distances; η Cha, Taurus-Auriga, and Upper-Scorpius are ~100–140 pc away.

Unfortunately, no planets have yet been discovered to orbit stars with circumstellar disks. Young stars are naturally variable, and the techniques that could be plausibly used, RV, transits, astrometry, and imaging must all overcome significant obstacles. For the strongest signal, RV detection requires an inclined orbit, but to avoid being hindered by the disk, would require a nearer face-on orientation. The same problem is faced by the transit method, requiring an almost perfect edge-on orientation. Imaging is perhaps the most promising, with detection of hot young planets embedded in their disks a plausible possibility for the next generation of larger telescopes. At the distance of Taurus and Upper Scorpius, a diffraction limited telescope needs to have a 30 m diameter—the size of the next generation of "extra large" telescope—to resolve a planet at 1 AU in the near-IR.

These observational difficulties mean not all stages of the planet formation process are visible. Thus, connecting planetary nurseries with full grown planets requires theoretical models. These models use the initial conditions set by observations of young stars and disks and attempt to reproduce the other observed boundary conditions, such as disk lifetimes and trends in extra-solar planets.

1.3 Disks and their Planets: Theory

Though the first cosmogonies were put forward over 200 years ago, the modern theory of planet formation is relatively young. Much of the theoretical groundwork was laid 30–40 years ago, with a number of seminal papers. The results from these works are still being used and improved on today. Highlights include; the size distribution of a "collisional cascade" (Dohnanyi, 1969), the formation of "planetesimals" by gravitational instability (Goldreich & Ward, 1973), the viscous evolution of circumstellar disks (Lynden-Bell & Pringle, 1974), and the book, *Evoliutsiia doplanetnogo oblaka*, published by Safronov (1969).

In the following sections, I cover some of the current theoretical understanding of disk evolution and planet formation. As with the observational picture, this field is far too large to cover in detail, so I outline the concepts relevant to this thesis, attempting to cover much of the material included in the Introductions to individual Chapters.

I have separated the theory into a hierarchy of stars–disks–planets, because each is influenced by the evolution of the preceding, but little by those after. For example, stellar evolution can change disk evolution and planet formation, but planets have little influence on the star. The evolution of disks and planets can be fairly closely linked, but disks will still evolve in the absence of planets.

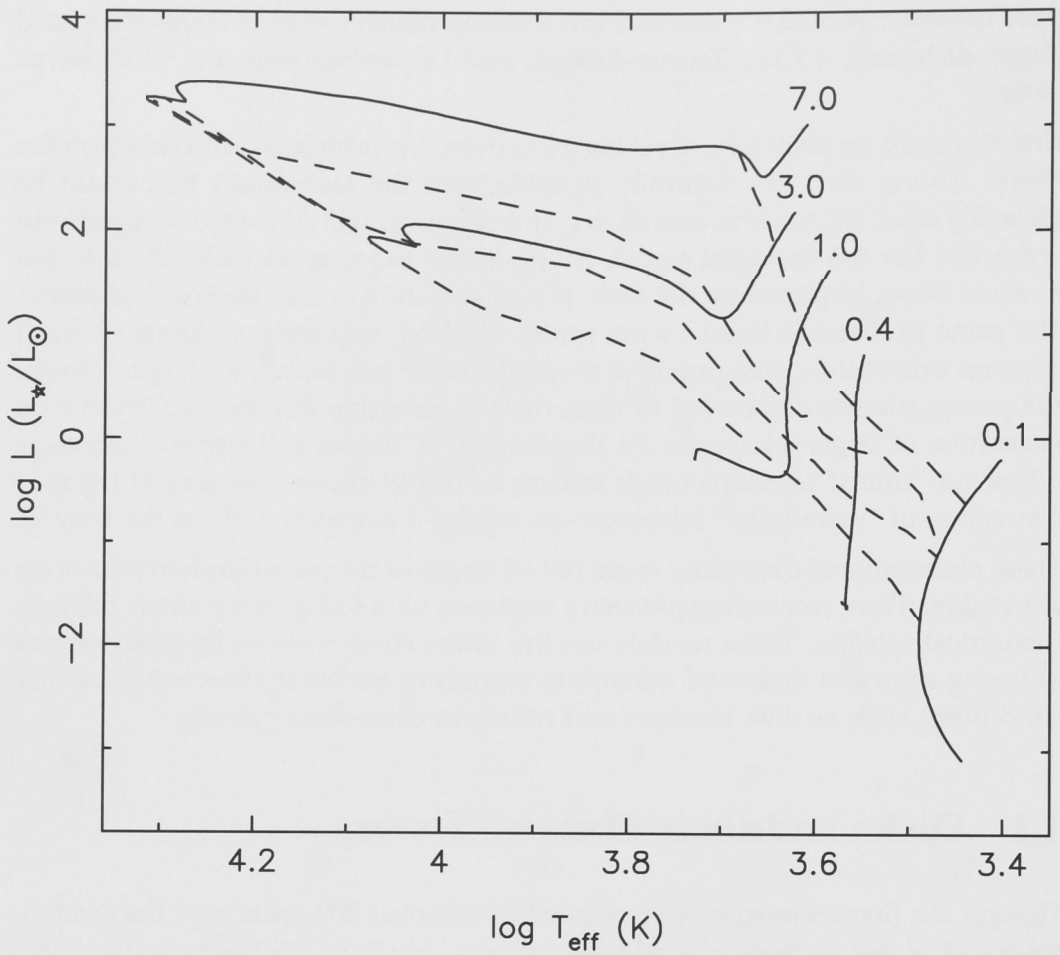

Figure 1.6 Hertzsprung-Russell diagram of PMS evolutionary tracks for a range of stellar masses (labeled in $M_\odot$, Siess et al., 2000). Dashed lines show lines of constant stellar age (isochrones) at 0.1, 1, 3, and 10 Myr.

1.3.1 Stellar Evolution

Understanding stellar evolution is one of the great astrophysical achievements of the last century. The first major steps were taken when Hertzsprung published his article "On the Luminosity of the Stars" in an obscure photographic journal in 1905,[†] and Russell published his now well-known diagram (Russell, 1914). Since the recognition of differences between stars termed "giants" and "dwarfs," models have been developed that explain essentially the entire life of a star. Most important for this thesis is development of models which take a star from its initial appearance at the "birth-line" (Stahler, 1983) through contraction to the MS, the period when a star + disk system forms planets.

[†]Zeitschrift fŸr Wissenschaftliche Photographie, 1905

Figure 1.6 shows this PMS evolution for a range of stellar masses (Siess et al., 2000). Low-mass stars contract on Hayashi tracks at constant effective temperature and are fully convective right down to the MS. solar and intermediate-mass stars begin contracting at near constant effective temperature. As the core temperature rises, increasing levels of ionisation decrease the optical depth, and the core becomes radiative. Energy escaping to the outer convective regions increase the effective temperature and luminosity as the star approaches the MS.

The important point for planet formation, is that both effective temperature and luminosity change significantly during the first 10-100 million years of a stars lifetime. The nature and timescale for these changes depends on the mass of the star. During the PMS evolution, changes in luminosity affect the disk temperature and the locations where different chemical species freeze into solids. How this evolution affects the location of the boundary between water vapour and ice—the "snow line"— is studied in Chapters 2 and 3.

1.3.2 Disk Structure and the Snow Line

A circumstellar disk is commonly parameterised by two or three main properties, from which many others can be derived. Central to any disk model is the surface density profile. This profile sets the mass of material in the disk at a given location and the total mass with definition of inner and outer disk radii. The MMSN (Weidenschilling, 1977b; Hayashi, 1981) is the most commonly used disk model. This relation usually follows a simple power law

$$\begin{aligned} \sigma_{\rm solid} &= \sigma_{0,\rm solid}\, f_{\rm ice}\, a_{\rm AU}^{-\delta} \\ \sigma_{\rm gas} &= \sigma_{0,\rm gas}\, a_{\rm AU}^{-\delta} \end{aligned} \tag{1.1}$$

In this case the radial distance a is in units of AU. The normalisation σ_0 depends on which disk component is being described. For the gaseous component $\sigma_{0,\rm gas} \sim 1700\,{\rm g\ cm^{-2}}$, and for the solid component $\sigma_{0,solid} \sim 10\,{\rm g\ cm^{-2}}$ (Hayashi, 1981). This normalisation defines the MMSN model, with a typical power law $\delta = 1.5$. This model provides sufficient material to build the terrestrial solar system planets (Chambers, 2001; Raymond et al., 2004; Kenyon & Bromley, 2006).

The factor $f_{\rm ice}$ refers to a change in disk structure at the "snow line," where the disk temperature becomes cold enough for water to be in the form of ice. The location of asteroids with hydrated minerals in the asteroid belt suggests a primordial distance of 2.7 AU (Abe et al., 2000; Rivkin et al., 2002). This concept has become part of the commonly used MMSN disk model (e.g. Ida & Lin, 2004a; Raymond et al., 2004), which typically uses the original factor ~4 increase in solid surface density outside the snow line (Hayashi, 1981). This factor is probably smaller, based on two modern results: the conclusion of the Deep Impact experiment that comets are probably icy-dirtballs rather than the

converse (Küppers et al., 2005) and updated solar abundances (Asplund et al., 2005). Water vapour contributes little to the overall gaseous disk component, so $f_{\rm ice}$ is not included, and the gas density follows a continuous power law decline.

The snow line—and other solid surface density enhancing effects (e.g. Stevenson & Lunine, 1988; Cuzzi & Zahnle, 2004; Kretke & Lin, 2007)—have at least in part been favoured because of their implications for forming Jupiter. Models typically find that without some increase in the surface density extrapolated from the terrestrial region, there is too little solid material to form Jupiter (Lissauer, 1987; Pollack et al., 1996; Thommes et al., 2003). These models find that at least $\sim$10 g cm^{-2} at 5 AU is needed, a factor 2–3 times increase over the MMSN.

In this thesis, an MMSN model essentially the same as Equation (1.1) is used with one additional parameter: how surface density varies with stellar mass. Based on observations (Natta et al., 2000; Andrews & Williams, 2005), this modification is made by simply adding a linear dependence. Thus, higher mass stars have more gas and dust available to form planets.

Because the snow line location is set by the disk temperature, it moves with time as the central star contracts and the disk accretion rate subsides. Chapter 2 is devoted to studying what this snow line movement might imply for forming large, icy planets around low-mass M-dwarfs. In Chapter 3, I extend this model to include energy liberated through viscous disk evolution and consider the implications for gas giant formation over a wide range of stellar masses.

There are more complex snow line models and alternatives that also yield departures from a power-law solid surface density profile. One of these is the "cold-finger" effect suggested by Stevenson & Lunine (1988) and updated by Cuzzi & Zahnle (2004). In this picture, a circumstellar disk has an initial equilibrium state with the water vapour concentration decreasing due to an increase in ice condensation beyond the snow line. As the disk diffuses and advects, ice continually condenses from gas passing beyond the snow line, thus enhancing the local surface density of solids and removing vapour phase water from the inner disk. Sublimation of planetesimals that drift inside the condensation radius by gas drag enhances this effect: the surface density beyond the snow line increases when water vapour from the sublimated planetesimals diffuses back outside the snow line (Cuzzi & Zahnle, 2004). This snow line model is used in Chapter 4 and simply results in a larger surface density enhancement at the snow line.

1.3.3 Disk Dispersal: Viscous Evolution and Photoevaporation

A circumstellar disk orbits at near Keplerian speed around the parent star for the bulk of its lifetime. However, disks are observed to evolve over time, accreting onto their parent stars and dispersing after several million years.

For stars to accrete, there must be some viscosity in the disk that leads to disk spreading over time. The bulk of the material is accreted, with a small fraction

at large distances retaining the initial angular momentum (Shakura & Syunyaev, 1973; Lynden-Bell & Pringle, 1974). However, molecular viscosity is too small to account for the observed disk lifetimes and more complex and specialised mechanisms have been sought. The most accepted source of this viscosity is the "Magneto-Rotational Instability" (Balbus & Hawley, 1991). This mechanism works by transferring angular momentum outward through magnetic field lines. The field lines link parcels of gas initially on similar orbits that become increasingly separated through Keplerian shear.

Accretion disk models lead to a disk that disperses steadily over several million years. If the viscosity is approximated as a power-law function of radius, then the equation describing the evolution of a thin accretion disk leads to a solution for the evolution of the accretion rate (Lynden-Bell & Pringle, 1974)

$$\dot{M}_{\rm accr}(t) = \frac{M_{\rm disk}(0)}{2\,t_\nu}\,\tau_\nu^{-3/2} \tag{1.2}$$

where $M_{\rm disk}(0)$ is the initial disk mass and $\tau_\nu = t/t_\nu + 1$ is a dimensionless time. The viscous timescale is defined at the scale radius R_0 by $t_\nu = R_0^2/(3\nu_0)$, where the viscosity is ν_0. Initially, $1/e$ of the disk mass lies outside R_0.

Though this evolution produces accretion rates comparable with observations (Hartmann et al., 1998), it is at odds with the observation that disks are rarely caught in the act of dispersing their disks: once significant mass loss begins, after several million years, the rest of the evolution takes only $\sim 10^5$ years (Skrutskie et al., 1990; Kenyon & Hartmann, 1995). This "two timescale" behaviour is a problem for pure accretion models.

The solution to this problem lies with photoevaporation, where disk material is lost to interstellar space near the star. If the gas can be ionised, it reaches temperatures of ~10,000 K. At disk locations where the thermal speed of this ionised gas is greater than the local Keplerian velocity, the gas is lost via a "wind" (Hollenbach et al., 1994, 2000). This mass loss may occur due to the central star, or high energy photons from massive stars in the local cluster environment (Adams et al., 2004).

By combining accretion and photoevaporation, Clarke et al. (2001) proposed a model that reproduces the two timescale behaviour. When the accretion rate drops below the wind loss rate, the inner disk is accreted rapidly. The outer disk is then subject to direct photoevaporation from the star and is removed in $\sim 10^5$ years, in line with observational results (Alexander et al., 2006). I use of a simplified version of this "UV switch" model (Alexander & Armitage, 2006) to study stellar mass dependent disk dispersal in Chapter 5.

1.3.4 Planet Formation

To form planets from micron sized grains, growth over a massive twelve orders of magnitude needs to occur. Models usually split this problem in two or three: how to form ~1 km "planetesimals," then how these form planets, and finally (or sometimes concurrently) how these planets evolve and interact to produce the observed extra-solar planets.

Aside from the complexities of modelling such a wide range of scales, this split is largely motivated by the influence of gas on growing objects. The gaseous disk component orbits at slightly sub-Keplerian speed due to pressure support from interior orbits—hydrostatic equilibrium. Objects much smaller than ~1 m follow the motions of the gas, and objects much larger are unaffected by gas drag. In between, ~1 m objects are most strongly affected. These objects want to move on normal orbits, but experience a "headwind" from the more slowly orbiting gas. The time for ~1 m objects to spiral into the star from 1 AU is astonishingly short; around 100 yr (Weidenschilling, 1977a). Thus, planetesimal formation models focus on ways to make ~1 km objects. Planet formation models assume this 1 m "barrier" has already been overcome and focus on the following evolution.

Early Planet Formation: Making Planetesimals

There are two fairly well studied ways to form planetesimals. The first, a small scale gravitational instability, sidesteps the 1 m barrier by forming planetesimals directly in the disk mid-plane, without the need to grow through 1 m size objects (e.g. Goldreich & Ward, 1973; Youdin & Shu, 2002). Although some studies suggest that turbulence may prevent this process (Weidenschilling, 1980), gravitational instability remains a plausible planetesimal formation mechanism (see Natta et al., 2007, for a recent review).

In the second picture—"coagulation"—small dust particles again settle toward the mid-plane of the disk. They collide and stick as they settle, which significantly shortens the timescale for growth (Safronov, 1969). Some recent models find the 1 m barrier less of a problem. Grains may grow so efficiently that fragmentation is needed to explain the observed disk lifetimes (Dullemond & Dominik, 2005). Gas drag may be reduced in the disk mid-plane, where the gas instead experiences "particle drag," and is pulled along at the Keplerian velocity for sufficient grain densities (Nakagawa et al., 1986).

Planet Formation: Making Planets

Once planetesimals form, growth of large objects is determined by the collision rate, $n v \sigma_{\rm coll}$, where n is the number density of objects and v is their velocity

dispersion. The collision cross section is

$$\sigma_{\rm coll} = \pi d^2 F_{\rm g} = \pi d^2 \left(1 + \frac{v_{\rm esc}^2}{v^2}\right), \tag{1.3}$$

where d is the planetesimal radius and $v_{\rm esc}$ is the escape velocity of the merged pair of planetesimals. The gravitational focusing factor $F_{\rm g}$ becomes important when the objects reach 1–10 km in size and accretion is no longer simply geometric.

When planetesimals form, dynamical friction from small objects damps the random velocities of the largest objects, leading to large gravitational focusing factors and "runaway" growth, where the largest objects grow much faster than small ones (Wetherill & Stewart, 1989; Kokubo & Ida, 1996). Runaway growth ends when the largest protoplanets start to stir the remaining small objects velocity dispersions, decreasing F_g and their rate of accretion onto large objects. This evolution may be self consistently treated though use of analytical relations for stirring and damping rates (Ohtsuki et al., 2002) and gas drag (Inaba et al., 2001).

The Hill radius

$$R_{\rm H} = a \left(\frac{M_{\rm planet}}{3 M_\star}\right)^{1/3} \tag{1.4}$$

is a recurring distance in the study of planet formation, since the dynamics can commonly be treated as a large set of three-body problems, where the third bodies only interact with larger objects (e.g. Chambers, 2001; Tsiganis et al., 2005).

During "oligarchic" growth (Kokubo & Ida, 1998)—where each oligarch dominates a dynamical annulus ~5–10 Hill radii wide —objects become isolated from their surroundings and try to accrete all mass within the annulus.

Formally, the isolation mass contains all the mass within an annulus $2\,B\,R_{\rm H}$ wide: $M_{\rm iso} = 4\,\pi\,B\,R_{\rm H}\,a\,\sigma$, where the spacing factor $B \sim 4$ is derived from numerical simulations of oligarchic growth (Kokubo & Ida, 1998). Substituting $M_{\rm iso}$ as the planet mass in $R_{\rm H}$ yields

$$M_{\rm iso} = \frac{(4\,\pi\,B\,\sigma\,a^2)^{3/2}}{(3\,M_\star)^{1/2}} \tag{1.5}$$

(e.g. Lissauer, 1993), where σ is the disk surface density. Isolation masses are ~Mars size near 1 AU and several Earth masses near 5 AU.

The isolation mass is a useful concept that appears throughout this thesis. It provides an estimate of the maximum protoplanet size for a given solid surface density and semi-major axis.

Protoplanetary growth rates can be estimated with analytic or numerical models (e.g. Lissauer, 1987; Thommes et al., 2003; Chambers, 2006a; Kenyon & Bromley, 2006). Despite the different methods used, these estimates generally find that the

growth rate depends on two fundamental parameters: the initial surface density of planetesimals and the local orbital period.

$$\tau_{\rm grow} \propto \frac{P}{\sigma} \tag{1.6}$$

Greater initial surface density leads to more rapid growth, as does a shorter orbital period. Thus, the enhancement in surface density due to the snow line can be important when considering whether gas giant "cores" have time to form before the gas disk disperses. This balance sets where gas giants form and is the subject of Chapter 3.

As shown in Equation (1.3), the growth rate also depends on the velocity dispersion of the objects being accreted. If planetesimals can be damped, then gravitational focusing factors are larger and growth is faster. Planetesimals can be damped by gas drag and provides another mechanism for increasing protoplanetary growth rates (Rafikov, 2004; Chambers, 2006b). I explore the consequences of these differences with a numerical model, in the context of migrating super-Earths in Chapter 4.

Gravitational scattering becomes important after isolation, when dynamical friction from remaining planetesimals no longer damps protoplanets random velocities. At this point, growth in the rocky region near Earth diverges from growth where the giant planets formed. Near 1 AU, $M_{\rm iso} \sim 0.1\,M_\oplus$; protoplanets must undergo a 10–100 Myr period of chaotic growth to attain larger masses (e.g. Chambers, 2001; Raymond et al., 2004; Kenyon & Bromley, 2006; Nagasawa et al., 2007).

Near 5 AU, the Jovian and Saturnian "cores" reached $M_{\rm iso} \sim 10\,M_\oplus$, sufficient to undergo "core accretion." However, not all cores go on to become gas giants. Simple analytical arguments and some numerical simulations suggest that cores are likely to be ejected when instability sets in (Goldreich et al., 2004; Ford & Chiang, 2007; Chiang et al., 2007). However, detailed numerical simulations suggest the orbits are more likely to spread to larger distances (Levison & Morbidelli, 2007).

The formation of gas giants by core accretion has two or three phases (Pollack et al., 1996; Ikoma et al., 2000; Shiraishi & Ida, 2008). Runaway and oligarchic growth first produce an isolated core of $\sim 10\,M_\oplus$. This core mass varies with opacity and planetesimal accretion rate (Ikoma et al., 2000; Rafikov, 2006). A phase of moderate accretion of gas may follow (but see Shiraishi & Ida, 2008), where growth is limited by energy deposited in the atmosphere by remaining icy planetesimals. When the mass of the envelope reaches approximately that of the core mass, the envelope is then no longer stable and undergoes a rapid collapse. The planet attracts several hundred Earth masses of gas from the nebula. When the supply of nebular gas is exhausted due to local or global disk effects, growth is complete.

The rapid final stage of gas giant formation suggests there should be a separation between solid and gaseous planets and a dearth of ~50–100 Earth-mass planets (Ida & Lin, 2004a). The histogram on the y-axis of Figure 1.3 shows that there are too few low-mass planets to verify this prediction.

Beyond Planet Formation: Migration and Scattering

The discovery of extra-solar planets in short-period orbits was a surprise, because it is unlikely that they formed *in situ*. The favoured way for them to arrive at the observed small semi-major axes is through some form of migration or scattering (Lin et al., 1996; Rasio & Ford, 1996).

Migration is a natural way to produce the observed short-period orbits of many extra-solar planets, provided it can be stopped before the planet falls onto the star. The theory of migration involves interaction between a planet and the gas disk.[†] The presence of a planet causes a departure from the axisymmetric potential of the star. This break in symmetry forms spiral density waves in the gas disk, whose total torques on the planet usually result in inward migration.

There are two main "types" of migration, which depend on the mass of the planet (Ward, 1997). Type I migration applies to relatively low-mass protoplanets, up to tens of Earth-masses and is predicted to be rapid; so rapid that it conflicts with formation of planetary systems (e.g. Ida & Lin, 2008). However, recent simulations find that the Type I migration rate is slower than predicted by analytic theory (Masset et al., 2006a). Several groups have recently begun to investigate the effects of vertically non-isothermal disks on Type I migration. Early results suggest that Type I migration can be stopped, or even reversed in these cases (Paardekooper & Mellema, 2006, 2008; Fouchet & Mayer, 2008).

Planets reaching gas giant masses are large enough that they open a gap in the gas disk. A rough criterion for gap opening is for the planets Hill radius to exceed the disk scale height. For these planets, the migration is called Type II, and the planets orbit evolves inward with the viscous evolution of the disk on million year timescales.

An alternative theory for placing extra-solar planets on short period orbits is scattering (Rasio & Ford, 1996). In this scenario, the orbits of two planets with relatively close semi-major axes become unstable. Once the instability sets in, the planets interact over ~10 million year timescales, exciting each other onto highly eccentric orbits. If the inner planet attains a small enough periastron distance, its orbit can be circularised through tidal interaction with the star, resulting in a short-period planet like those observed. Scattering models are also capable of reproducing the eccentricity distribution of extra-solar planets (Ford & Rasio, 2008). An important prediction of this theory is that systems with planets in

[†]Except migration through a planetesimal disk (see Levison et al., 2007).

short-period orbits should also contain longer period planets on eccentric orbits (Rasio & Ford, 1996; Ford & Rasio, 2008).

Migration and scattering have been essential for describing extra-solar planetary systems, but each has its strengths and weaknesses. Migration models do not naturally produce planets on eccentric orbits, and scattering cannot produce planets in circular orbits at large semi-major axes.

Given the low-eccentricity and relatively wide orbits, the application of these mechanisms to the solar system must be more subtle. A number of recent studies investigating Type II migration in a solar system context find that the migration of a Jupiter-like planet can be modified by a lighter, outer giant planet (like Saturn). If the outer planet is captured into the 2:3 resonance, the gaps opened in the gas disk by the two planets overlap, and the migration can be halted or even reversed.

This discovery leads naturally to solar system like scenarios, without modifying the results for extra-solar systems. The solar system appears to have a unique configuration compared to extra-solar systems, which tend to have planets whose mass increases with semi-major axis. Thus, Jupiter-Saturn systems like the solar system tend to migrate little, whereas Saturn-Jupiter systems migrate significantly. This theoretical picture is consistent with the typical configuration of extra-solar planetary systems, which tend to have a larger planet orbiting outside a less massive one.[†]

This picture naturally predicts initial conditions for the favoured model for explaining the architecture of outer solar system planets. The "Nice" model[‡] suggests the orbits of the outer solar system planets were originally in a more compact configuration and became more spread out though gravitational interactions with each other and an outer planetesimal disk (see also Thommes et al., 1999). I study this type of initial compact configuration using isolation masses when looking at gas giant core forming regions in Chapter 3.

[†]Noted in a talk at the Harvard-CfA, 2007, by A. Morbidelli on simulations published in Morbidelli et al. (2007).

[‡]Developed in Nice, France; and does a nice job of explaining the orbits in the outer solar system (Tsiganis et al., 2005), the late heavy bombardment (Gomes et al., 2005), Jupiter's Trojan asteroids (Morbidelli et al., 2005), Saturn's rings (Charnoz et al., 2008), and the structure of the Kuiper belt (Levison et al., 2008).

1.4 Thesis Outline

Having outlined the observational and theoretical state of the art, I now briefly describe each Chapter that follows. In general, I study the consequences of changing the mass of the central star in disk evolution and planet formation models and the observational consequences. The first three studies appear in *The Astrophysical Journal* and the fourth is currently under review.

The methods used in these Chapters fairly closely resembles the theory outlined above. I commonly use simple scaling relations, the result of detailed numerical calculations. In many cases, the approach becomes semi-analytical, due to the inclusion of results from PMS stellar evolution models. In Chapter 4, I use a numerical oligarch formation and migration code, which is a simplified version of a model developed by Chambers (2006a).

Chapter 2: The Moving Snow Line and Super-Earths

This Chapter (Kennedy et al., 2007) looks at the effects of early stellar evolution on planet formation around a low mass star. Using a simple semi-analytic model, I consider how the decreasing luminosity of an M-dwarf causes the snow line to move inward as it contracts to the MS. The changing surface density profile sets where and when super Earth-mass planets are likely to form.

In this thesis, I use a refereed version of the paper that appeared in the conference proceedings following the "Fifth Stromlo Symposium: Disks, Winds and Jets—From Planets to Quasars." This version is simply a clearer and updated version of the original article, published in *The Astrophysical Journal Letters* (Kennedy et al., 2006).

Chapter 3: The Snow Line and Giant Planet Frequency

This Chapter (Kennedy & Kenyon, 2008b) again uses the snow line as part of the motivation, but looks at the consequences for gas giant formation over a range of stellar masses. This article is in part motivated by the treatment of the snow line by Ida & Lin (2005), which assumes $a_{\rm ice} \propto M_\star^2$. Using a semi-analytic model, I show that this assumption—based on an optically thin disk—is oversimplified and makes it hard to form gas giants around intermediate-mass stars. I extend the model of Chapter 2, including the energy liberated by viscous disk evolution in calculating the snow line location. Our model suggests that giant planets should form more frequently around these stars, because they tend to have more massive disks. This paper was published at about the same time

as Johnson et al. (2007a), which reported an increased giant planet frequency for intermediate-mass stars relative to solar and lower-mass stars.[†]

Chapter 4: Hot Super-Earths

This Chapter (Kennedy & Kenyon, 2008a) studies the results predicted for forming super Earth-mass planets over a range of stellar masses. Using analytic and numerical models, I show that Type I migration leads to an increased frequency of super-Earths in short-period orbits for lower-mass stars. I focus on planets in close-in orbits because these will be targeted by current and future transit surveys, which aim to find many Earth-like planets. I show how the frequency of these planets can be independent of stellar metallicity. I also qualitatively consider the further atmospheric evolution of these planets in close proximity to the parent star.

Chapter 5: Stellar Mass Dependent Disk Dispersal

This Chapter (Kennedy & Kenyon, 2008c, submitted to *The Astrophysical Journal* in October 2008) looks for observational evidence of different disk lifetimes for different stellar masses. These differences are important for gas giant formation, because these planets must form and migrate before the disk disperses. I find some evidence for a stellar mass dependence for intermediate-mass stars, though the statistical significance is limited by sample numbers. A simple photoevaporation model matches the observations well, much better than the null hypothesis that disk dispersal is independent of stellar mass. Stronger significance can be attained with future observations. I consider possible consequences for planet formation, suggesting that the larger orbits of planets around intermediate-mass stars may be caused by a lack of migration due to shorter disk lifetimes.

Chapter 6: Summary and Future Directions

I conclude with a summary of the achievements from Chapters 2–5 and some possible future directions.

[†]A talk by J. Johnson at the Harvard-CfA in early 2007 prompted a more detailed look at the predictions of our model for planet frequency.

CHAPTER 2

PLANET FORMATION AROUND M-DWARFS: THE MOVING SNOW LINE AND SUPER-EARTHS

Kennedy, Kenyon, & Bromley (2007)

Abstract

Planets result from a series of processes within a circumstellar disk. Evidence comes from the near planar orbits in the solar system and other planetary systems, observations of newly formed disks around young stars, and debris disks around main-sequence stars. As planet-hunting techniques improve, we approach the ability to detect systems like the solar system and place ourselves in context with planetary systems in general. Along the way, new classes of planets with unexpected characteristics are discovered. One of the most recent classes contains super Earth-mass planets orbiting a few AU from low-mass stars. In this contribution, we outline a semi-analytic model for planet formation during the pre–main-sequence contraction phase of a low-mass star. As the star contracts, the "snow line," which separates regions of rocky planet formation from regions of icy planet formation, moves inward. This process enables rapid formation of icy protoplanets that collide and merge into super-Earths before the star reaches the main sequence. The masses and orbits of these super-Earths are consistent with super-Earths detected in recent microlensing experiments.

2.1 Introduction

Planets form in circumstellar disks. The strongest evidence is contained in the nearly flat orbital structure of the solar system. The near ubiquity of infra-red excesses around young stars (Haisch et al., 2000)—starlight reprocessed by a dusty disk—argues strongly for planetary formation as a common and robust process.

The abundance of low-mass stars in the Milky Way and evidence that they harbour circumstellar disks and planets makes them potentially fruitful and important locales for planet formation. The recent microlensing discoveries of ~5–10 $M_\oplus$ planets orbiting at distances of a few AU provide additional evidence that planetary systems with planet/star mass-ratios similar to Neptune/Sun are common (Beaulieu et al., 2006; Gould et al., 2006).

The discovery of super Earth-mass planets—dubbed "super-Earths"—around low-mass stars challenges our understanding of planet formation. With orbital semi-major axes $a \sim 2$–3 AU, these planets are probably ice giants roughly similar in structure to Uranus and Neptune in the solar system.

Boss (2006b) proposes that these planets form in two stages. After gravitational instability produces a gas giant, photoevaporation of the gas giant atmosphere leaves behind an icy core with $M \sim 10$–$20\,M_\oplus$. This mechanism requires a massive disk to initiate the instability and a nearby O-type star to photoevaporate the giant planets atmosphere. Boss notes that this process should yield (i) super-Earths around M dwarfs formed in rich star clusters and (ii) gas giants around M dwarfs formed in low-mass stellar associations.

Beaulieu et al. suggest that super-Earths favour coagulation models, where collisions of 1–10 km objects eventually produce icy planets with $M \sim 10\,M_\oplus$ at 1–10 AU. Although numerical calculations appear to preclude gas giants at 1–10 AU around M dwarfs (Laughlin et al., 2004), there has been no demonstration that coagulation produces icy planets on reasonable timescales in a disk around an M dwarf.

Here we outline a semi-analytic coagulation model, which shows that contraction of the central star along a pre–main-sequence (PMS) Hayashi track sets the initial conditions for planet formation around low-mass stars. Our results indicate that icy protoplanets with $M \sim 0.1$–$1\,M_\oplus$ form in ~0.1–1 Myr at 1–4 AU. Over 50–500 Myr, collisions between protoplanets produce super-Earths with masses similar to those detected in microlensing surveys.

We start with the motivation for our study in §2.2, discuss the coagulation model of planet formation and the moving snow line in §2.3, develop the disk evolution model in §2.4, and apply the model to super-Earth formation in §2.5. We end with a brief summary in §2.6.

2.2 Motivation: Planet Formation in the Disk of a Low-Mass Star

To motivate our study, we contrast planet formation around low-mass stars and those moderately more massive that the Sun (intermediate mass stars). As intermediate mass stars approach the main-sequence, the luminosity increases. Thus, the star is not at the main-sequence luminosity when protoplanets form in the first 0.1–1 Myr. The same is also true for low mass stars. For stars with masses $\lesssim 0.5\,M_\odot$, the luminosity fades by a factor of 10–100 on the PMS track. During this evolution, the "snow line"—the point that separates the inner region of rocky planet formation from the outer region of icy planet formation—also moves inward.

Previous studies of planet formation (e.g. Ida & Lin, 2005) have used the main-sequence luminosity when setting the location of the snow line. This assumption overlooks the movement of the snow line during the PMS contraction and thus implies the snow line is too close to (far from) the central star for low-mass (intermediate-mass) stars.

Here we investigate the consequences of a moving snow line for low-mass stars and how it sets where super-Earth building blocks form.

2.3 Coagulation and the Moving Snow Line

In this section we briefly review the coagulation model of solar system formation, where planets grow from repeated collisions and mergers of small objects in a circumstellar disk of gas and dust (Safronov, 1969). Nearly all stars in sufficiently young clusters show these excesses (Haisch et al., 2000), which disappear over timescales of several million years as grains grow and the disk becomes optically thin.

To create a model disk in which planets grow, the solar system planets are augmented to solar metallicity and distributed evenly over concentric annuli. The radial profile of this "minimum mass solar nebula" (MMSN, Hayashi, 1981) is

$$\sigma(a) = \sigma_0\, a_{\rm AU}^{-3/2}\ , \tag{2.1}$$

where $\sigma_0 \sim 8\,{\rm g\ cm^{-2}}$ is the surface density in solids at 1 AU and $a_{\rm AU}$ is the radial distance from the star in units of AU. The surface density of gas follows a similar relation, increased by a factor of about 100.

An important part of the MMSN model is the snow line at ~3 AU. This distance marks where the temperature becomes low enough for ices to condense from the nebular gas and where $\gtrsim M_\oplus$ protoplanets form in the solar system.

Models of growth by coagulation commonly start with the MMSN. As the disk forms, micron-sized grains settle to the mid-plane of the disk. The settling rate depends on particle size, so grains begin to collide and stick as they settle, greatly increasing the rate of growth (Safronov, 1969). Upon reaching the mid-plane, growth continues until 1–10 km "planetesimals" form (Weidenschilling, 1980). The timescale for this growth is short—on the order of several thousand orbital periods—so repeated fragmentation is needed to explain the much longer observed disk lifetimes (Dullemond & Dominik, 2005).

Once objects reach ~km sizes, they are largely free from influence by the nebular gas (but see comments on migration below) and processes are dynamical.

The size distribution of objects evolves roughly as a power-law, with a few large objects and many more small ones. Dynamical friction from small objects damps the orbital eccentricities of the largest objects, leading to "runaway growth," where the largest objects grow much faster relative to smaller objects (Wetherill & Stewart, 1989). Throughout runaway growth, the largest protoplanets stir up the leftover planetesimals. Eventually, the leftovers have velocity dispersions comparable to the escape velocities of the largest protoplanets and runaway growth ends. The ensemble of planetesimals and protoplanets then enters "oligarchic" growth, where the largest objects—oligarchs—accrete at rates roughly independent of their size (Kokubo & Ida, 1998).

During oligarchic growth, protoplanets become isolated from their surroundings. If an oligarch accretes all of the mass in an annulus with width $2\,B\,R_{\rm H}$, where the factor $B \sim 4$ and $R_{\rm H} = a\,(M_{\rm iso}/3\,M_\star)^{1/3}$ is the Hill radius, its isolation mass is

$$M_{\rm iso} \approx 4\,\pi\,a\,B\,R_{\rm H}\,\sigma \propto (B\,\sigma)^{3/2}\,a^3\,M_\star^{-1/2}\ , \tag{2.2}$$

(e.g. Lissauer, 1993). However, both theoretical and numerical calculations show that oligarchic growth probably ends when oligarchs contain ~50% of the total mass in solids and dynamical friction from small objects no longer keeps the large objects in circular orbits (Goldreich et al., 2004; Kenyon & Bromley, 2006).

To reach isolation, protoplanets must overcome type I migration, where the object is torqued by density waves excited in the gas disk (e.g. Tanaka et al., 2002). Type I migration timescales are typically very short—of the order 10^4 yr for the Jovian core. Icy protoplanets in general may suffer similar problems. However, the extremely short timescale has lead some researchers to include other effects. A likely important effect is magnetohydrodynamic (MHD) turbulence generated by the magneto-rotational instability, a likely source of the viscosity needed to explain disk accretion onto young stars. MHD turbulence causes the migration of $\lesssim 10\,M_\oplus$ protoplanets to become a random walk in semi-major axis rather than a steady decline, resulting in diffusion during oligarchic growth (see Papaloizou et al., 2007, and references therein for a recent review).

Growth beyond isolation is different in the inner and outer planetary regions of the solar system. The boundary is marked by the snow line, where it becomes

cold enough for ices to condense from the nebular gas into solids.

In the terrestrial region, isolated protoplanets have masses $\sim 0.1\,M_\oplus$ and are rocky because volatile materials remain in the gas. In numerical models of the solar terrestrial zone, collisions and mergers of 10–20 oligarchs yield 2–5 planets with masses comparable to the mass of the Earth, on timescales of 10–100 Myr (e.g. Kenyon & Bromley, 2006). The timescale for oligarchs to merge into planets is proportional to P/σ, where P is the orbital period.

Outside the snow line, ice condensation enhances the surface density and promotes the formation of larger oligarchs. For a density $\rho \sim 1.5\,\mathrm{g\,cm^{-3}}$ and $\sigma \sim 3$–$6\,\mathrm{g\,cm^{-2}}$ at 5 AU, isolated oligarchs with $M_{\rm iso} \sim 5$–$10\,M_\oplus$ form on timescales $t_{\rm iso} \sim 1$ Myr. These icy oligarchs accrete gas directly from the nebula and grow into gas giant planets in several million years (Pollack et al., 1996).

The time to reach isolation is important for two reasons. It determines when isolation occurs during the PMS contraction of the central star and also determines whether a large protoplanet can form early enough to accrete a significant atmosphere. The timescale to reach isolation varies as (Goldreich et al., 2004)

$$t_{\rm iso} \propto \rho^{1/2}\, a^{3/2}\, \sigma^{-1/2}\ . \tag{2.3}$$

Because the timescale for planetesimal and oligarch formation is short compared to the 0.1–1 Gyr PMS contraction time (e.g. Siess et al., 2000), the timing of planetesimal formation sets the nature of icy/rocky planets with distance from a star. Just outside the moving snow line, ice condensation increases σ ($M_{\rm iso}$) by a factor of ~3 (5) using solar oxygen abundances from Asplund et al. (2005). If the planetesimal density decreases by 2–3 times, $t_{\rm iso}$ decreases by a factor of ~3.

2.4 Evolution of a Disk Around a Contracting Star

In the standard MMSN model, σ is fixed in time (e.g. Hayashi, 1981). However, as a low-mass star contracts to the main-sequence, the snow line moves inward and the surface density may change as the temperature drops below the ice condensation temperature.

To construct a model for disk evolution, we adopt

$$\sigma(t) = \sigma_0\, \eta\, f_{\rm ice}\, \frac{M_\star}{M_\odot}\, a_{\rm AU}^{-3/2} \tag{2.4}$$

where $f_{\rm ice} = 3$ is the increase in surface density applied beyond the snow line and η allows us to vary the disk mass (relative to $M_\star$). For reference, with $\eta = 1$ and $1\,M_\odot$, the disk mass $M_{\rm disk} \approx 0.025\,M_\star$ (integrated to 60 AU). To derive the snow line distance, we adopt the temperature profile of a flat circumstellar disk, $T \propto T_\star\,(R_\star/a)^{3/4}$ (Kenyon & Hartmann, 1987). Consistent with observations (e.g.

Natta et al., 2000), we scale σ and the disk mass linearly with the stellar mass. For further details, we refer the reader to Kennedy et al. (2006).

With these ingredients, we derive the evolution of $a_{\rm snow}$, σ, $M_{\rm iso}$ and $t_{\rm iso}$ as the star contracts to the main sequence using Siess et al. (2000) PMS tracks. This evolution has two main features. Initially, the snow line is at ~4 AU from the luminous PMS star. Well inside the snow line, rocky oligarchs form and reach $M_{\rm iso}$ before the star contracts significantly. At a few AU, the isolation timescale at the snow line is long compared to the initial contraction time. As the star contracts, ices condense out of the nebula and the snow line moves inward. For the inner region, this icy material coats the growing oligarchs, leftover planetesimals, and the surrounding debris with an icy veneer that may extend the oligarchic growth phase and produce more massive oligarchs. The snow line is at ~1 AU when the gas disk dissipates in 1–10 Myr. At a few AU, ice condensation reduces the isolation timescale by increasing σ and decreasing ρ.

2.5 Super-Earth Formation

To explore the consequences of this picture, we consider a $0.25\,M_\odot$ M dwarf with a disk with mass $M_{\rm disk}/M_\star = 0.063$. This disk is $\eta = 2.5$ times more massive than the $M_\star$ scaled MMSN and about half the mass of the most massive observed disks (e.g. Natta et al., 2000). Alternatively, the disk could have an increased metallicity and retain $M_{\rm disk} = 0.025\,M_\star$. Figure 2.1 shows isolation mass evolution for this system at several distances from the central star. The figure shows clear increases when the snow line crosses specific points in space and ices condense out of the gas.

Interior to $a_{\rm snow}$ at isolation ($a \lesssim$ 1–2 AU), rocky oligarchs with $M_{\rm iso} \sim 0.1\,M_\oplus$ form in $\lesssim 10^5$ yr. This time is probably somewhat limited by the disk and planetesimal formation time and not as short as equation 2.3 and the figure suggest. At 1.5 AU, continued movement of the snow line replenishes σ and enables further growth of oligarchs to $M_{\rm iso} \sim 0.3\,M_\oplus$ in several 10^5 yr. At $a \sim$ 2–3 AU, ice condensation during runaway growth promotes the formation of oligarchs with $M_{\rm iso} \sim 0.5\,M_\oplus$ in $\sim 10^5$ yr.

This analytic prescription for protoplanet growth suggests that oligarchs with $M_{\rm iso} \sim 0.1$–$0.5\,M_\oplus$ can form at ~1–3 AU in $\lesssim$ 1 Myr. The model predicts ~10 oligarchs at 1.5–4 AU. Thus, the building blocks for observable super-Earths can form on timescales much shorter than disk lifetimes derived from measurements of dust emission from low-mass PMS stars (e.g. Plavchan et al., 2005). We find it unlikely that icy protoplanets form interior to ~1 AU for $0.25\,M_\odot$ stars, in contrast to Ida & Lin (2005).

There are two main considerations for the final stages of coalescence into super-Earths. Goldreich et al. (2004) point out that interactions are more likely to lead

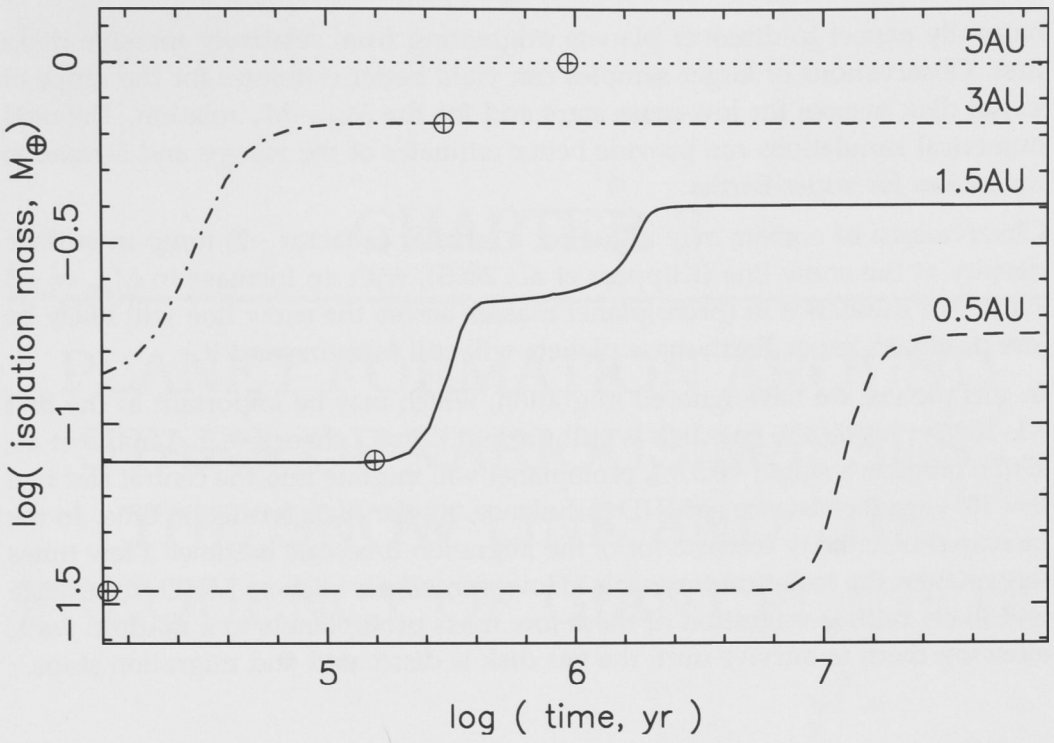

Figure 2.1 Isolation masses at fixed radii over time around a $0.25\,M_\odot$ star with $M_{\rm disk}/M_\star = 0.063$. The isolation time for each distance is marked by a ⊕. As the snow line moves inwards, ice condensation increases σ (and hence $M_{\rm iso}$), which leads to more rapid formation of more massive oligarchs. The dip in the 1.5 AU line at ~ 1 Myr is caused by deuterium burning in the star briefly stabilising the contraction.

to ejections when the escape velocity from a planet is greater than the local orbital velocity, which allows us to set planetary mass limits as a function of distance from the star. In this picture we expect to form $\sim 5\,M_\oplus$ planets at 1–2 AU, $\sim 3\,M_\oplus$ planets at 2–3 AU and 1–2 $M_\oplus$ planets at 3–4 AU. If we simply adapt the collisional history of Earth formation to a planetesimal disk around a 0.25 $M_\odot$ star, mergers of ~10 oligarchs should yield planets with masses ~1–2 $M_\oplus$ at 1 AU and ~3–5 $M_\oplus$ at 2.5 AU.

To consider whether oligarchs can merge into super-Earths on reasonable timescales, we use the scaling relation for Earth formation $t_{\rm form} \propto 10\text{–}100\,P/\sigma_0$ Myr. The expected merger timescale for oligarchs at 1–3 AU around a $0.25\,M_\odot$ star is ~2–5 times longer than for the terrestrial zone around a solar-type star. Thus, coagulation can produce super-Earths around low-mass stars on timescales of ~50–500 Myr.

The main uncertainties in our picture are the probability of the initial disk mass and the details of the final accretion stage when 1–2 $M_\oplus$ planets evolve into 3–5 $M_\oplus$ planets. Since we expect planet masses to increase with disk mass, we

naturally expect to discover planets originating from relatively massive disks first. Observations of larger samples can yield better estimates for the range of initial disk masses for low-mass stars and for the $M_{\rm disk}$–$M_\star$ relation. Detailed numerical simulations can provide better estimates of the masses and formation timescales for super-Earths.

Observations of comets may argue for a smaller (a factor ~2) jump in surface density at the snow line (Küppers et al., 2005), with an increase in $M_{\rm iso}$ of ~3. While the difference in (proto)planet masses across the snow line will likely be less dramatic, super Earth-mass planets will still form beyond it.

In this picture we have ignored migration, which may be important in the first ~1–10 Myr while the gas disk is still present. Type I theory (e.g. Tanaka et al., 2002), predicts a single $\sim 0.5\,M_\oplus$ protoplanet will migrate into the central star in a few 10^5 yr in the absence of MHD turbulence, similar to its formation time. In the increased metallicity scenario for η, the migration timescale becomes a few times longer than the isolation timescale. However, effects such as MHD turbulence will likely reduce migration of these low mass protoplanets to a random walk, allowing them to survive until the gas disk is dissipated and migration stops.

2.6 Summary

We have developed an analytic prescription for snow line evolution and planet formation by coagulation around low-mass stars and applied it to super-Earth formation around a $0.25\,M_\odot$ star. At 1–5 AU, isolated oligarchs can grow to masses ~ 0.1–$1\,M_\oplus$ in ~0.1–1 Myr, short compared to the ~ 100 Myr PMS contraction time. These oligarchs merge into super-Earths with masses ~ 2–$5\,M_\oplus$ as the star contracts to the main sequence. Thus, coagulation can produce planetary systems similar to those detected in recent microlensing events.

We acknowledge support from the *NASA Astrophysics Theory Program* through grant NAG5-13278 (SK, BB) and an Australian Postgraduate Award (GK). We thank T. Currie, M. Geller, the ANU Planetary Science Institute planet group for helpful comments on the project. We thank the referee Pawel Artymowicz for a thorough review of the manuscript.

CHAPTER 3

PLANET FORMATION AROUND STARS OF VARIOUS MASSES: THE SNOW LINE AND THE FREQUENCY OF GIANT PLANETS

Kennedy & Kenyon (2008b)

Abstract

We use a semi-analytic circumstellar disk model that considers movement of the snow line through evolution of accretion and the central star to investigate how gas giant frequency changes with stellar mass. The snow line distance changes weakly with stellar mass; thus giant planets form over a wide range of spectral types. The probability that a given star has at least one gas giant increases linearly with stellar mass from $0.4\,M_{\odot}$ to $3\,M_{\odot}$. Stars more massive than $3\,M_{\odot}$ evolve quickly to the main-sequence, which pushes the snow line to 10–15 AU before protoplanets form and limits the range of disk masses that form giant planet cores. If the frequency of gas giants around solar-mass stars is 6%, we predict occurrence rates of 1% for $0.4\,M_{\odot}$ stars and 10% for $1.5\,M_{\odot}$ stars. This result is largely insensitive to our assumed model parameters. Finally, the movement of the snow line as stars $\gtrsim 2.5\,M_{\odot}$ move to the main-sequence may allow the ocean planets suggested by Léger et al. to form without migration.

3.1 Introduction

In the last ten years, the discovery of more than 200 extra-solar planets,[1] and more than 200 debris disks,[2] suggests that planet formation is a common and robust process. Planet masses inferred from debris disks range from terrestrial to Jovian, at distances as great as tens of AU from the central star (e.g. Kenyon & Bromley, 2004a; Greaves et al., 2005). The nature and sensitivity of radial velocity surveys means that most of the planets are ~Jupiter mass gas giants in close orbits around Sun-like stars. However, recent discoveries as diverse as icy ~Neptune-mass planets orbiting M dwarfs (e.g. Rivera et al., 2005), and debris disks around A-type stars (e.g. Rieke et al., 2005) show that planet formation occurs over a wide range of spectral types.

Current theory suggests that planets form in similar ways around all stars. Thus, the increasing diversity of stellar hosts and planetary systems provides an opportunity to test these theories. For this reason, the types of planets most likely to form around stars of differing spectral types has become a renewed area of study (e.g. Ida & Lin, 2005; Boss, 2006a; Kornet et al., 2006; Kennedy et al., 2006), after the idea was first explored by Nakano nearly 20 years ago (Nakano, 1987, 1988a,b).

Theories of solar system formation generally include the "snow line," where ices condense from the nebular gas. The snow line distance is usually fixed in a disk with a time independent surface density and temperature profile around a main-sequence star (e.g. Ida & Lin, 2005). In a more realistic picture, the disk and stellar properties evolve considerably during the 1–10 Myr pre–main-sequence (PMS) lifetime when planets probably form (e.g. Lissauer, 1987; Pollack et al., 1996). As the disk temperature evolves with time, movement of the snow line may therefore influence the properties of theoretical planetary systems (e.g. Kennedy et al., 2006; Garaud & Lin, 2007).

Here, we begin to develop a time dependent model for the formation of gas giant cores that considers the PMS evolution of the star and surrounding accretion disk. We introduce a simple semi-analytic disk model, based on the "minimum mass solar nebula," that links movement of the snow line through evolution of disk accretion and stellar luminosity. In contrast to previous studies (e.g. Ida & Lin, 2005; Kornet et al., 2006), our analysis suggests that gas giant formation around stars more massive than the Sun is more likely than around less massive stars.

We cover the background important to our story in §3.2, consider the snow line in §3.3, and outline our model in §3.4. We present our results in §3.5, and discuss and conclude in §3.6 and §3.7.

[1] http:exoplanet.eu

[2] http://www.roe.ac.uk/ukatc/research/topics/dust/identification.html

3.2 Background

Planetary systems form in circumstellar disks, which evolve on timescales comparable to the pre–main-sequence (PMS) stage of stellar evolution. Observations indicate a wide range of disk masses $M_{\rm disk} \sim 0.01$—$0.1\,M_\star$ (where $M_\star$ is the stellar mass, e.g. Osterloh & Beckwith, 1995; Natta et al., 2000; Andrews & Williams, 2005; Eisner & Carpenter, 2006; Scholz et al., 2006) and radii ~100–1000 AU (McCaughrean & O'Dell, 1996). The lifetime of the primordial, optically thick, dusty component of the disk is $\lesssim$10 Myr, with a median timescale of ~3 Myr (e.g. Strom et al., 1993; Haisch et al., 2001b). Though harder to observe, the gaseous component of the disk is probably removed by viscous accretion (Lynden-Bell & Pringle, 1974) and photoevaporation (e.g. Hollenbach et al., 2000; Adams et al., 2004; Alexander et al., 2006) on similar timescales (Zuckerman et al., 1995; Pascucci et al., 2006).

These timescales place strict observational limits on the important stages of planet formation. Planetesimals must form rapidly to enable further grain growth and protoplanet formation by coagulation (e.g. Safronov, 1969). To attract significant atmospheres and form gas giants, protoplanets need to reach masses of 5-10 $M_\oplus$ (e.g. Pollack et al., 1996; Ikoma et al., 2000) before the nebular gas is removed.

In coagulation models, dust particles on near circular orbits with small relative velocities grow through repeated collisions and mergers in circumstellar disks. Further dynamical evolution through "runaway" (Wetherill & Stewart, 1989; Kokubo & Ida, 1996) and "oligarchic" (Kokubo & Ida, 1998) growth leads to "isolated" protoplanets, whose mass $M_{\rm iso}$ and spacing depend on their radial distance a from the central star via the Hill radius $R_{\rm H} = a\,(M_{\rm iso}/3M_\star)^{1/3}$ (e.g. Lissauer, 1987; Lissauer & Stevenson, 2007)

$$M_{\rm iso} = \frac{(4\,\pi\,B\,\sigma\,a^2\,)^{3/2}}{(3\,M_\star)^{1/2}}\,, \tag{3.1}$$

where σ is the disk surface density. Protoplanets are spaced at $2\,B\,R_{\rm H} \sim 8\,R_{\rm H}$ intervals (Kokubo & Ida, 1998). Used in combination with equation (3.1), the "minimum mass solar nebula" (MMSN, Weidenschilling, 1977b; Hayashi, 1981) with $\sigma \propto a^{-\delta}$ (where δ = 1–1.5), gives a simple model of protoplanet formation.

The "snow line"—the point in the disk that separates the inner region of rocky planet formation from the outer region of icy planet formation—is an important feature of the MMSN (e.g. Sasselov & Lecar, 2000; Ida & Lin, 2005; Ciesla & Cuzzi, 2006). Condensation of ices outside the snow line increases the disk surface density by a factor $f_{\rm ice} \sim 3$,[3] which leads to factor of 5 larger isolation masses (eq. 3.1). In an MMSN model with $\sigma = 10$ g cm^{-2} at 1 AU and $\delta = 3/2$,

[3]The usual value is ~4, but recent solar abundance figures for oxygen (Asplund et al., 2005) indicate 3 is more reasonable. Recent composition data from 9P/Tempel 1 may argue for an even lower ice/rock ratio (Küppers et al., 2005).

$M_{iso} \approx 0.1\ (1)\ M_\oplus$ at 1 (5) AU. To achieve the probable core mass of 5–10 $M_\oplus$ for Jupiter (Saumon & Guillot, 2004) the MMSN can be augmented beyond the snow line by a factor ~4. Alternatively, if $\delta = 1$ then $M_{iso} \approx 5 M_\oplus$ at 5 AU. Models that relax the assumption of a smooth radial profile find an enhanced surface density near the snow line (e.g. Cuzzi & Zahnle, 2004; Ciesla & Cuzzi, 2006). A common theme among both MMSN and more detailed models is the surface density added by ice condensation.

Because the timescale for planet growth is $t \propto P/\sigma \propto a^3$ for $\sigma \propto a^{-3/2}$, where P is the orbital period (e.g. Lissauer, 1987, see also Goldreich et al. (2004)), ice condensation also leads to shorter growth times. Numerical simulations by Kenyon & Bromley (2004a,b) find the time to form 1000–3000 km objects agrees with this relation. Numerical estimates of the time to form the Jovian core range from ~10^5–10^6 yr (e.g. Lissauer, 1987; Pollack et al., 1996; Inaba et al., 2003; Chambers, 2006b). In general, the time to reach isolation t_{iso} provides an estimate of whether protoplanets form early enough to accrete gas and become giant planets. Short gas disk lifetimes (e.g. Zuckerman et al., 1995; Pascucci et al., 2006), imply a relatively short isolation time and place strong constraints on the time to form gas giants by core accretion.

Gas giant formation by core accretion occurs when protoplanet core masses are sufficient to attract gas from the nebula. The core mass sets the timescale for gas giant formation (Ikoma et al., 2000; Hubickyj et al., 2005). Cores with masses smaller than ~5 $M_\oplus$ attract atmospheres (e.g. Inaba & Ikoma, 2003), but are unable to form a gas giant before the nebular gas is removed on timescales of 1–10 Myr. Beyond the snow line the critical core mass where significant gas accretion occurs is $M_{crit} \sim 7 M_\oplus \dot{M}_{core}^{0.25} \kappa^{0.25}$ (where $\dot{M}_{core}$ is the rate at which planetesimals are accreted onto the core in units of $10^{-7} M_\oplus$ yr^{-1} and κ is the grain opacity in units of cm^2 g^{-1}, Ikoma et al., 2000, see also Rafikov (2006)). The critical core mass required to form Jupiter in several Myr ($M_{iso} \sim$ 5–10 $M_\oplus$, Pollack et al., 1996; Hubickyj et al., 2005)—which implies $\sigma \sim 10$ g cm^2 at 5 AU—is consistent with the core mass inferred from current structural models (e.g. Saumon & Guillot, 2004).

3.2.1 Previous Work

Most planet formation theories are based on a static MMSN disk around a solar-mass star. There are several motivating factors for extending these theories to a range of stellar masses: (1) the increasing stellar mass range of extra-solar planet hosts, (2) observed trends with stellar mass, such as accretion rate and disk mass, and (3) theoretical relations with variables that change with stellar mass, such as orbital period and isolation mass. This extension of solar system theory to a range of spectral types began with a series of papers by Nakano nearly twenty years ago (Nakano, 1987, 1988a,b). More recently, Kornet et al.

(2006) considered formation of planets around stars of various masses *in situ*, while Ida & Lin (2005) examined observable planetary systems resulting from type II migration.

Kornet et al. consider disk evolution prior to the growth of large objects. In their models, the increased inward migration rate for planetesimals around low-mass stars results in higher absolute surface densities from 0.1–100 AU at 1 Myr. Thus low-mass stars are more likely to form giant planets. This result is influenced by their choice of an approximately constant initial disk mass for all stellar masses. They do not consider planet formation beyond 5 AU.

Ida & Lin base their Monte-Carlo study on the MMSN. Type II migration—where a planet with sufficient mass opens a gap in the disk and whose orbit is subsequently coupled to the viscous evolution of the disk (e.g. Lin & Papaloizou, 1985)—is central to their model. In their attempt to reproduce the observed distribution of extra-solar planets, they find that close-in icy Neptune-mass planets should be much more common than close-in Jupiter-mass planets around M dwarf stars (see also Laughlin et al., 2004). In contrast to the Kornet et al. study, they find that the likelihood of a star harbouring gas giants increases with stellar mass up to solar-mass stars. Their results are influenced by scaling the snow line distance as $a_{\rm snow} \propto M_\star^2$, based on the main-sequence luminosity $L_\star \propto M_\star^4$. As we show below, this simplification places the snow line too close to (far from) the central star for stars with masses less than (greater than) a solar mass when protoplanets form.

In this paper we consider movement of the snow line as disk accretion subsides and the central star evolves to the main-sequence. Using our prescription for the snow line position over a range of stellar and disk masses, we locate regions where gas giant cores form. Assuming stars are born with disks from a distribution of masses, we then predict how gas giant frequency varies with stellar mass.

3.3 Location of the Snow Line

In this section we consider evolution of the disk mid-plane temperature and the snow line distance, with a simple model that includes accretion and PMS evolution. In particular, we are interested in the stellar mass dependence, rather than a detailed derivation for a single star. As we show in §3.5, ~1 AU differences between our model and more detailed treatments (e.g. Sasselov & Lecar, 2000; Lecar et al., 2006) do not affect our conclusions.

The disk mid-plane, where the gas density is highest, is probably where most ices condense and has a temperature

$$T_{\rm mid}^4 = T_{\rm mid,accr}^4 + T_{\rm irr}^4, \tag{3.2}$$

where $T_{\rm mid,accr}$ is the mid-plane temperature arising from viscous forces within the disk and $T_{\rm irr}$ is temperature due to external irradiation of the disk by the central star.

The effective disk temperature from viscous accretion is (Lynden-Bell & Pringle, 1974)

$$T^4_{\rm eff,accr} = \frac{3}{8\pi}\frac{GM_\star \dot{M}}{\sigma_{\rm sb} a^3}\left(1 - \sqrt{\frac{R_\star}{a}}\right), \tag{3.3}$$

where $\dot{M}$ is the accretion rate, $R_\star$ is the stellar radius, and $\sigma_{\rm sb}$ is Stefan's constant. In optically thick regions near the snow line, the mid-plane temperature is $T^4_{\rm mid,accr} \sim 3\tau T^4_{\rm eff,accr}/8$ (Hubeny, 1990), where $\tau = \kappa\sigma_g/2$. The opacity κ is a function of temperature (Bell & Lin, 1994) and the gas surface density σ_g is 100 times greater than that of solids. The figure of 100 is used in converting mm dust observations to total disk masses (e.g. Natta et al., 2000) based on the interstellar gas/dust ratio and is similar to the solar metallicity (Z) fraction of 0.0122 (Asplund et al., 2005). The accretion rate varies with stellar mass as approximately $\dot{M} \propto M_\star$ for the range of stellar masses we consider (0.2–4 $M_\star$, Muzerolle et al., 2003) and with time as $\dot{M} \propto (t/10^6\,{\rm yr})^{-\gamma}$. Hartmann et al. (1998) derive γ = 1.5–2.8. The uncertainty is due to the limited age range of their sample and a large range of accretion rates at a given age. The value γ = 1.5 is their "preferred result." We scale $\dot{M}$ with surface density, which accounts for the observed trend with stellar mass (if disk mass scales linearly with stellar mass, see §3.4) and is consistent with expected viscous evolution (where $\dot{M} \propto \nu\sigma$ and ν is the disk viscosity). For ~1 Myr old solar-type stars $\dot{M} \sim 10^{-8}\,M_\odot$ yr^{-1} (Hartmann et al., 1998). We set $\dot{M} = 10^{-8}\,M_\odot$ yr^{-1} for an initially three-fold enhanced MMSN disk, as this disk decays to the "typical" observed ~MMSN mass disk by ~1 Myr (Hartmann et al., 1998).

A more complete treatment of the optical depth to the mid-plane would include evolution of the gas surface density, allowing the mid-plane temperature to drop somewhat faster than described above as σ_g decreases in the inner disk (Lynden-Bell & Pringle, 1974). The solid surface density, which largely resides near the mid-plane and determines protoplanet characteristics, remains largely unaffected by the gas disk evolution (aside from snow line evolution).

The disk temperature contribution from irradiation is

$$T_{\rm irr} = T_\star \left(\frac{\alpha}{2}\right)^{1/4}\left(\frac{R_\star}{a}\right)^{3/4}, \tag{3.4}$$

where $\alpha \approx 0.005/a_{\rm AU} + 0.05\,a_{\rm AU}^{2/7}$ for a flared disk in vertical hydrostatic equilibrium (e.g. Adams & Shu, 1986; Kenyon & Hartmann, 1987; Chiang & Goldreich, 1997). Here $a_{\rm AU}$ is a in units of AU. When the disk is optically thick to radiation at this temperature, $T_{\rm irr}$ is approximately the interior temperature for a flared disk (Chiang & Goldreich, 1997).

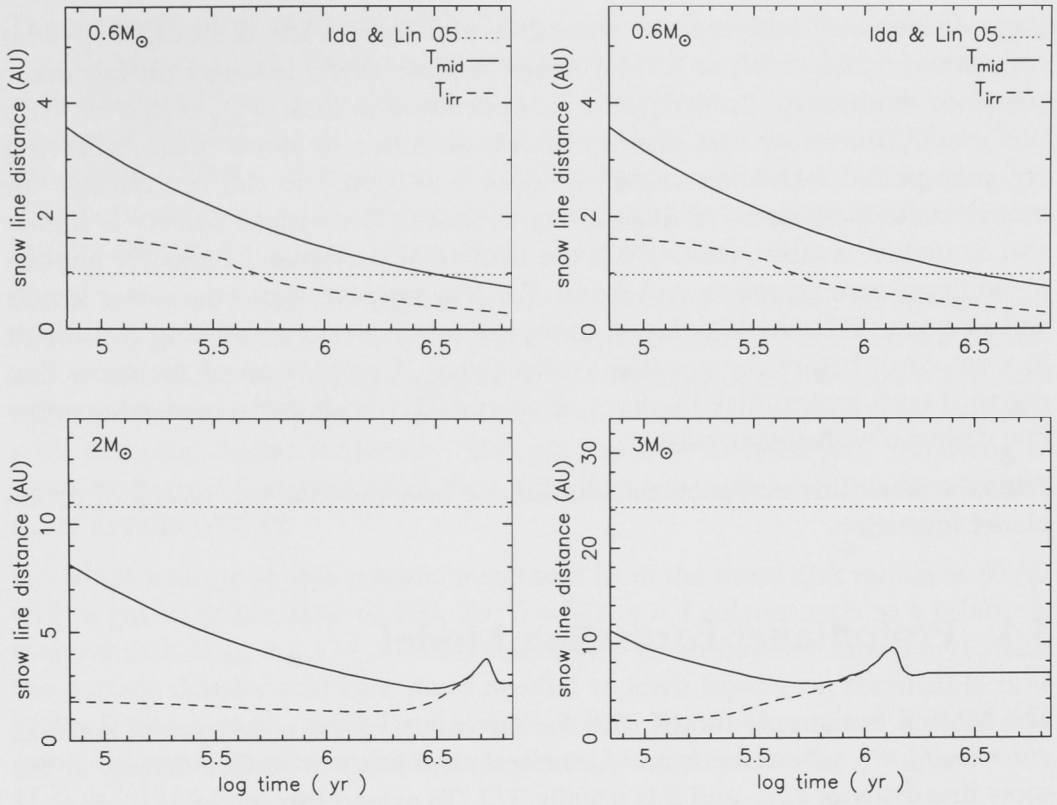

Figure 3.1 Location of the snow line (a at $T_{\rm mid} = 170\,{\rm K}$) over time for 0.6, 1, 2, and $3\,M_\odot$ stars (*left to right, and down*) with irradiation only (using Palla & Stahler (1999) PMS tracks, *dashed line*) and irradiation + accretion (*solid line*). The disks have surface densities $\sigma = \sigma_{\rm MMSN}\, M_\star/M_\odot$. Included for reference is $a_{\rm snow} = 2.7\, M_\star/M_\odot$ AU as used by Ida & Lin (2005) (*dotted line*).

Figure 3.1 shows the location of the snow line in disks with $\sigma = \sigma_{\rm MMSN}\, M_\star/M_\odot$ for several different stellar masses over time for irradiation only, and for accretion + irradiation. We locate the snow line where $T_{\rm mid} = 170\,{\rm K}$. More detailed derivations of this temperature (e.g. Podolak & Zucker, 2004; Lecar et al., 2006) do not change the snow line distance significantly. For PMS stellar properties we use Palla & Stahler (1999) tracks. For comparison, we also show the (fixed) snow line distance for stars on the main-sequence (e.g. Ida & Lin, 2005).

Looking first at the solar case, the snow line moves inward over time. This movement is always determined by viscous accretion and its decay over time. Our snow line crosses the "canonical" distance of 2.7 AU at 5×10^5 yr. For disks with accretion rates so low that irradiation dominates, the snow line still moves inward over time, as illustrated by the dashed line for $T_{\rm irr}$.

For more massive stars, $T_{\rm irr}$ begins to dominate as accretion subsides and the star quickly evolves to a significantly greater main-sequence luminosity. Irradiation becomes important at a few Myr for $2\,M_\odot$ stars and ~1 Myr for $3\,M_\odot$ stars. The

large discrepancy between our snow line and that of Ida & Lin (2005) (who considered $0.2\,M_\odot < M_\star < 1.5\,M_\odot$) arises because theirs is based on the main-sequence luminosity ($L_\star \propto M_\star^4$) and an optically thin disk ($T_{\rm disk}^4 \propto L_\star\, a^{-2}$). With our model, the snow line distance is less sensitive to stellar mass, allowing icy protoplanet formation relatively close (~5–10 AU) to the central star for intermediate mass stars. At these closer distances, the surface density is higher and formation is faster, making it more likely that protoplanets massive enough to undergo core accretion will form. For less massive stars, the snow line is still at a few AU, where isolation times are relatively long, making it difficult to form cores before the gas disk is dissipated. Comparison of the snow line distance with typical disk lifetimes of several Myr leads to an increasing snow line distance with stellar mass.

With the snow line evolution established, we now describe our model of protoplanet formation.

3.4 Protoplanet Formation Model

The MMSN is a simple model disk for the origin of the solar system and has $\sigma(a) = \sigma_0\, f_{\rm ice}\, a^{-\delta}$, where the factor $f_{\rm ice}$ represents a jump in surface density at the snow line distance $a_{\rm snow}$ and δ is usually 3/2. To extend this model to a range of stellar masses requires consideration of how disk mass varies with stellar mass. Observations indicate $M_{\rm disk} \propto M_\star$ (Natta et al., 2000; Scholz et al., 2006); however, there is a wide range of disk masses at any given stellar mass. Thus, to extend the MMSN model to a range of stellar and disk masses, we adopt the surface density relation

$$\sigma(a,t) = \sigma_0\, \eta\, f_{\rm ice}\, \frac{M\star}{M_\odot}\, a_{\rm AU}^{-\delta}\,, \tag{3.5}$$

where $\sigma_0 = 10\,{\rm g\ cm^{-2}}$. The factor η changes the disk mass relative to the star ("relative disk mass") and is varied to account for the observed range of disk masses at fixed stellar mass. Current observations suggest $\eta \sim 0.5$–5 ($M_{\rm disk} = 0.01$–$0.1\,M_\star$); $\eta \sim 10$ is the upper limit for disk stability ($M_{\rm disk} \sim 0.25\,M_\star$). To provide a smooth transition from $f_{\rm ice} = 1$ for $a \lesssim a_{\rm snow}$ to $f_{\rm ice} = 3$ for $a \gtrsim a_{\rm snow}$, we set $f_{\rm ice} = 1 + (\Delta_{\rm ice} - 1)/(1 + e^x)$ where $\Delta_{\rm ice} = 3$, $x = (a_{\rm snow} - a)/\Delta a_{\rm snow}$ and $\Delta a_{\rm snow}$ is the radial distance equivalent to a 5 K temperature change.

Combined with the local orbital period, the surface density sets the time to form protoplanets and sets whether protoplanets form early enough to accrete gas and become gas giants. We introduce a stellar mass dependence, so our isolation timescale, based on numerical simulations by Kenyon & Bromley (2004a,b), becomes

$$t_{\rm iso} \propto (\eta\,\sigma)^{-1}\, a^{3/2}\, M_\star^{-1/2}\,. \tag{3.6}$$

The normalisation of equation (3.6) depends on the size of the small objects (e.g. Goldreich et al., 2004; Chambers, 2006b). We use 10^5 yr for $\sigma = 10\,\mathrm{g\ cm^{-2}}$ at 5 AU, based on the likelihood of small fragmented bodies to accrete (e.g. Kenyon & Bromley, 2004a) and the consequent short growth times (Rafikov, 2004; Chambers, 2006b). Hubickyj et al. (2005) infer $t_{\rm iso} \lesssim 5{\times}10^5$ yr for much larger 100 km planetesimals. As long as the Jovian timescale is somewhat shorter than the gas disk lifetime, this choice affects our results little.

Under the assumption that stars all form disks in $\sim 10^5$ yr (based on an infall rate of $10^{-5}\,M_\odot\ \mathrm{yr}^{-1}$, Palla & Stahler, 1999) and that planetesimal formation is relatively fast (Weidenschilling, 2000; Dullemond & Dominik, 2005), we add a constant offset of 10^5 yr to the isolation timescale to reconcile the timing of isolation with disk and stellar evolution. Though this time is uncertain, removing or moderately modifying the offset does not affect our results significantly because $t_{\rm iso}$ is usually $\gtrsim 10^5$ yr.

We adopt a range of disk masses, integrated from the inner disk radius to 60 AU, with a gas to solids ratio of 100. For $\delta = 3/2$, $\eta = 4$ corresponds to a relatively massive disk $M_{\rm disk} = 0.1\,M_\star$. This enhancement is our baseline model and yields the surface density and core mass needed to form Jupiter on reasonable time scales (Pollack et al., 1996; Ikoma et al., 2000). For $\delta = 1$, smaller η yields the same disk mass because more mass is placed at larger radii. For $\eta = 1$ and $\delta = 1$, $M_{\rm disk} = 0.12\,M_\star$.

3.5 Regions that Form Gas Giant Cores

The successful formation of a gas giant planet by core accretion requires satisfaction of two main conditions. A core must form while the gaseous component of the circumstellar disk is still present and it must be massive enough to attract a large atmosphere before this gas is dispersed. Prior to isolation, accreted planetesimals and a sub-critical protoplanet mass limit gas accretion. After isolation, if a protoplanet is massive enough and forms while the gas disk is still present, significant gas accretion proceeds. This separation into two classes, gas giants and "failed cores," reflects the expected paucity of 20–100 $M_\oplus$ planets over a range of stellar masses (Ida & Lin, 2005).

To form a gas giant in less than 10^7 yr, various studies suggest a minimum core mass of 5–10 $M_\oplus$ (Ikoma et al., 2000; Inaba et al., 2003; Hubickyj et al., 2005). Although the core mass depends on the planetesimal accretion rate and the opacity, the derived sensitivity is weak ($M_{\rm core} \propto \dot{M}^{0.25}$; Ikoma et al., 2000, see also Rafikov (2006)). A limited reservoir of planetesimals to accrete after isolation means high accretion rates cannot be sustained (and $\dot{M}$ will decrease), while low accretion rates lower $M_{\rm core}$. Thus, we adopt a minimum core mass $M_{\rm core} = 10\,M_\oplus$ as a baseline and consider $M_{\rm core} = 5\,M_\oplus$ in §3.5.4.

The timescale for gas dissipation sets our second restriction. The gaseous component of the disk disperses in $\lesssim$10 Myr (Zuckerman et al., 1995; Pascucci et al., 2006). With $\dot{M} \propto \sigma$, the dissipation timescale for a viscous disk $t_d \propto M_{\rm disk}/\dot{M} \sim$ constant for our assumptions. Because the disk mass decreases significantly (~60%) in 1 Myr, we adopt $t_{\rm core}$ = 1 Myr as a typical maximum core formation time for all disks. Henceforth we reserve the word "core" for a protoplanet with $M_{\rm iso} > M_{\rm core}$ and $t_{\rm iso} < t_{\rm core}$. Relatively little is known about the evolution of the gaseous component of the disk; we comment further on the consequences of varying $t_{\rm core}$ and other parameters in §3.5.4.

To investigate locations within circumstellar disks where gas giant cores form, we first derive results for a $1\,M_\odot$ star and then consider a range of stellar masses. We restrict our study to stars with masses 0.2–4 $M_\odot$. For stars with masses <0.2 $M_\odot$ our model does not form gas giants. The short main-sequence lifetime of massive stars ($M_\star > 4\,M_\odot$) makes them much less likely targets for planet detection. Some oligarchs do not reach masses sufficient for core accretion. Those cores that do form compete with other cores for dynamical space in the disk. We defer consideration of these objects to §3.5.3.

3.5.1 The Solar Example

In this subsection we show how the MMSN disk model, the moving snow line, and the isolation mass and time combine to give a picture of the solar system structure at ~1 Myr.

Figure 3.2 shows isolation masses for the MMSN model beyond the snow line with $\eta = 4$, as a function of time and radial distance from the Sun. The isolation mass and timescale are calculated from the equations described in §3.4. Accretion and PMS tracks from Palla & Stahler (1999) set $a_{\rm snow}$ as described in §3.3.

When the first objects reach isolation, the Sun is in the early stages of its PMS contraction and the accretion rate is $\sim 10^{-7}\,M_\odot$ yr^{-1}. Consequently the snow line is at ~6 AU, which determines where the innermost icy protoplanet forms. This protoplanet is massive enough to become a gas giant (a core), so we refer to this position as the inner edge of the core-forming region. In the absence of significant migration from disk interaction, this result may help explain why Jupiter is at 5 AU. As the Sun continues to contract and accretion decreases, isolation is reached at ever increasing distances beyond the snow line. Eventually, the isolation time becomes longer than $t_{\rm core}$ and protoplanets form too late to undergo core accretion. Isolation masses increase with distance from the Sun, so $t_{\rm core}$ always sets the outer edge of the core-forming region and the number of cores that form. If the cores are spaced by $8\,R_{\rm H}$ at isolation (as in Figure 3.2), then ~4 cores form in this region and the region extends from ~6–11 AU, similar to the region containing Jupiter and Saturn today.

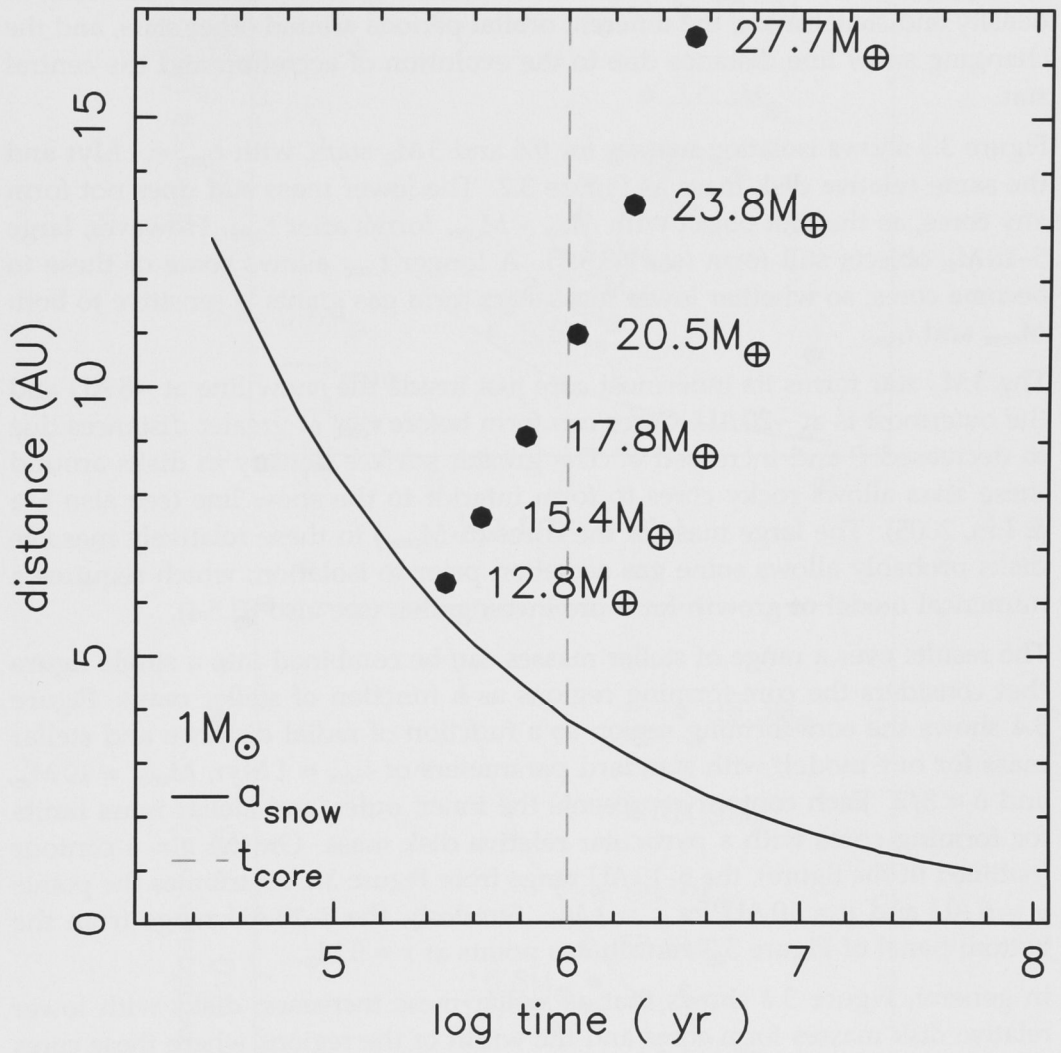

Figure 3.2 Isolation mass (*filled circles*, labelled with $M_{\rm iso}$) as a function of radial distance and PMS model time, for a solar mass star with the MMSN model with $\eta = 4$ and $\delta = 3/2$. Masses are spaced at $8\,R_{\rm H}$ intervals and only shown outside the snow line. The solid line shows $a_{\rm snow}$ over time and the dashed vertical line is the time $t_{\rm core} = 1\,$Myr.

3.5.2 A Range of Stellar Masses

We now consider how the core-forming region for a solar mass star changes with stellar mass between $0.2\,M_\odot$ and $4\,M_\odot$. The processes described in §3.5.1 still apply, but differences arise due to the linear relation between disk surface density and stellar mass, the different orbital periods around other stars, and the changing snow line distance due to the evolution of accretion and the central star.

Figure 3.3 shows isolation masses for 0.6 and $3\,M_\odot$ stars, with $t_{\rm core} = 1\,$Myr and the same relative disk mass as Figure 3.2. The lower mass star does not form any cores, as the first object with $M_{\rm iso} > M_{\rm core}$ forms after $t_{\rm core}$. However, large 5–$10\,M_\oplus$ objects still form (see §3.5.3). A longer $t_{\rm core}$ allows some of these to become cores, so whether lower mass stars form gas giants is sensitive to both $M_{\rm core}$ and $t_{\rm core}$.

The $3\,M_\odot$ star forms its innermost core just inside the snow line at ~8 AU and the outermost is at ~20 AU. Cores can form before $t_{\rm core}$ at greater distances due to decreased P and increased σ. The greater surface density in disks around these stars allows rocky cores to form interior to the snow line (see also Ida & Lin, 2005). The large mass of the cores ($\gg M_{\rm core}$) in these relatively massive disks probably allows some gas accretion prior to isolation, which requires a numerical model of growth for more investigation (see also §3.5.4).

The results over a range of stellar masses can be combined into a single figure that considers the core-forming regions as a function of stellar mass. Figure 3.4 shows the core-forming region as a function of radial distance and stellar mass for our model, with standard parameters of $t_{\rm core} = 1\,$Myr, $M_{\rm core} = 10\,M_\oplus$, and $\delta = 3/2$. Each contour represents the inner, outer, and stellar mass limits for forming cores with a particular relative disk mass. On the $\eta = 4$ contour (outlined in the figure), the 6–10 AU range from Figure 3.2 contributes the points $y = 6\,$AU and $y = 10\,$AU for $x = 1\,M_\odot$. Similarly, the 8–20 AU range from the bottom panel of Figure 3.3 contributes points at $x = 3\,M_\odot$.

In general, Figure 3.4 shows that as stellar mass increases, disks with lower relative disk masses form cores and the width of the regions where these cores form increases. Stars more massive than $\sim 1.2\,M_\odot$ form rocky cores interior to the snow line for relatively high disk masses. The core-forming region expands outward with increasing relative disk mass because the isolation timescale becomes shorter. Doubling the disk mass allows a to increase by a factor of ~1.6 to keep the same $t_{\rm iso}$ (eq. 3.6).

As stellar mass increases, cores form in disks with decreasing relative disk mass. As η decreases, the inner edge of the core-forming region moves inward, because the accretion rate is lower and the disk has lower optical depth (so the mid-plane is cooler) and the snow line has evolved closer to the star by the time isolation

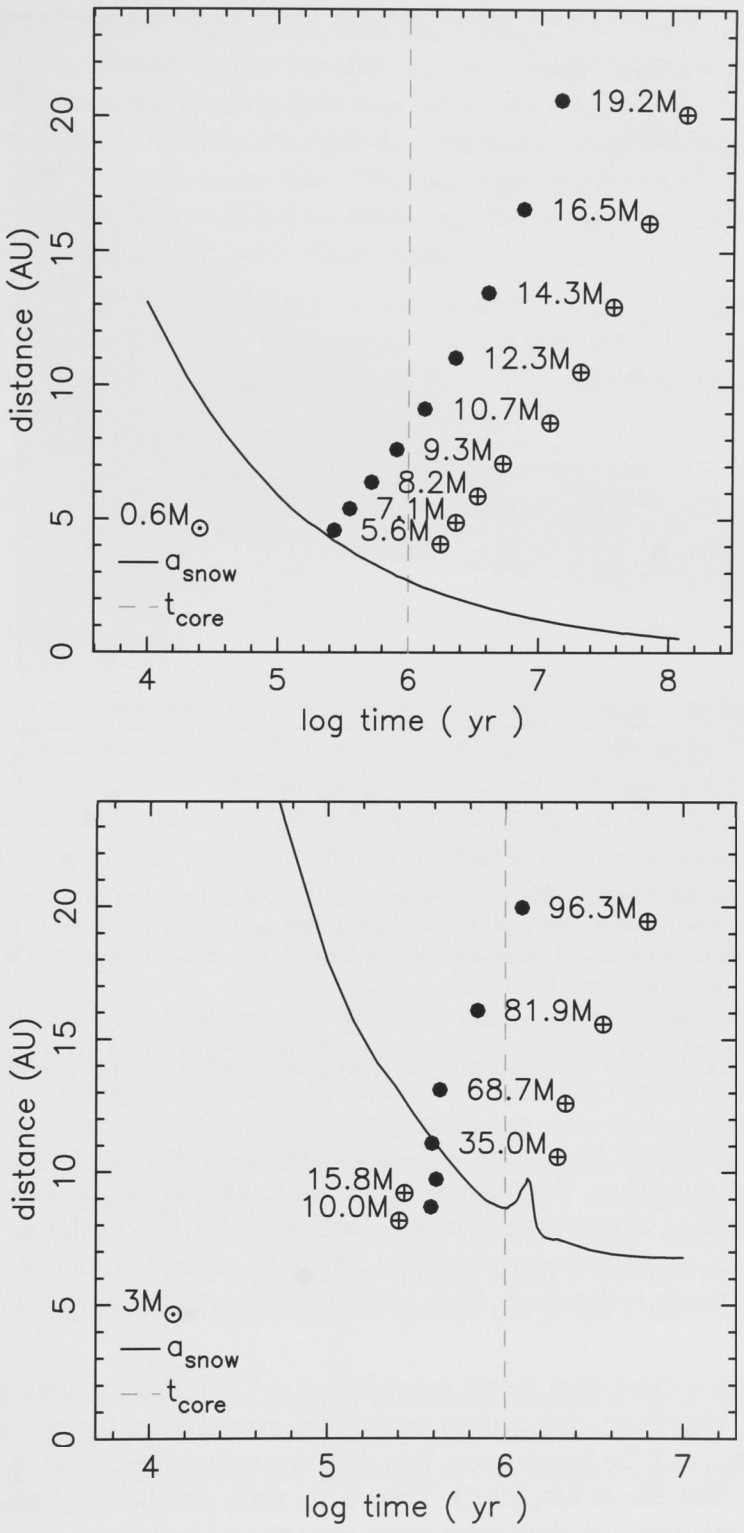

Figure 3.3 Same as Figure 3.2, but for $0.6\,M_\odot$ (*top*) and $3\,M_\odot$ (*bottom*). Isolation masses are only plotted outside the snow line, or where $M_{\rm iso} > M_{\rm core}$.

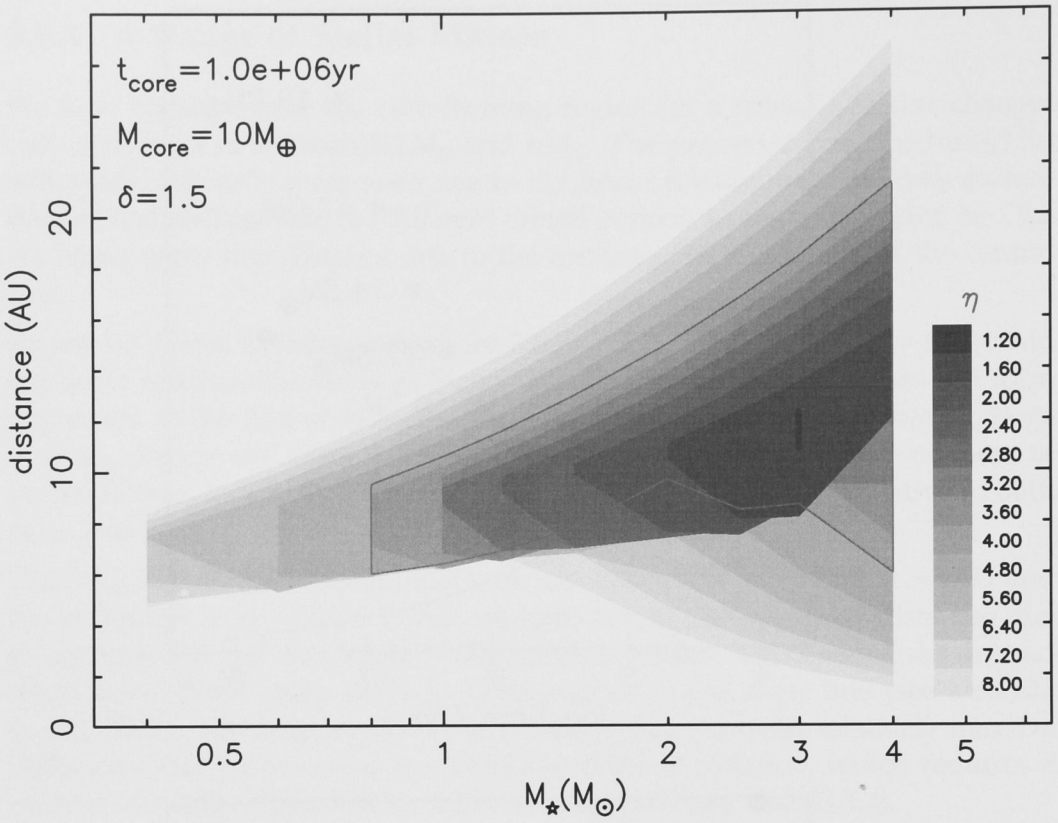

Figure 3.4 Regions where $10\,M_\oplus$ cores form in $\leq 10^6$ yr as a function of radial distance and stellar mass. Each contour represents the inner, outer, and stellar mass limits for a particular η (and corresponding $M_{\rm disk}$), as shown by the legend. Our baseline model, $\eta = 4$ is outlined. For $\eta = 1.2$, only $3\,M_\odot$ stars form cores.

is reached. The snow line is roughly the lower edge of the darker (lower η) contours.

If $M_{\rm iso}$ does not jump to a value >$M_{\rm core}$ due to $f_{\rm ice}$ at the snow line, a core still forms further out. Thus, the inner edge moves to greater distances as the stellar mass—and hence absolute disk mass—decreases for fixed relative disk mass. However, the $t_{\rm core}$ restriction means that oligarchs around sufficiently low-mass stars do not reach isolation in time and that all contours have a lower stellar mass limit.

The lowest disk mass that forms cores has $\eta = 1.2$ and only does so for $3\,M_\odot$. For more massive stars, irradiation overcomes accretion as the star reaches the main-sequence and the larger snow line distance makes formation of cores more difficult (see also Ida & Lin, 2005). Thus $3\,M_\odot$ stars are the most likely to form at least one gas giant, as they form cores over the widest range of disk masses.

The width of the regions where cores form increases with stellar mass (Figure 3.4, Ida & Lin, 2005). The spacing of cores remains roughly constant with different

stellar mass ($M_{\rm iso} \propto \sigma^{3/2}/\sqrt{M_\star} \propto M_\star$ and $R_{\rm H} \propto (M_{\rm iso}/M_\star)^{1/3}$ for $\delta = 3/2$, see also Figs. 3.2 & 3.3). However, the number of cores is not linearly related to the region width, since the spacing becomes wider with increasing distance. The width of the regions depends strongly on disk mass, particularly for disks that form cores interior to the snow line. The increasing width of the core-forming regions suggests that the number of cores (and therefore planets) in individual planetary systems increases with stellar mass.

To summarise, the range of relative disk masses that form gas giant cores increases with stellar mass, as does the width of the regions they form in. The first result leads to the expectation that the likelihood of forming gas giants increases with stellar mass. We make a quantitative prediction in §3.6.1.

While the core-forming regions are our primary interest, there are large regions of parameter space where oligarchs are relatively massive, but will not form gas giants. We consider these planets now.

3.5.3 Other Planets

The discovery of extra-solar planets with masses smaller than Neptune suggests that planet formation might often yield failed cores—oligarchs that did not accrete gas from the disk. Neptune and Uranus may be considered failed cores. Several theoretical studies (e.g. Laughlin et al., 2004; Ida & Lin, 2005, this paper) suggest that failed cores are more common around low mass stars.

Failed Cores

In our model, there are three ways to produce failed cores. Objects that form too late ($t_{\rm iso} > t_{\rm core}$), or form with insufficient mass to accrete gas ($M_{\rm iso} < M_{\rm core}$) are failed cores. Although all cores within the core-forming region can potentially accrete gas, dynamical interactions among the cores may eject one or more into regions with a small gas surface density (e.g. Thommes et al., 1999) or from the system entirely (e.g. Goldreich et al., 2004; Ford & Chiang, 2007). This mechanism occurs in a random (and currently unquantifiable) fraction of models with $M_{\rm iso} > M_{\rm core}$ and $t_{\rm iso} < t_{\rm core}$. In our model failed cores are more common around low-mass stars because isolation masses are smaller and isolation times are longer.

Apparent failed cores may also form by collisions over long timescales (Kennedy et al., 2006). The mass of these icy planets may be limited by the likelihood of collisions vs. ejections during the final stages of coalescence (Goldreich et al., 2004).

Ocean Planets

The diversity of observed extra-solar planets led Léger et al. (2004) to suggest that 1–10 $M_\oplus$ icy planets that form in the region beyond the snow line may migrate inward to ~1 AU, where the outer layers subsequently "melt." With masses too low to accrete much gas, these planets are less dense than a rocky planet of equivalent mass and harbour deep oceans. Hence Léger et al. call these "ocean planets."

The increase in luminosity of stars with masses $\gtrsim 2.5\,M_\odot$ as they reach the main-sequence provides an alternative *in situ* formation mechanism for ocean planets, as they may have insufficient mass for significant migration. We outline the concept briefly, because these planets are difficult to detect. At times $\gtrsim$1–10 Myr, the snow line moves to ~10 AU as the disk becomes optically thin.[4] Failed cores in the range 1–10 $M_\oplus$ can therefore achieve their final mass outside the snow line in ~1 Myr and without migrating, later find themselves in a much warmer region when the star reaches the main-sequence.

Though all stars more massive than the Sun undergo an increase in luminosity as they settle onto the main-sequence (e.g. Palla & Stahler, 1999), the temperature at the early snow line distance of ~7 AU must increase enough to melt ice and maintain oceans. For 2.5 $M_\odot$, there is ~1 AU overlap between the early snow line and the final habitable zone distance—at an equilibrium temperature of ~245 K (Kasting et al., 1993)—with room for a few cores that form *in situ* just beyond the snow line.

3.5.4 Sensitivity to Model Assumptions

Our model is simplified, but captures some important concepts. In this section, we show that our results remain for realistic variations on our model assumptions.

We use a simple model for the temperature profile of an irradiated, accreting, flared disk, which sets the location of the snow line. As shown in Figure 3.4, ~AU changes in the snow line distance affects where the innermost cores originate, but there is little change in the range of disk masses that forms massive cores for a given stellar mass.

The disk surface density profile is uncertain: the MMSN assumes the solar system planets formed *in situ*. In the standard MMSN model, $\delta = 3/2$ and $\eta = 4$ yield the surface density needed to form a massive core near Jupiter. If $\delta = 1$ and $\eta = 1$, then $M_{\rm iso} \approx 5\ (13)\,M_\oplus$ at 5 (10) AU, which are similar to the inferred core masses for Jupiter and Saturn (Saumon & Guillot, 2004). Figure 3.5 shows the core-forming regions for $\eta = 1$, $\delta = 1$ and $M_{\rm core} = 5\,M_\oplus$. The lower σ in the

[4]The snow line has less meaning at these times, since there is little gas to condense into ices. The equilibrium temperature of objects is a more relevant concept.

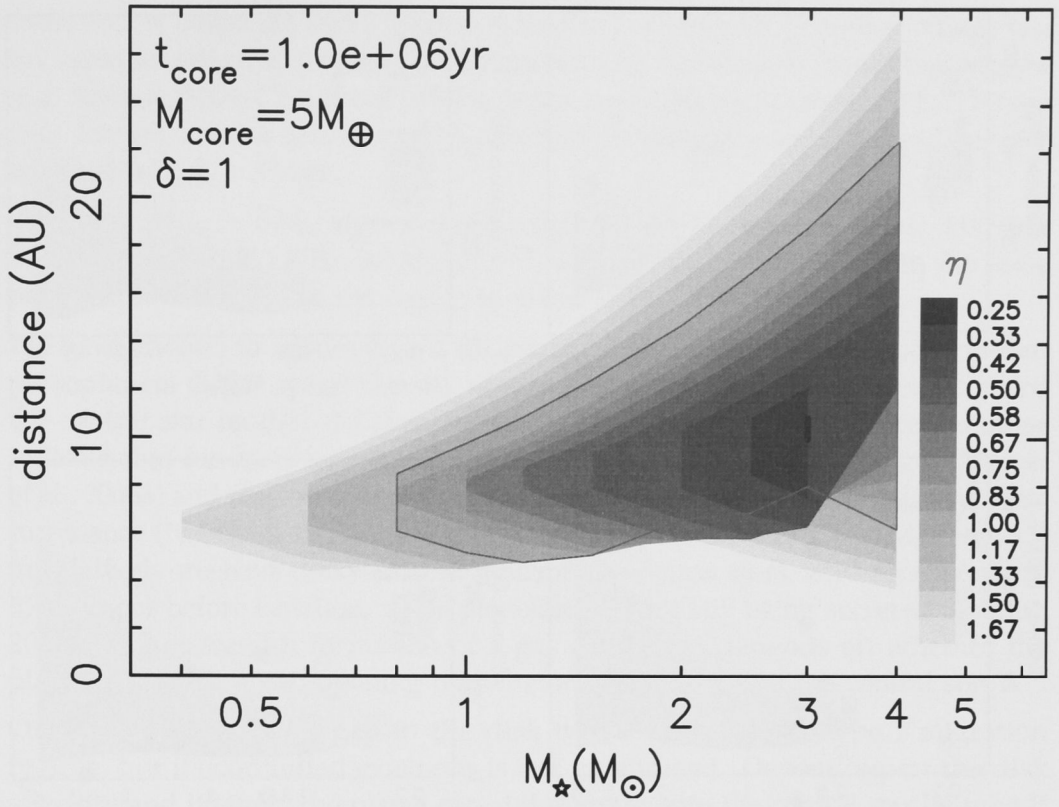

Figure 3.5 Same as Figure 3.4, but for $\delta = 1$ and $M_{\rm core} = 5\,M_\odot$. For $\eta = 0.25$, only $3\,M_\odot$ stars form cores. Though the $\delta = 1$ disk has different η, it covers the same range of disk masses as Figure 3.4 with $\delta = 3/2$, with the exception of the lowest disk mass ($\eta = 1.2$) from that figure.

core-forming regions needed to keep the same disk mass makes it harder to form cores with $M_{\rm core} = 10\,M_\oplus$, but with $M_{\rm core} = 5\,M_\oplus$ the regions are similar to our baseline model.

There is little observational constraint of gaseous inner disk lifetimes, so the least certain of the parameters we specify is $t_{\rm core}$. The isolation time is $t_{\rm iso} \propto a^3$ (when $\delta = 3/2$), so doubling $t_{\rm core}$ allows the outer edge to move outward by a factor of about 1.3. Figure 3.6 shows how changing $t_{\rm core}$ alters the core-forming region with $\eta = 4$ for $M_{\rm core} = 5\,M_\oplus$ and $10\,M_\oplus$, and $\delta = 1$ and $3/2$. Longer gaseous disk lifetimes lead to more gas giant cores. The general trend is to extend the regions to lower stellar masses and to greater radial distances. Cores that take longer to form—due to smaller P or σ—can reach isolation before the gas disk is dissipated.

Dust disks around spectral types earlier than ~G have somewhat shorter lifetimes than disks around lower mass stars (Haisch et al., 2001a; Currie et al., 2007). If gas is removed on timescales similar to infra-red excesses for a range of spectral types, $t_{\rm core}$ is shorter and the outer edge of the core-forming region for these stars

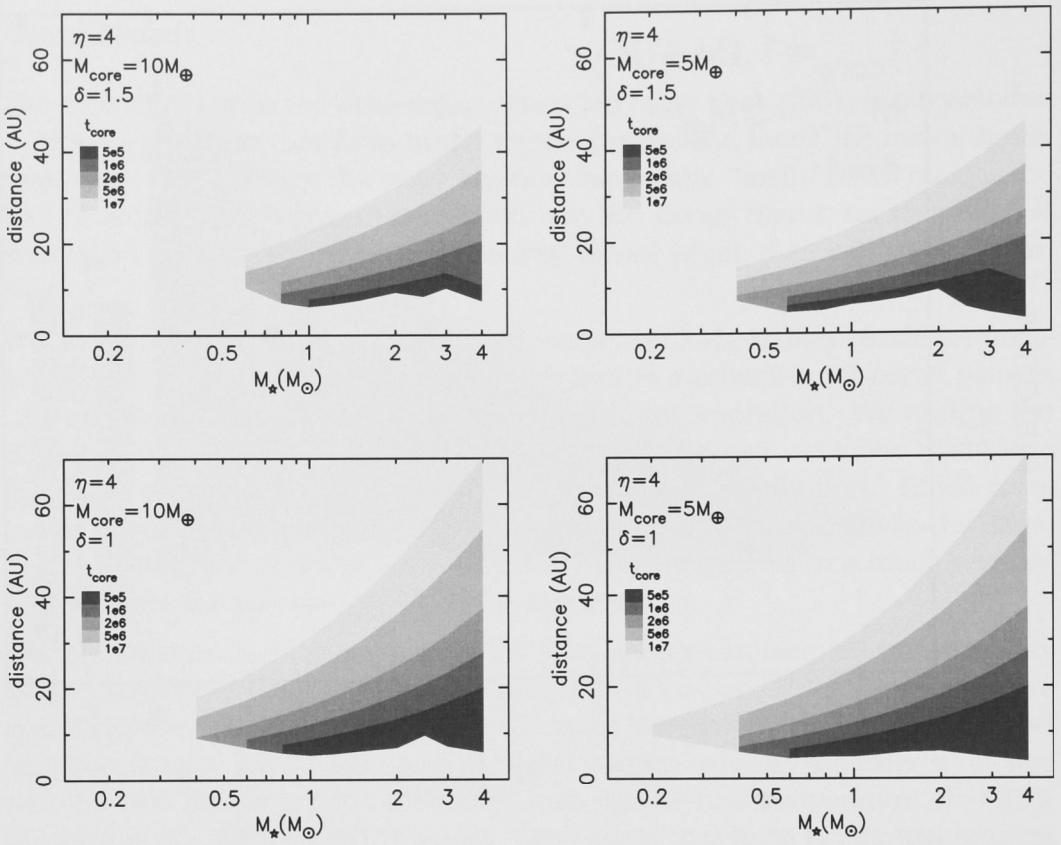

Figure 3.6 Similar to Figure 3.4, but for fixed $\eta = 4$. Contours represent different $t_{\rm core}$ as indicated by legends. Top (bottom) panels are $\delta = 1.5$ ($\delta = 1$) and left (right) panels are $M_{\rm core} = 10\,M_\oplus$ ($M_{\rm core} = 5\,M_\oplus$).

moves in (Fig. 3.6). Observations of evolved stars can test whether a strongly stellar mass dependent $t_{\rm core}$ (or some other process) defines an upper stellar mass limit for gas giant formation.

The short timescale for disk removal by the central star—inferred from the lack of transition disks (e.g. Kenyon & Hartmann, 1995; Clarke et al., 2001; Alexander et al., 2006)—and the likely large radial distance in the disk for external influence by massive stars (Adams et al., 2004), supports our assumption that the location of photoevaporation is unimportant. Although the expected distance for external photoevaporation in "typical" clusters reaches closer to the central star for low-mass stars (Adams et al., 2004), it lies outside the core-forming region for our standard case of $M_{\rm core} = 10\,M_\oplus$, $t_{\rm core} = 10^6\,{\rm yr}$ and $\delta = 1.5$. The core-forming and external photoevaporation regions begin to overlap for $M_\star \lesssim 0.5\,M_\odot$ and $t_{\rm core} \gtrsim 5 \times 10^6\,{\rm yr}$.

The size of planetesimals is uncertain, as is the isolation time that results from their accretion by oligarchs. Our choice of $10^5\,{\rm yr}$ for the Jovian core is relatively

short and is based on likely fragmentation (e.g. Kenyon & Bromley, 2004a) and the rapid accretion of small ~100 m planetesimals in the shear dominated regime (e.g. Rafikov, 2004; Chambers, 2006b). If planetesimals are larger and t_{iso} is longer (e.g. 1 Myr), similar results can be obtained by simply using a longer (yet still reasonable) $t_{core} \sim 3$ Myr.

Choosing $M_{core} = 5 M_{\oplus}$ allows core formation in less massive disks. Halving M_{core} allows a disk 1.6 times ($M_{iso} \propto \sigma^{3/2}$) less massive to form cores in the same region and also extends the region to lower stellar masses (Fig. 3.6).

We have chosen to ignore type I migration, where linear theory predicts that protoplanets excite spiral density waves in the gas disk and migrate toward the central star on 0.01–0.1 Myr timescales (Tanaka et al., 2002). Recent studies indicate that for cores less massive than $\sim 10 M_{\oplus}$ the timescale is longer (Masset et al., 2006a) and may be reduced to a random walk due to magnetohydrodynamic turbulence (Nelson & Papaloizou, 2004). For cores with masses $\gg 10 M_{\oplus}$ (Fig. 3.3) in relatively massive disks around intermediate mass stars, core accretion will likely occur before isolation, while planetesimals are still being accreted (Rafikov, 2006). The successful formation of a gas giant then depends on whether the planet can reach a gap-opening mass before migrating into the central star.

Once a planet opens a gap in the disk it has survived the type I migration regime, but its continued existence is not guaranteed. Depending on the disk viscosity and lifetime, the planet can still migrate onto the central star by type II migration.

In summary, the simplicity of our model means that reasonable changes in the input parameters change the results little. Future development of the model can include a more complete treatment of more complicated physical processes.

3.6 Discussion

The age of direct planet detection is approaching (e.g. NICI Campaign on Gemini South), where discoveries will be pushed to larger semi-major axes. Already, microlensing probes distances of several AU around $\lesssim M_{\odot}$ stars (e.g. Beaulieu et al., 2006). In addition, radial velocity surveys now extend over a wider range of stellar masses (e.g. Frink et al., 2002; Butler et al., 2006; Johnson et al., 2007a,b). Our goal is to develop a theory of planet formation that extends over the observational range to make testable predictions and to develop greater insight into the processes that produce the observed diversity of planetary systems.

For planets orbiting giant stars, there is a downward shift in the planet-metallicity distribution by ~0.3 dex (Pasquini et al., 2007). This result is not surprising in the context of our model. In Figure 3.4, the lowest relative disk mass that forms cores roughly halves from 1 to $2 M_{\odot}$, which corresponds to a −0.3 dex change in metallicity. Thus, we naturally expect the lower end of the metallicity distribution

of higher mass stars to be shifted. However, we do not expect the high metallicity end of the distribution to move, since these disks can still form cores.

There are now sufficient planet discoveries to start quantifying trends across a range of stellar masses, which allows the first steps towards comparison with planet formation theories that consider the mass of the central star (e.g. Ida & Lin, 2005). Though sample numbers are small, studies of $\gtrsim 1.3\,M_\odot$ giants indicate that giant planet frequency increases with stellar mass in the range 0.1–2 $M_\odot$ (Johnson et al., 2007a). We now calculate what our model predicts for the probability of forming gas giants as a function of stellar mass.

3.6.1 Gas Giant Frequency and Stellar Mass

Assuming all stars are born with a distribution of disk masses, we can estimate the probability $P_{\rm GG}$ of a star forming at least one gas giant as a function of stellar mass. Though comparison with observed disk masses is uncertain, we follow Ida & Lin (2005) and adopt a Gaussian distribution in terms of $x = \log M_{\rm disk}/M_\star$, where $P_{\rm disk} \propto \exp\left(-(x-\mu)^2/2\,\sigma_{\rm ln}^2\right)$ with standard deviation $\sigma_{\rm ln} = 1/3$, centred on $M_{\rm disk} = 0.03\,M_\star$ (e.g. $\mu \approx -1.5$). This distribution is similar to data compiled by Natta et al. (2000), which is sensitive to all disk masses that form a core in our baseline model. Because our model is based on parameters that change with stellar mass (such as isolation time and disk mass), the relative probability of forming gas giants is our main concern. Effects that may set the absolute probability, such as survival of migrating planets, are not included. To make contact with observations, we therefore normalise our results to 6% for solar-mass stars (Udry et al., 2007).

Figure 3.7 shows the likelihood of a star harbouring at least one gas giant planet as a function of stellar mass for our baseline model (Fig. 3.4) and a model with $\delta = 1$ and $M_{\rm core} = 5\,M_\oplus$ (Fig. 3.5), normalised to 6% at $1\,M_\odot$. To illustrate the difference between a static, main-sequence scaled snow line and our evolving one, we include a model with $a_{\rm snow} \propto 2.7\,M_\star^2$ AU, similar to the main model of Ida & Lin (2005). Each point is the probability a star has a disk in the range that forms cores in Figure 3.4. This plot assumes that if one or more cores form, at least one will result in a gas giant. For comparison to current observations, it also assumes that as they accrete gas, cores generally migrate or scatter a stellar-mass independent fraction to observable distances, where the 6% normalisation applies. Like our baseline model, different $M_{\rm core}$, $t_{\rm core}$, and δ have lines of approximately constant slope ($P_{\rm GG} = m\,M_\star - c$) up to $\sim 3\,M_\odot$. Our baseline model has $m = 0.20$ and $c = 0.06$; very few gas giants form by core accretion below $0.3\,M_\odot$.

With the normalisation, our baseline model predicts 1% of $0.4\,M_\odot$ stars and 10% of $1.5\,M_\odot$ stars will harbour at least one gas giant. Increasing $\sigma_{\rm ln}$ decreases the range of probabilities, because disk masses come from a less strongly varying

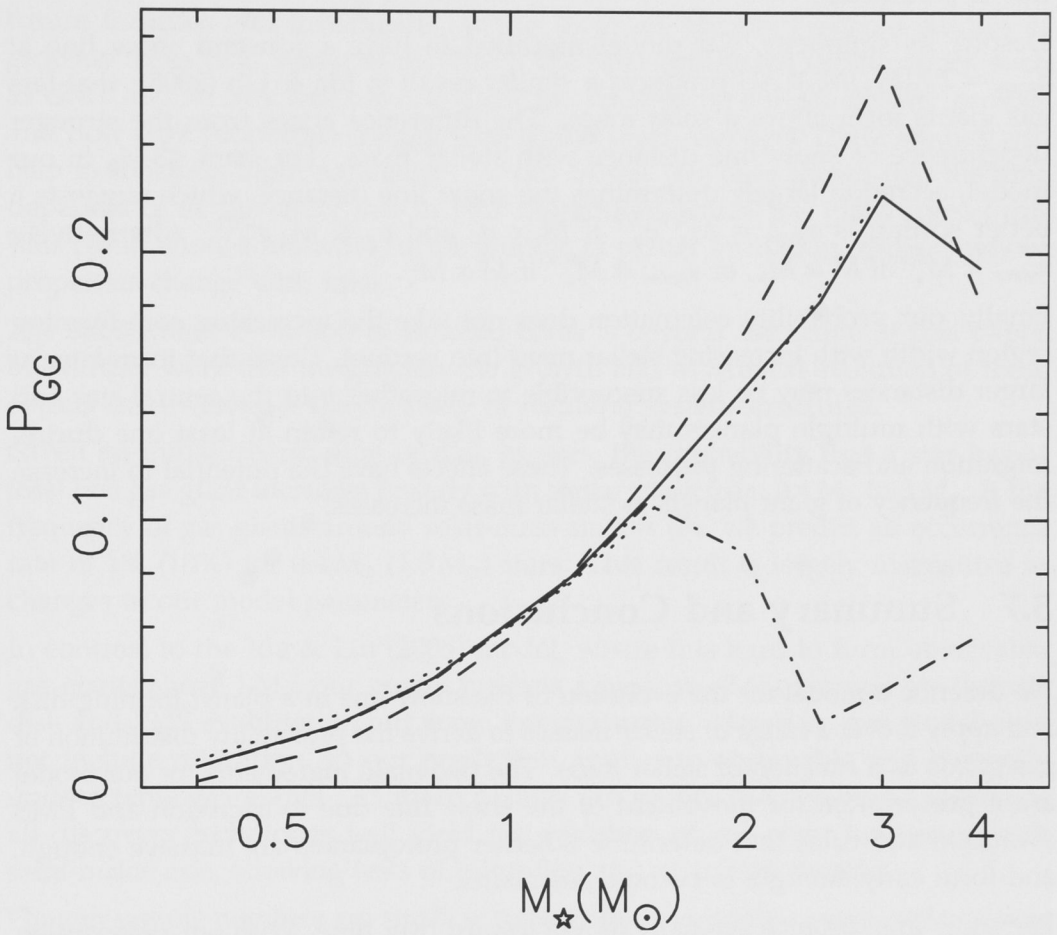

Figure 3.7 Probability of a star harbouring at least one gas giant planet as a function of stellar mass for our baseline model (*solid line*) and $\delta = 1$ and $M_{\rm core} = 5\,M_\oplus$ (*dashed line*). The thin dotted line is a fitted line of constant slope $P_{\rm M_\star} = 0.20\,M_\star - 0.06$. The dot-dashed line has $a_{\rm snow} \propto 2.7 M_\star^2$ AU, for comparison with Ida & Lin (2005). All curves are normalised to 6% at $1\,M_\odot$ via a straight line fit.

section of the overall distribution. For example, $\sigma_{\ln} = 1$ yields 4% and 8% for $0.4\,M_\odot$ and $1.5\,M_\odot$ stars respectively.

Our result is robust to changes in our assumed model parameters (in the range 0.4–1.5 $M_\odot$), because the range of core forming disk masses generally remains the same and the 6% normalisation removes absolute differences for different model parameters.

Despite its simplicity, our model modified to have a constant snow line at $a_{\rm snow} = 2.7\,(M_\star/M_\odot)^2$ AU produces a similar result to Ida & Lin (2005): that less gas giants form above a solar mass. The difference arises from the stronger dependence of snow line distance with stellar mass. For stars $\lesssim 3\,M_\odot$ in our model, accretion largely determines the snow line distance, which suggests a better scaling is $a_{\rm snow} \propto M_\star^{4/9}\sigma_0^{2/9}$ if $\dot{M} \propto \sigma_0$ and $\sigma_g \propto M_\star\, a^{-3/2}$. Alternatively, $a_{\rm snow} \propto M_\star^{6/9}$ if $\dot{M} \propto M_\star$, or $a_{\rm snow} \propto M_\star^{8/9}$ if $\dot{M} \propto M_\star^2$.

Finally, our probability calculation does not take the increasing core-forming region width with increasing stellar mass into account. Cores that form later at larger distances may be less susceptible to migrating into the central star and stars with multiple planets may be more likely to retain at least one during migration and scattering processes. These effects have the potential to increase the frequency of giant planets as stellar mass increases.

3.7 Summary and Conclusions

We describe a model for the evolution of the snow line in a planet forming disk and apply it over a range of stellar masses to derive the probability distribution of gas giants as a function of stellar mass. The two main ingredients for our model are a prescription for movement of the snow line due to accretion and PMS evolution and rules that determine whether protoplanets are massive enough, and form early enough, to become gas giants.

The snow line distance generally moves inward over time. With our prescription for the accretion rate, accretion dominates over irradiation for stars with $M_\star \lesssim 2\,M_\odot$. For $\gtrsim 3\,M_\odot$ stars, irradiation dominates at times $\gtrsim 1$ Myr as the star moves up to its main-sequence luminosity. The transition is at a few Myr for $\sim 2\,M_\odot$ stars. Over the wide range of observed accretion rates for any fixed stellar mass, the snow line in some disks may be set entirely by irradiation.

The snow line generally sets where the innermost gas giant cores form. In relatively massive disks around intermediate mass stars, rocky cores form interior to the snow line. The location of the outermost core is always set by the gas dissipation timescale. The range of disk masses that form cores and the radial width of the region in the disk where they form, increase with stellar mass. Lower mass disks produce failed icy cores, which are probably similar to Uranus, Neptune, and the observed "super-Earths."

The outward movement of the snow line as stars more massive than the Sun reach the main-sequence, and as the disk becomes optically thin, allows the ocean planets suggested by Léger et al. (2004) to form *in situ*. The change in disk temperature is only large enough for these planets to harbour oceans around stars $\gtrsim 2.5\,M_{\odot}$.

Our model includes several poorly determined parameters, which current and future facilities will investigate. While there are current resolved studies of gaseous disks (e.g. Bitner et al., 2007), the next generation of telescopes such as GMT and ALMA will provide more information on surface density profiles and how disk properties change with stellar mass and age. These studies will help to constrain input parameters for our model. We have shown that the time dependence of the snow line in part determines where gas giant cores form. This result should motivate future studies of planet formation in disks whose properties change with time.

The subsequent evolution of isolated cores is beyond the scope of this paper, but further work that investigates the growth and dynamical evolution of these objects can investigate the diversity of resulting system structures.

Given an initial distribution of disk masses, the probability that a star has at least one gas giant increases linearly with stellar mass from $0.4\,M_{\odot}$ to $3\,M_{\odot}$. If the frequency of gas giants around solar-mass stars is 6%, we predict an occurrence rate of 1% (10%) for $0.4\,M_{\odot}$ ($1.5\,M_{\odot}$) stars. This result is largely insensitive to changes in our model parameters.

In contrast to the Ida & Lin (2005) model, where it is hard to form observable gas giants above $1\,M_{\odot}$, our model predicts a peak at $\sim 3\,M_{\odot}$ because we include disk and PMS evolution in our snow line derivation. However, our model does not include migration, so our prediction applies to observable and currently undetectable gas giants. As more planets are found, the combined results of all discovery techniques will yield the variation of gas giant frequency with semi-major axis, allowing tests of migration and scattering theories.

Though sample numbers are small, it appears that observable gas giant frequency increases with stellar mass across a wide range of host masses (Johnson et al., 2007a). Larger samples of stars that host giant planets, particularly low and intermediate-mass stars, will solidify this result. These studies, and the extension of the results to a wider range of semi-major axes, will provide a basis for comparison with our model predictions.

We acknowledge support from an Australian Postgraduate Award, a Smithsonian Astrophysical Observatory pre-doctoral fellowship (GK), and the *NASA Astrophysics Theory Program* through grants NAG5-13278 and NNG06GH25G (SK). We thank T. Currie, J. Johnson and the ANU Planetary Science Institute planet group for helpful discussions. We thank the anonymous referee for comments that improved the manuscript.

CHAPTER 4

PLANET FORMATION AROUND STARS OF VARIOUS MASSES: HOT SUPER-EARTHS

Kennedy & Kenyon (2008a)

Abstract

We consider trends resulting from two formation mechanisms for short-period super-Earths: planet-planet scattering and migration. We model scenarios where these planets originate near the snow line in "cold-finger" circumstellar disks. Low-mass planet-planet scattering excites planets to low periastron orbits only for lower mass stars. With long circularisation times, these planets reside on long-period eccentric orbits. Closer formation regions mean planets that reach short-period orbits by migration are most common around low-mass stars. Above $\sim 1\,M_{\odot}$, planets massive enough to migrate to close-in orbits before the gas disk dissipates are above the critical mass for gas giant formation. Thus, there is an upper stellar mass limit for short-period super-Earths that form by migration. If disk masses are distributed as a power-law, planet frequency increases with metallicity because most disks have low masses. For disk masses distributed around a relatively high mass, planet frequency decreases with increasing metallicity. As icy planets migrate, they shepherd interior objects toward the star, which grow to $\sim 1\,M_{\oplus}$. In contrast to icy migrators, surviving shepherded planets are rocky. On reaching short-period orbits, planets are subject to evaporation processes. The closest planets may be reduced to rocky or icy cores. Low-mass stars have lower EUV luminosities, so the level of evaporation decreases with decreasing stellar mass.

4.1 Introduction

With nearly 300 known extra-solar planets, there are now several clear correlations between the properties of the planets and their host stars. The most well known trend is the increase in gas giant frequency with host star metallicity (e.g. Fischer & Valenti, 2005). Recent radial velocity surveys suggest that giant planet frequency also increases with stellar mass (Johnson et al., 2007a).

These trends provide tests of planet formation theories. In the core accretion model for example, gas giant planets form by coagulation of small planetesimals near the "snow line" that separates rocky and icy regions in a circumstellar disk. Once icy protoplanets reach a critical core mass, they accrete gas rapidly (Pollack et al., 1996). Cores benefit from extra planet building material provided by enhanced metallicities and an increase in disk masses with stellar mass. The model is thus consistent with current observations (Ida & Lin, 2004b, 2005; Kennedy & Kenyon, 2008b).

Gravitational instability (GI) is an alternative formation mechanism for gas giant planets, where a relatively massive disk cools enough to fragment into Jupiter-mass clumps. Although GI operates over a wide range of stellar masses, there is still debate about predicted trends with metallicity (Durisen et al., 2007). Given observational biases in the current sample of extra-solar planets, GI cannot be ruled out as a formation mechanism (Durisen et al., 2007).

Core accretion and GI models suggest that short-period "hot Jupiters" reside too close to their parent stars to have formed *in situ*. Thus, these planets must migrate or scatter from more distant formation regions to arrive at their final orbits (Lin et al., 1996; Rasio & Ford, 1996). A combination of these two mechanisms probably operates to produce the observed distribution of extra-solar giant planets. Scattering can reproduce most of the observed eccentricity distribution, but has trouble accounting for planets in circular orbits at distances too far from their host stars for tidal circularisation (Ford & Rasio, 2008). Migration theories can explain systems with planets in mean-motion resonances (Lee & Peale, 2002), but they may not reproduce the observed eccentricity distribution (e.g. Tremaine & Zakamska, 2004).

With the discovery of the first super-Earths in relatively short period orbits, migration and scattering remain possible mechanisms for planets to reach these radii (Brunini & Cionco, 2005; Terquem & Papaloizou, 2007; Raymond et al., 2008). However, the discovery of low-mass planets in systems already harbouring giant planets suggests new formation mechanisms (Zhou et al., 2005). Because these models require gas giants, they predict trends with metallicity and stellar mass for low-mass planets similar to those for giant planets. Though some low-mass planets may have formed with help from giant planets, a flatter metallicity distribution (Udry et al., 2007) and the absence of giant planets in some low-mass

planet systems (e.g. GL581 and GJ674, Bonfils et al., 2005, 2007) indicate other formation mechanisms.

Here, we consider trends that may arise in forming short-period and/or transiting icy/rocky planets in systems with no gas giants, over a range of stellar masses. The close-in planets that form are therefore the most massive in the planetary system. We first cover some background in §4.2. In §4.3 we use n-body simulations to show that $10\,M_\oplus$ planet-planet scattering is unlikely to result in transiting planets for all but the lowest mass stars. With long circularisation timescales, planets in these systems are hard to detect. We consider migration scenarios using analytic, semi-analytic and n-body models in §4.4. With migration, short-period low-mass planets most likely form around low-mass stars. Above a certain stellar mass, it is hard to form any short-period planets without giant atmospheres. Trends with metallicity depend on the disk mass distribution. Migration to short-period orbits results in significant amounts of material being shepherded inward, which affects the final structure of these systems. We discuss our results, subsequent planetary evolution, and conclude in §4.5.

4.2 Background

4.2.1 General Picture

Planets form in circumstellar disks. Therefore disk structure plays a key role in setting the final configuration of planetary systems. In most planet formation models, disk structure is characterised by an outwardly decreasing radial surface density profile. This profile usually includes an increase in surface density at the "snow line," where the temperature becomes low enough for water to freeze.

Planets form by accumulating solids in the disk. Therefore the expected increase in surface density at the snow line is often associated with the formation of gas giants like Jupiter. Forming Jupiter requires the relatively rapid growth of a ~5–10 $M_\oplus$ icy core, followed by a period of gas accretion (Pollack et al., 1996). Gas accretion must be complete before the gas disk disperses in ~3 Myr (e.g. Haisch et al., 2001b). In the minimum mass solar nebula model (MMSN, Weidenschilling, 1977b; Hayashi, 1981), forming the icy core rapidly requires factor of 5–10 surface density enhancements relative to the terrestrial region (Lissauer, 1987; Pollack et al., 1996; Thommes et al., 2003). This factor is larger than the factor of 2–3 enhancements expected from solar abundances (Asplund et al., 2005), or suggested by comet composition (Küppers et al., 2005), and the factor of ~4 derived in the original MMSN model (Hayashi, 1981).

The need for larger surface density enhancements inspired "cold-finger" disk models, which produce much larger snow line enhancements in a relatively narrow ($\lesssim$AU) radial region near the snow line (Stevenson & Lunine, 1988; Cuzzi

& Zahnle, 2004). In this picture, a circumstellar disk has an initial equilibrium state with the water vapour (ice) concentration decreasing (increasing) beyond the snow line. As the disk diffuses and advects, water continually condenses from gas passing beyond the snow line, thus enhancing the local surface density of solids and removing vapour phase water from the inner disk. Sublimation of planetesimals that drift inside the condensation radius by gas drag enhances this effect: the surface density beyond the snow line increases when water vapour from the sublimated planetesimals diffuses back outside the snow line (Cuzzi & Zahnle, 2004).

The first cold-finger models predict a factor of ~10-100 increase in the surface density of icy material in a relatively narrow region near the snow line (Stevenson & Lunine, 1988; Cuzzi & Zahnle, 2004). Using a more complex global disk model, Ciesla & Cuzzi (2006) suggest surface density enhancements closer to 10 than 100. In their simulations, the enhancement regions are several AU wide at half the maximum planetesimal surface density.

The main differences expected for planet formation models using cold-finger instead of MMSN disks are threefold. Due to the nature of the surface density enhancement: (1) fewer large planets form, (2) large planets form in relatively low-mass disks, and (3) planets form from material with much higher ice/rock ratios. In addition, material lost to inward planetesimal drift by gas drag (Thommes et al., 2003) may be returned to the cold-finger region, allowing continued growth. Reducing the removal of drifting planetesimals enhances growth rates and allows formation of more massive icy planets.

4.2.2 Mathematical Formalism

In the standard coagulation model, planets grow in a circumstellar disk through repeated collisions and mergers of smaller objects (Safronov, 1969). First, roughly kilometre size planetesimals form rapidly, whether by coagulation (e.g. Weidenschilling, 2000) or direct collapse (e.g. Goldreich & Ward, 1973). Little knowledge of which process dominates means the size distribution of the first planetesimals is poorly constrained. Planetesimals initially grow through a rapid phase of "runaway" growth (Kokubo & Ida, 1996). During the period of "oligarchic" growth that follows (Kokubo & Ida, 1998), protoplanetary growth rates depend on the surface density of planetesimals σ_s, the local orbital frequency Ω, the gravitational reach of the growing protoplanet, and the random velocities of the smaller planetesimals (Inaba et al., 2001)

$$\dot{M}_{\rm pl} \propto \sigma_s R_H^2 \Omega P_{\rm col}(\tilde{e}, \tilde{i}) . \tag{4.1}$$

Here $R_H = a\left(M_{\rm pl}/3M_\star\right)^{1/3}$ is the Hill radius and a is semi-major axis. The eccentricity $\tilde{e}$ and inclination $\tilde{i}$ are in units of the growing protoplanets Hill

radius (i.e. $\tilde{e} = e/R_H$). The collision probability P_{col} largely determines how growth proceeds: growth is fastest when planetesimals are small enough ($\lesssim$1 km) to be damped by gas drag (e.g. Rafikov, 2004). In this "shear-dominated" regime, when $\tilde{e}$ and $\tilde{i}$ are $\lesssim$1, growth depends on Keplerian shear in the disk, rather than objects random velocities. Growth slows strongly with increasing radial distance, because $\Omega \propto a^{-3/2}$ and $\sigma_s \propto a^{-\delta}$, where $\delta \sim$ 1–1.5.

Eventually, protoplanets accrete most of the nearby material and reach the "isolation" mass (Lissauer, 1987)

$$M_{iso} = \frac{(4\pi B \sigma_s a^2)^{3/2}}{(3M_\star)^{1/2}}. \tag{4.2}$$

Numerical simulations indicate that isolated oligarchs are spaced at $2BR_H \sim 8R_H$ intervals (e.g. Kokubo & Ida, 1998). In the terrestrial region around the Sun, the isolation mass is $\sim 0.1\,M_\oplus$, and the timescale for Earth formation by the chaotic growth that follows is ~10–100 Myr (e.g. Kenyon & Bromley, 2006).

Further out in the disk, larger isolation masses allow formation of gas giant planets. The critical core mass for gas accretion depends on opacity and planetesimal accretion rates, but is $\gtrsim 10\,M_\oplus$ (e.g. Ikoma et al., 2000; Rafikov, 2006). This mass is reached more easily further out in the disk because M_{iso} increases with a. However, growth slows rapidly with increasing radial distance; thus, there is an optimum region where cores are massive enough to accrete gas and to form giant planets before the gas disk is dissipated (Kennedy & Kenyon, 2008b). This region is sufficiently far from the star that *in situ* formation of "hot-Jupiters" is unlikely, thus motivating theories of migration and scattering.

4.2.3 Migration

Type I migration is a potential barrier to the formation of both terrestrial and giant planets (Goldreich & Tremaine, 1980; Ward, 1997; Tanaka et al., 2002; Papaloizou et al., 2007). When protoplanets reach near an Earth mass, the excitation of spiral density waves in the gaseous disk causes planets to experience a torque and migrate inward. The timescale for a planet to spiral into the central star is (Tanaka et al., 2002)

$$\tau_{mig} = (2.7 + 1.1\delta)^{-1} \frac{(M_\star M_\odot)^2}{M_{pl}\,\sigma_{gas}\,a^2} \frac{h^2}{\Omega}, \tag{4.3}$$

where $h \approx 0.05$ is the disk aspect ratio, and the stellar mass $M_\star$ is in units of solar masses. For a planet of mass $M_{pl} = 1\,M_\oplus$ in a disk with $\sigma_{gas} = 1700$ g cm^{-2} at 1 AU around a solar-mass star, $\tau_{mig} = 1.6 \times 10^5$ yr. Because this timescale is shorter than the ~3 Myr disk lifetime (Haisch et al., 2001b) and comparable with growth timescales, type I migration theory conflicts with terrestrial and giant planet formation in the solar system (but see Chambers, 2006b).

Recent work suggests a reduced migration efficiency can resolve this problem (Ida & Lin, 2008). This "offset" applies to planets $\lesssim 15 M_{\oplus}$ (D'Angelo et al., 2002, 2003) and arises from corotation torques by coorbital material (Masset et al., 2006a). Other ways of reducing (and even reversing) type I migration rates include turbulence arising from the magneto-rotational instability (e.g. Nelson & Papaloizou, 2004) and eccentricity driven by planet-planet interactions (Papaloizou & Larwood, 2000).

If planets do not fall onto the central star, migration is a possible mechanism for producing planets on short-period orbits (Lin et al., 1996; Brunini & Cionco, 2005; Terquem & Papaloizou, 2007).

4.2.4 Scattering

Planet-planet scattering can also produce planets with short-period, or low periastron (q) orbits. Originally proposed to explain hot-Jupiters (Rasio & Ford, 1996), this scenario has not been applied to low-mass planets.

Scattering favours giant planets on short-period orbits. When a gas giant scatters into a low periastron orbit, tidal interaction with the star can circularise the orbit on reasonable timescales, with $a \sim 2q$ (Rasio & Ford, 1996). For lower mass planets, long circularisation timescales make circular orbits unlikely (Raymond et al., 2008). However, if the initial scattering region is sufficiently close, as for low-mass stars, detection of low-periastron eccentric planets is possible.

We now consider two different scenarios that form short-period and/or transiting low-mass planets that begin growth near the snow line, across a range of stellar masses. When the snow line enhancement is small, many planets migrate toward close orbits. This scenario has already been studied for solar-mass stars by Terquem & Papaloizou (2007). Here, we instead consider cold-finger type disks, where a few planets forming near the snow line dominate others forming elsewhere in the disk. We first consider a scattering scenario resulting from *in situ* growth and then a migration scenario. We defer discussion of subsequent planetary evolution in final orbits to §4.5.

4.3 Scattering

Planet-planet scattering is a likely outcome of oligarchic growth. In migration scenarios, protoplanets interact strongly with the gas disk and they migrate to close-in orbits. However, if the gas disk disperses before planets have time to migrate, or if migration results in no net inward movement, planets form *in situ*. During oligarchic growth, protoplanets grow on orbits near the limits of dynamical stability, with damping provided by small bodies (e.g. Stewart & Wetherill, 1988; Kokubo & Ida, 1998). At later stages near isolation, their orbits

can become unstable as remaining small bodies are accreted (Goldreich et al., 2004; Kenyon & Bromley, 2006).

When planets start interacting dynamically, the boundary in semi-major axis between stable and unstable configurations is very sharp. Thus, two planets with orbits that become too close experience the sudden onset of a dynamical instability caused by close encounters (Gladman, 1993).

In previous studies of giant planet scattering, planets begin at ~AU distances from the central star, with spacings just inside the stability limit. After many interactions, one planet sometimes attains a highly eccentric orbit with a small periastron distance (e.g. Rasio & Ford, 1996; Ford & Rasio, 2008). Tidal interaction with the central star then circularises the orbit with $a \sim 2q$.

While tidal forces can circularise gas giant orbits, the timescales for 1–10 $M_\oplus$ planets on highly eccentric orbits are long ($\gtrsim$Gyr, Raymond et al., 2008). Although these planets maintain eccentric long-period orbits, transits are possible in favourable circumstances. Because planets form at shorter orbital periods around low-mass stars, these provide the best opportunity for transit observations.

cold-finger disks provide an ideal environment for oligarchic growth followed by planet-planet scattering. The width of the cold-finger region allows several protoplanets to form (Ciesla & Cuzzi, 2006). Once protoplanets reach isolation, further chaotic growth may occur if their escape velocity $v_{\rm esc}$ is less than the local Keplerian velocity $v_{\rm K}$ ($\mathcal{R} \equiv v_{\rm esc}/v_{\rm K}$, Goldreich et al., 2004). In the terrestrial region of solar-type stars, $\mathcal{R} \sim 1/4$. For gas giants, $\mathcal{R} \gg 1$. For $M_{\rm pl} = 10\,M_\oplus$ with density $\rho = 4.5\,{\rm g\ cm^{-2}}$, $\mathcal{R} \approx 1.3$ outside the snow line. Thus, ~10 $M_\oplus$ protoplanets present an approximate division between coalescence and scattering/ejection and an order of magnitude estimate of the maximum planet mass. This mass is similar to the minimum needed for gas accretion, so scattering of super-Earths to close-in orbits appears difficult.

For less massive stars, scattering to low periastron orbits is easier. At fixed a, smaller $v_{\rm K}$ leads to larger $\mathcal{R}$ and a greater chance of scattering. However, the snow line also moves inward as stellar mass decreases ($a_{\rm snow} \propto M_\star^{1-2}$, e.g. Ida & Lin, 2008; Kennedy & Kenyon, 2008b), so scattering remains difficult. For $a_{\rm snow} \propto M_\star$, $v_K(a_{\rm snow})$ is constant for different stellar masses. However, for a fixed time period, a greater number of conjunctions for low-mass stars allows dynamical evolution to greater eccentricities.

4.3.1 Scattering Simulations

To measure the likelihood of planet-planet scattering, we performed simulations over a range of stellar masses with the MERCURY integrator (Chambers, 1999). We initialised integrations with two 10 $M_\oplus$ planets spaced near the Hill stability criterion to ensure close encounters (Gladman, 1993). This planet mass is an

Table 4.1 Scattering simulation outcomes and fraction with low periastra.

$M_\star(M_\odot)$	collisions	ejections	survival	$q < 0.1$ AU
0.25	95%	2.5%	2.5%	4%
0.5	95%	0%	5%	0%
1	94%	0%	6%	0%
2	84%	0%	16%	0%

approximate maximum mass before cores accrete gas to become gas giants and thus offers the best chance for scattering over coalescence. To represent a linearly stellar mass dependent snow line, the inner planet was placed at $a_{\rm in} = 3\,M_\star$ AU. The outer planet begins at a random a in the range 0.9–1 $a_{\rm in}\,(1 + \Delta_{\rm crit})$, where $\Delta_{\rm crit} = 3\left(M_{\rm pl}/M_\star\right)^{1/3}$ (Gladman, 1993; Ford & Rasio, 2008). Both planets begin in circular orbits with random inclinations less than 3°; the remaining orbital elements are chosen randomly. Simulations were run with a 5 day time step for 1 Gyr around stars of 0.25, 0.5, 1, and $2\,M_\odot$, or halted earlier in the case of collisions (we assume perfect mergers) or ejections. A total of 520 simulations were run, 130 for each stellar mass.

4.3.2 Scattering Results

The simulations result in three different outcomes: collisions, ejections, or survival of both planets for 1 Gyr. No planets achieved periastra low enough to fall onto the central star. Most (> 85%) simulations resulted in collisions (Table 4.1). Some systems survived for the full simulation. The only ejections were for $0.25\,M_\odot$.

With so few systems remaining after 1 Gyr, we use the smallest periastron distance reached in each simulation to characterise the success of planet-planet scattering, shown in Figure 4.1. As expected, the closer snow line distance for the $0.25\,M_\odot$ allows smaller periastra after scattering.

For simulations of $0.25\,M_\odot$ stars, 5/130 (4%) planets reach periastra less than 0.1 AU. A shorter orbital period allows many more conjunctions. Thus, systems evolve further than for more massive stars. For the three ejections, the lowest periastra were reached just before a series of close encounters, which resulted in the ejection. For the three surviving systems, the lowest periastra were reached near the end of the integrations. These orbits have eccentricities ≈0.5 and semi-major axes ≈0.5 AU, corresponding to an orbital period of around 260 days. Circularisation times for these planets are ~10 Gyr (Goldreich & Soter, 1966; Raymond et al., 2008).

Therefore, in the case of $10\,M_\oplus$ planet-planet scattering, only the lowest mass stars have planets with periastra close enough for transiting orbits. However, long circularisation timescales mean these planets will likely remain on highly

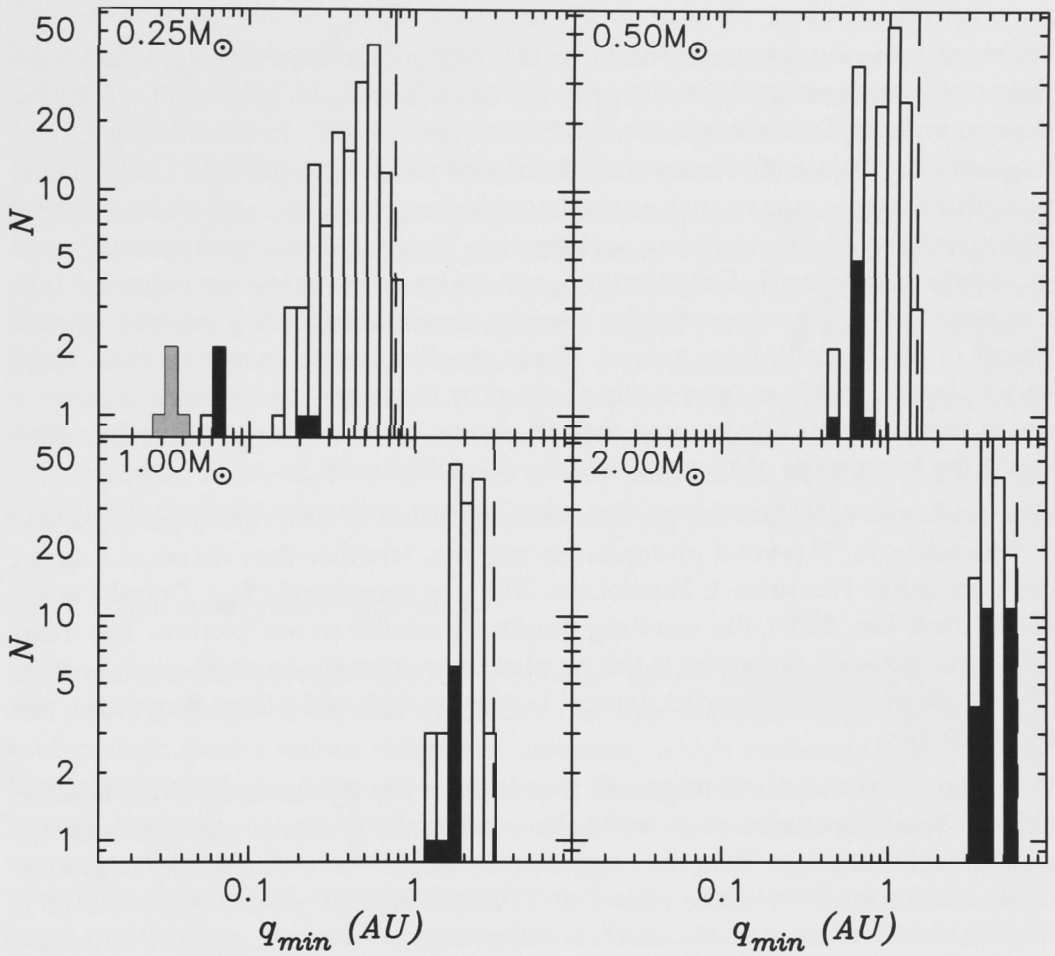

Figure 4.1 Smallest periastra of scattering simulations for all non-stable orbits. Black filled bars: simulations in which both planets survived until 1 Gyr. Grey bars: ejections (orbits going beyond 1000 AU). Unfilled bars: collisions/mergers. The dashed line shows the starting a (and q) of the inner planets (circular) orbit. Planets are scattered to lower periastra for low-mass stars because of more conjunctions and starting closer to the central star.

eccentric orbits, with periods long enough to make radial velocity and transit detections difficult.

4.4 Migration

We now turn to a migration scenario. In this picture, the largest protoplanets form near the snow line by oligarchic growth. Once they reach masses of ~1–10 $M_\oplus$, these icy protoplanets migrate towards the central star. In a cold-finger disk, migrating icy objects dominate smaller interior rocky protoplanets. Long chaotic growth timescales mean that as the icy object migrates through the terrestrial region, interior rocky objects are not accreted. They are instead scattered outward or shepherded inward. Shepherding—where interior objects are captured into mean-motion resonances—results in rocky protoplanets being pushed inward ahead of the migrating icy planet. These smaller objects merge to form large rocky planets, which are eventually accreted by the larger icy migrator or survive on an interior orbit. We assume that all objects halt their migration when they reach the inner edge of the gas disk, at ~10 stellar radii.

Our goal is to calculate the growth and migration of individual protoplanets in this scenario. If several protoplanets migrate, whether they do so as a set in resonant orbits (Terquem & Papaloizou, 2007), or successively (e.g. Daisaka et al., 2006; Ida & Lin, 2008), the resulting trends are similar in our picture. The main difference between outcomes is the number of icy planets on short-period orbits. The trends our models predict depend largely on disk and planet properties, not multiplicity.

When an icy protoplanet migrates, it only interacts dynamically with interior objects. Because collision cross sections are essentially geometric, the timescale for growth is much longer than the migration timescale. For example, the migration timescale for an Earth-mass planet at 1 AU (several 10^5 yr, or several 10^6 yr if migration is less efficient) is much smaller than the chaotic growth timescale ($\tau_{\rm chaotic} \sim \rho R_{\rm pl}/\sigma_{\rm s}\Omega \sim 10^8$ yr, where $R_{\rm pl}$ is the planet radius, Goldreich et al., 2004). Thus, the migrating protoplanet does not accrete terrestrial protoplanets; outward scattering or inward shepherding are the most likely outcomes.

The evolution of interior protoplanets depends on their random velocities. Chaotically growing objects with high eccentricities are scattered outward by the migrating protoplanet. These may interact with another migrating protoplanet or resume chaotic growth. If interior objects have finished chaotic growth and are damped by the gas disk onto more circular orbits, shepherding by capture onto resonant orbits is possible. Shepherded objects merge and form rocky planets as their orbits are pushed together by the migrating icy protoplanet. Shepherding by giant planets undergoing type II migration has been proposed as a way to

form super Earth-mass planets (Zhou et al., 2005). However, studies have yet to consider shepherding by super-Earths undergoing type I migration.

While some planets are stranded at intermediate radii as the gas disk dissipates, most planets that begin to migrate reach the inner disk edge and might fall onto the star. Because the torque on the migrating planet changes when the disk gas surface density profile varies rapidly, as happens at the inner disk edge, this fate may be avoided (Tanaka et al., 2002). Here, corotation torques affect migration and allow for planets to cease migration before reaching the stellar surface (Masset et al., 2006b). In our migration simulations, we therefore assume migration stops inside the inner disk edge (Terquem & Papaloizou, 2007).

In the rest of this section, we consider three models that explore different aspects of the migration scenario and observable trends that probe stellar and disk properties. We consider the simplest scenario—when growth is so fast that planets reach isolation before migration begins—with an analytic model in §4.4.1. As the planetesimal size increases, growth slows; the timescale becomes comparable to that for migration. The assumption made in the analytic model no longer applies and we use a semi-analytic model to study concurrent growth and migration in §4.4.2. Finally, we use n-body simulations in §4.4.3 to show the shepherding effects migrating super-Earths have on terrestrial material.

4.4.1 An Analytic Approach

If we assume that protoplanets reach isolation before migration starts, then we can create a simple analytical model for our migration scenario. At isolation, protoplanets have a known migration timescale, which is shorter than the disk lifetime if they are to reach the central star. To remain in the super-Earth mass regime, the mass of a protoplanet is smaller than the critical core mass for gas accretion. Because the isolation mass changes with surface density—and thus with disk mass—only a certain range of disk masses satisfy these conditions for fixed stellar mass. To consider a range of different stars, we also consider how the snow line—where these migrating planets form—changes with stellar mass. The range of disk masses that satisfy the conditions changes with stellar mass, resulting in potentially observable trends that test migration models.

To begin, we adopt a relation for the surface density of solid material in the disk. In the standard MMSN model,

$$\sigma_s = \sigma_0 f_{\rm ice} a_{\rm AU}^{-\delta}, \tag{4.4}$$

where $\sigma_0 = 8\,{\rm g\ cm^{-2}}$, $\delta = 1$–1.5 and $a_{\rm AU}$ is a in units of AU. The factor $f_{\rm ice} \sim 2$–3 is the enhancement from ice condensation beyond the snow line. This disk has a mass $\sim 0.01\,M_\odot$.

To generalise this relation, we add terms to account for differences in disk mass and metallicity around stars with a range of masses. Disks around young stars

have a large dispersion in mass (Natta et al., 2000; Andrews & Williams, 2005, 2007). Setting the disk mass $M_{\rm disk} \propto \eta M_\star^\beta$ allows us to treat the observed trends with stellar mass—$M_{\rm disk} \propto M_\star^\beta$, with $\beta \approx 1$—and a range (η) of disk masses at fixed stellar mass. Adopting a factor $\mathcal{M} \propto 10^{\rm [Fe/H]}$ for the metallicity of the stars and the disk yields

$$\sigma_{\rm s} = \sigma_0 \, \eta \, f_{\rm ice} \, \mathcal{M} M_\star^\beta \, a_{\rm AU}^{-\delta} . \tag{4.5}$$

For simplicity, we combine $f_{\rm ice}$ and $\mathcal{M}$ into a single factor $\Delta = f_{\rm ice}\mathcal{M}$, which quantifies the enhancement of solid material relative to gas where these planets form. For a cold-finger disk, we use $f_{\rm ice} = 10$. Thus, for typical ranges in $\mathcal{M}$ (~1/3–3) and $f_{\rm ice}$ (2–10), the plausible range of Δ is 0.6–30. We concentrate on higher Δ, because these are cold-finger disks.

For the surface density of the gas disk, we set $\sigma_g = 100\,\sigma_{\rm s}/\Delta$. Thus, the gas mass depends on η and δ and is independent of metallicity and the enhancement in ices at the snow line. We adopt $\delta = 3/2$.

How the snow line varies with stellar mass is uncertain. The existence of gas giant planets suggests that the stages of planet formation up to isolation occur while the gas disk is still present. During these stages the snow line distance is set by viscous accretion of the gas disk. If the accretion rate onto the star is $\dot{M} \propto M_\star^{1-2}$, then $a_{\rm snow} \propto M_\star^{6/9-8/9}$ (Kennedy & Kenyon, 2008b). Later, when the star has reached the main-sequence and the gas disk has been dissipated, the main-sequence luminosity is more important and $a_{\rm snow} \propto M_\star^2$ (Ida & Lin, 2005). Because we model oligarchic growth, and $\dot{M} \propto M_\star^2$ (Muzerolle et al., 2005), we adopt the snow line distance $a_{\rm snow} = 2.7\,M_\star$ AU. Variation of the snow line with time and stellar mass is a key component of planet formation models that consider a range of spectral types (Kennedy & Kenyon, 2008b).

Substituting our adopted surface density into the isolation mass yields

$$M_{\rm iso} \propto \frac{(\sigma_{\rm s}\, a^2)^{3/2}}{(M_\star)^{1/2}} = \frac{\left(\eta \, f_{\rm ice} \, \mathcal{M} M_\star \, a^{1/2}\right)^{3/2}}{M_\star^{1/2}} . \tag{4.6}$$

The isolation mass increases with any parameter that increases the surface density. The increasing disk mass with stellar mass ($M_\star$ in numerator) is stronger than the decreasing Hill radius ($M_\star$ in denominator). Thus, at fixed a the isolation mass increases with stellar mass. For our scenario, we are interested in planets that form at the snow line, so the changing snow line distance ($a = a_{\rm snow} \propto M_\star$) makes the stellar mass dependence stronger.

Substituting $a = 2.7\,M_\star$ AU, equation (4.6) yields the isolation mass *at the snow line* for a range of stellar and disk masses, and metallicities and snow line enhancements

$$M_{\rm iso} = 0.12 \, (\Delta\,\eta)^{3/2} \, M_\star^{7/4} M_\oplus . \tag{4.7}$$

Applying the same approach to type I migration yields

$$\tau_{\rm mig} \propto \frac{M_\star^2\, h^2\, f_{\rm mig}}{a^2\, M_{\rm pl}\, \Omega\, \sigma_{\rm gas}} = \frac{M_\star^{1/2}\, h^2\, f_{\rm mig}\, a}{M_{\rm pl}\, \eta}\,, \tag{4.8}$$

where the offset $f_{\rm mig}$ allows us to consider reduced migration rates. At fixed a, migration takes longer as stellar mass increases and speeds up as planet mass increases. If planet masses vary less strongly with radial distance than $M_{\rm pl} \propto a$, then the migration timescale increases outward and planets cannot catch up to interior ones. Even with isolated objects ($M_{\rm iso} \propto a^{3/2}$), planets may not catch up to interior ones due to the strong slowing of growth with semi-major axis. At the snow line distance, migration slows even more strongly with increasing stellar mass due to lower gas density and slower orbital periods at larger radii.

Again substituting $a = 2.7\, M_\star$ AU, the timescale to migrate from the snow line to the star is

$$\tau_{\rm mig} = 9.1 \times 10^5\, \frac{f_{\rm mig}\, M_\star^{3/2}}{M_{\rm pl}\, \eta}\ {\rm yr}\,, \tag{4.9}$$

where we have set $h = 0.05$ (e.g. Papaloizou et al., 2007). At fixed $M_\star$, massive planets in massive disks migrate to the inner disk edge fastest. The migration timescale increases with $M_\star$ because the snow line is further away.

If the migration time is shorter than the disk lifetime (i.e. $\tau_{\rm mig} \lesssim \tau_{\rm disk} \sim 1\,{\rm Myr}$), then protoplanets reach short-period orbits. This inequality leads to

$$M_{\rm pl} > \frac{0.91\, f_{\rm mig}\, M_\star^{3/2}}{\eta}\, M_\oplus\,. \tag{4.10}$$

This result yields the minimum mass for a planet to migrate to a close orbit. Substituting the isolation mass (eq. 4.7) for $M_{\rm pl}$ and solving for η gives a lower relative disk mass limit of

$$\eta > \eta_{\rm low} = \frac{2.2\, f_{\rm mig}^{2/5}}{M_\star^{1/10}\, \Delta^{3/5}}\,. \tag{4.11}$$

Disks more massive than this η form protoplanets massive enough to migrate to short-period orbits before the gas disk dissipates. Planets in slightly less massive disks still migrate, but are stranded at intermediate radii as the disk disperses.

The critical $\sim 10\, M_\oplus$ core mass for gas accretion provides an upper limit for the protoplanet mass. Solving $M_{\rm iso} < 10\, M_\oplus$ for η yields

$$\eta < \eta_{\rm hi} = \begin{cases} \frac{18.6}{M_\star^{7/6}\, \Delta} & \frac{18.6}{M_\star^{7/6}\, \Delta} < 30 \\ 30 & \frac{18.6}{M_\star^{7/6}\, \Delta} \geq 30 \end{cases}\,, \tag{4.12}$$

where the additional constraint of a reasonable disk mass sets $\eta \lesssim 30$ ($M_{\rm disk} \lesssim 0.3\, M_\star$) as an upper limit (e.g. Ida & Lin, 2005). Because we assume growth is

fast, planetesimal accretion drops significantly at later stages. The core mass for gas accretion is then somewhat smaller (Ikoma et al., 2000; Rafikov, 2006).

The two limits on disk mass yield a simple relation between the stellar mass, migration offset, and enhancement factor. Equating $\eta_{\rm low}$ and $\eta_{\rm hi}$,

$$M_{\star,\rm max} = \frac{7.3}{\left(f_{\rm mig}\,\Delta\right)^{3/8}} \tag{4.13}$$

in units of solar masses.[1] This equation has a simple physical interpretation. For massive stars ($M_\star > M_{\star,\rm max}$), the only protoplanets massive enough to migrate to the central star before the gas disk disperses are above the critical core mass for gas accretion. These planets therefore become gas giants, rather than forming hot super-Earths. For lower stellar masses, the closer snow line distance allows planets smaller than the critical core mass to migrate to the host star. Thus, $M_{\star,\rm max}$ is the maximum stellar mass for hot super-Earths produced by type I migration.

Making an estimate of $M_{\star,\rm max}$ requires an assumed $f_{\rm mig}$ and Δ. For solar metallicity $\mathcal{M} = 1$ and a cold-finger enhancement $f_{\rm ice} = 10$–20, $\Delta = 10$–20. For a migration offset $f_{\rm mig} = 10$, $M_{\star,\rm max} \sim 1\,M_\odot$. Transit and radial velocity surveys routinely probe these stellar masses. Independent of the disk mass distribution, this result is therefore a simple testable prediction of hot super-Earth formation by type I migration.

Figure 4.2 shows the range of planet masses that reach short-period orbits for a range of stellar masses. For the analytic model (*thick grey lines*) the upper limit is constant at $10\,M_\oplus$. The lower limit decreases as stellar mass and snow line distance decrease. The expected range of planet masses decreases with increasing stellar mass, while the average mass increases to $10\,M_\oplus$, where the lines meet at $M_{\star,\rm max} = 1.3\,M_\odot$.

In addition to this maximum stellar mass, we can derive the probability of forming hot super-Earths around stars with $M_\star < M_{\star,\rm max}$. This estimate requires an adopted distribution of η (i.e. disk masses). If relative disk masses ($M_{\rm disk}/M_\star$) are distributed as a power-law with index ~ -1.75 (Andrews & Williams, 2005), the (relative) probability of forming a close-in planet as a function of stellar mass for a given Δ is

$$P_{\rm p}(M_\star, \Delta) \propto \int_{\eta_{\rm lo}}^{\eta_{\rm hi}} \eta^{-1.75}\,d\eta\,. \tag{4.14}$$

Alternatively, disk masses may be distributed around some "typical" relative disk mass (e.g. Ida & Lin, 2005)

$$P_{\rm g}(M_\star, \Delta) \propto \int_{\eta_{\rm lo}}^{\eta_{\rm hi}} \exp\left(-\frac{(\log(\eta) - \mu)^2}{2\,s^2}\right) d\eta \tag{4.15}$$

[1] Equating (4.11) and (4.12) has two solutions for $M_\star$ because of the upper limit of 30. The other solution is at $M_\star$ far too small to be interesting.

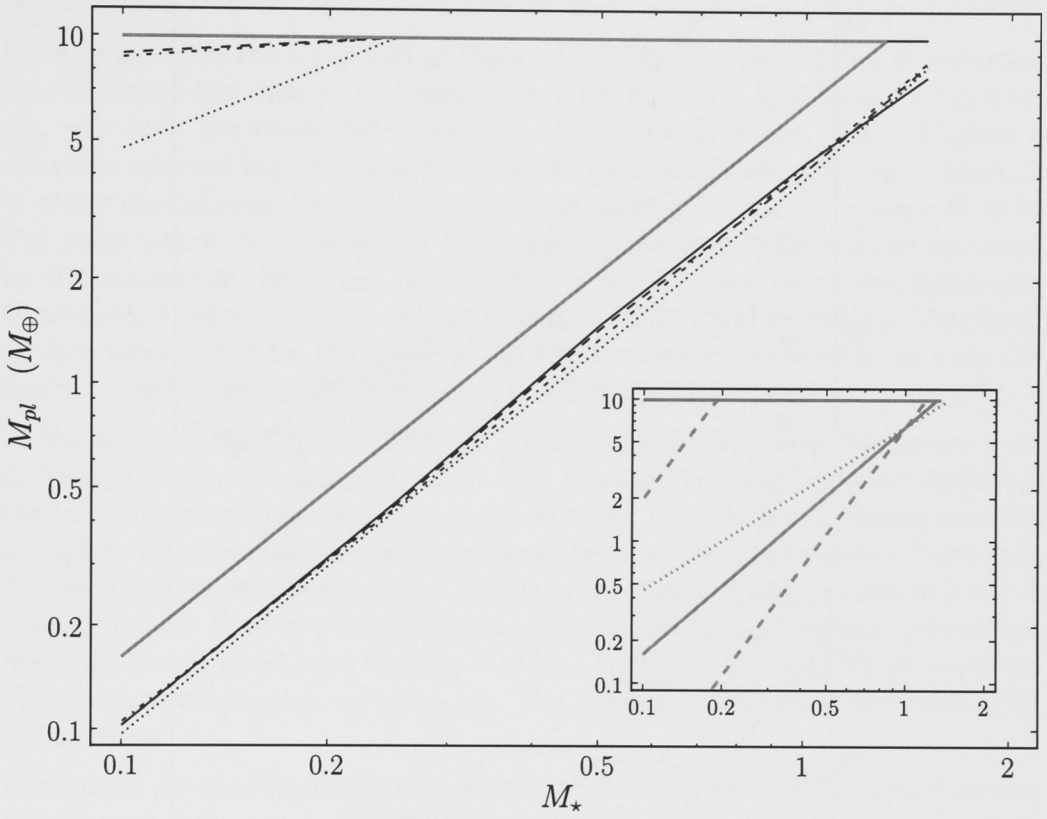

Figure 4.2 The range of planet masses that reach close-in orbits as a function of stellar mass. The thicker grey line line shows results from the analytic model using equations (4.7), (4.11), and (4.12). Other lines show upper and lower mass limits for a range of planetesimal sizes from the semi-analytic model (see §4.4.2) for $\Delta = 10$: $r = 10\,\mathrm{m}$ (*solid*), 100 m (dashed), 1 km (*dot-dashed*), and 10 km (*dotted*). The range of planet masses reaching short-period orbits decreases with increasing stellar mass because the snow line distance is greater. The inset panel (same axes) shows how different snow line relations affect the model (using $a_{\,\mathrm{snow}} = 2.7\,M_\star^{\alpha}$ AU). Lines are for $\alpha = 1/2$ (*dotted*), 1 (*solid*), and 2 (*dashed*) A more strongly varying snow line distance ($\alpha = 2$) yields smaller M_{iso} (due to smaller R_{H}) at much closer snow line distances as stellar mass decreases.

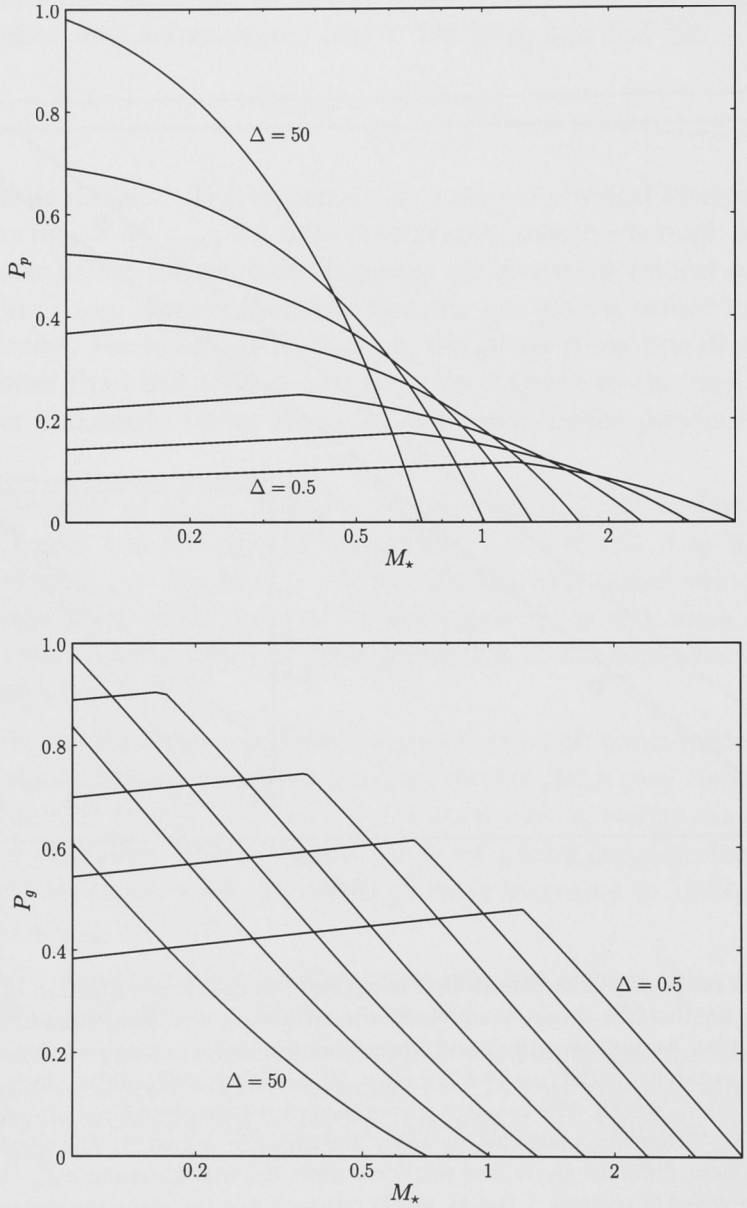

Figure 4.3 Probability distributions for power-law (*top*) and Gaussian with $\mu = 1$ (*bottom*) disk mass distributions of $\lesssim 10\,M_\oplus$ planets as a function of stellar mass. For $f_{\rm mig} = 10$, lines are for $\Delta = 0.5$, 1, 2, 5, 10, 20, and 50 from right to left where curves cross the x-axis. Thus $M_{\star,\rm max}$ decreases with increasing Δ and is independent of the disk mass distribution). Each plot is arbitrarily normalised to 1 for the most likely Δ at $M_\star = 0.1\,M_\odot$.

where we choose the standard deviation $s = 1$. This distribution is plausible because opacities may underestimate disk masses by as much as an order of magnitude, due to mass locked up in boulder size objects (Andrews & Williams, 2007). Therefore mm observations see disks not only with a range of masses, but in a range of evolutionary states. Unlike the case for giant planets, there is no observational anchor point, so we present these results as relative probabilities.

For a range of Δ, the top panel of Figure 4.3 shows the probability distribution for the power-law disk mass distribution with $f_{\rm mig} = 10$. Results are similar for $f_{\rm mig} = 1$, with the main difference that $M_{\star,\rm max}$ is higher (eq. 4.13). Higher Δ are most relevant here because low values describe MMSN disks, which result in many similar-mass migrating planets originating from a wide range of radii. The point where lines break and decrease toward lower stellar masses is caused by the maximum disk mass condition $\eta < 30$. In these cases the maximum short-period planet mass is not set by gas accretion and is $<10 M_\oplus$. This limit applies when $\Delta \lesssim 5$ for the lower of the stellar masses we consider, so does not apply to cold-finger disks with $f_{\rm ice} \gtrsim 10$ unless they have metallicity $\mathcal{M} \lesssim 0.5$.

At the lowest stellar masses, there is a clear increase in planet frequency with Δ. With a power-law distribution of disk masses, the most common disks are the least massive; these require large Δ to allow them to form planets massive enough to migrate (and satisfy condition 4.11). Near $M_{\star,\rm max}$, there is an optimum Δ, which is a balance between the likelihood of different disk masses and the Δ needed to form close-in planets from those disks. At $M_{\star,\rm max}$, the only planet that reaches a short-period orbit has $M_{\rm pl} = 10\,M_\oplus$. Therefore the range of short-period planet masses decreases up to $M_{\star,\rm max}$. The average planet mass increases with stellar mass.

The bottom panel of Figure 4.3 shows the probability distribution for the Gaussian distribution with $\mu = 1$. The most common disk mass is thus $\sim 0.1\,M_\star$. As Δ increases, the probability of forming a short-period planet decreases once the disk mass distribution is not truncated by the condition $\eta < 30$. In contrast to the power-law distribution, the low-mass disks requiring large Δ are uncommon. Thus, as Δ increases, isolation masses are pushed over the gas accretion mass, and the likelihood of forming close-in $\lesssim 10\,M_\oplus$ planets decreases. While the curves are different from the top panel, the point $M_{\star,\rm max}$ is the same for a given Δ. With $\mu = 0$ (i.e. distributed about $M_{\rm disk} = 0.01\,M_\star$) the probability distribution is qualitatively similar to the power-law disk distribution.

In summary, the simple analytical model yields testable predictions for an ensemble of super-Earths that migrate into short-period orbits from the snow line. For reasonable input parameters, we predict a maximum stellar mass $\sim 1\,M_\odot$ for stars with close-in super-Earths. If circumstellar disks tend to have similar snow line enhancements, this maximum mass decreases with the metallicity of the host star. For a range of stellar masses, the frequency of hot super-Earths depends on the initial distribution of disk masses. For a power-law (Gaussian)

distribution of disk masses, the model predicts more (fewer) hot super-Earths around more metal-rich stars.

To give the these trends some context, the first transiting low-mass planet orbits a star with sub-solar mass and metallicity (GJ436b, Gillon et al., 2007). The current sample of low minimum-mass planets also indicates a flatter metallicity distribution than exists for giant extra-solar planets (Udry et al., 2007). While both disk mass distributions suggest that low stellar mass host is likely, the power-law distribution argues against a low metallicity host. The Gaussian disk mass distribution, centred on a relatively high disk mass is consistent with an increasing giant planet frequency with metallicity and a flatter or decreasing frequency for lower mass planets.

Disks with $\eta > \eta_{\rm hi}$ form gas giants. Their relative probabilities can thus be calculated by integrating equations (4.14) and (4.15) from $\eta_{\rm hi}$ to 30. However, because $\eta_{\rm low}$ only weakly depends on $M_\star$, giant planet frequency is roughly some constant minus the hot super-Earth frequency (i.e. generally increases with $M_\star$). This trend is essentially the result arrived at by previous theoretical studies (e.g. Ida & Lin, 2005; Kennedy & Kenyon, 2008b) and is at least qualitatively consistent with the observed trend (Johnson et al., 2007a).

In constructing the above model we simplified some parameters and assumed values for others. We now briefly consider model sensitivity to these and whether observations may constrain them. The most uncertain simplification is how the snow line distance varies with stellar mass. Within our framework, relaxing the distance to $a_{\rm snow} = 2.7 M_\star^\alpha$ AU results in changes to Equations (4.12), (4.11), and (4.13) for $\alpha = 1/2$–2 (Fig. 4.2 inset). A more strongly varying snow line distance ($\alpha = 2$) yields much closer $a_{\rm snow}$ and smaller $M_{\rm iso}$ (due to smaller $R_{\rm H}$) for low mass stars. A more complex snow line model could include how $a_{\rm snow}$ varies with $M_{\rm disk}$ at fixed stellar mass, or some time dependence (e.g. Ciesla & Cuzzi, 2006; Kennedy & Kenyon, 2008b).

Another uncertain parameter is δ, the disk surface density power-law index. While we used $\delta = 3/2$, many models also consider $\delta = 1$. With $\delta = 1$, the main results of Figure 4.2 are unchanged, with stronger migration accounting for lower mass planets as the snow line distance decreases. It is unlikely observations of short-period super-Earths can constrain α or δ based on Figure 4.2, because they affect lower limits to planet masses, which will be hard to detect.

The efficiency of type I migration is also unclear. Our choice of $f_{\rm mig} = 10$ is based on numerical simulations, but may also be probed by future discoveries. The maximum stellar mass $M_{\star,\rm max}$ is not very sensitive to the snow line distance or disk profile, so for fixed snow line and metallicity enhancements (Δ), observations probe values for $f_{\rm mig}$.

Our final major assumption is that planets form rapidly and reach isolation before migrating. If planetesimals are small and growth is shear dominated, this assumption is generally true. With larger planetesimals however, growth is slower

and planets may leave their formation regions while still growing. Planetary growth and migration are then coupled and must be calculated simultaneously. Recently, Chambers (2006a,b) showed how a semi-analytic model of oligarchic growth can take different planetesimal sizes into account and estimate their effect on growth rates (see also Thommes et al., 2003; Brunini & Benvenuto, 2008). We now turn to a similar, yet simplified model to estimate the effects of planetesimal size on growth and migration.

4.4.2 Semi-Analytic Model

If planets grow fast enough, the isolation mass sets the range of disk masses that form migrating planets. If planetesimals are large enough, growth is not shear dominated and is slower. Migration then begins before planets reach isolation. To follow this evolution, a model treating concurrent accretion and migration is necessary. Our model tracks damping of planetesimal random velocities by gas drag and stirring by a growing protoplanet. The random velocities set how growth proceeds relative to migration, allowing comparison with the analytic model.

In the model, a single protoplanet of mass $M_{\rm pl}$ grows on a circular orbit from a planetesimal disk of small bodies of radius r. We adopt the accretion rate of Inaba et al. (2001) with the atmosphere enhanced accretion radius of Inaba & Ikoma (2003). To account for accretion of other nearby protoplanets, the growth rate is increased by 50% (Chambers, 2006b). Planetesimal random velocities are stirred by the growing protoplanet (Ohtsuki et al., 2002) and damped by gas drag (Inaba et al., 2001). The protoplanet accretes and stirs material within an annulus of half-width $4\,R_{\rm H}$ and undergoes type I migration at the rate derived by Tanaka et al. (2002), modified by the offset $f_{\rm mig}$. We use a ten times less efficient migration rate, motivated by numerical (D'Angelo et al., 2002, 2003; Masset et al., 2006a) and Monte-Carlo simulations (Ida & Lin, 2008). Objects have mass density $\rho = 1.5\,{\rm g\ cm^{-3}}$ outside the snow line. Simulations are started with planetesimals in an equilibrium between protoplanet stirring and gas drag. Because we consider growth only near the snow line (see below), planetesimals do not undergo radial motions due to gas drag. Planetesimals lost to gas drag can be returned to the growth region by the cold-finger mechanism (Cuzzi & Zahnle, 2004). The system is evolved using 4th order Runge-Kutta integration with an adaptive step-size (Press et al., 1992).

As before, we model protoplanets that form just outside the snow line. These are the largest objects that migrate to the central star in a cold-finger disk and are largely unaffected by interior objects. However, a migrating protoplanet shepherds material inward as it migrates and will accrete some terrestrial material. This accretion cannot be treated by the semi-analytic model, so protoplanets cease accretion once they pass inside the snow line in the semi-analytic model.

We model shepherding with n-body simulations in §4.4.3. We vary η to form 1–10 $M_\oplus$ planets and use $\Delta = 10$.

Protoplanets begin with masses $1 \times 10^{-4}\, M_\oplus$, at $4\, R_H$ outside the snow line. This starting condition allows them to reach isolation if growth is faster than migration. The disk is split into 1000 equally spaced radial bins. However, because accretion inside the snow line is turned off, objects grow from material in ~100 bins outside the snow line.

The snow line distance and gas disk are as in §4.4.1 (eq. 4.5 and following text), but the surface density of the gas disk decays exponentially with an e-folding time of 1 Myr. We place the inner edge of our disk at $0.2\, M_\star$ AU, though planets that reach a few tenths of an AU are migrating so rapidly that the exact value matters little.

To test our code, we compare growth at 5 AU with Figure 1 from Chambers (2006b). His figure compares isolation times for different r with the type I migration timescale. The smallest size planetesimals allow protoplanets to reach isolation before migration starts. Growth was simulated at 5 AU around a solar-mass star, with a solid surface density of 10 g cm^2 (so $M_{\rm iso} \approx 10\, M_\oplus$) and a gas/solids ratio of 90. Migration was not included and the isolation time was simply compared to the analytic estimate of Equation (4.3).

Figure 4.4 shows growth in the absence of migration at 5 AU around a solar-mass star for a range of r with similar initial conditions. The time to reach isolation is fastest for the smallest r (100 m), because growth is always shear dominated. For $r = 1$ km, the growing protoplanet excites the small body random velocities. Growth ceases to be shear dominated at several 10^3 yr. For higher r, isolation takes even longer, due to the decreasing effectiveness of gas drag on larger planetesimals. Compared with Figure 1 from Chambers (2006b), the time to reach $10\, M_\oplus$ is in good agreement. Our explicit calculation of eccentricities and inclinations accounts for differences in how growth proceeds (c.f. Fig. 3 of Chambers, 2006a).

Models with sufficiently small planetesimals reach isolation before migration. With $f_{\rm mig} = 1$, $r \lesssim 100$ m, and for $f_{\rm mig} = 10$, $r \lesssim 1$ km. Thus, even with a reduced migration rate, protoplanets may still migrate before isolation.

Semi-Analytic Model Results

For the range of disk masses (η) that forms 1–10 $M_\oplus$ planets around stars with masses 0.25–2 $M_\odot$, Figure 4.5 shows semi-major axis and mass evolution for $r = 100$ m. The choice of $1\, M_\oplus$ is somewhat arbitrary, but represents a rough lower limit for detection. We first describe the solar case and then look at differences as the stellar mass and r change.

For a solar mass star, growth is not always fast enough for migration to occur before the gas disk is dispersed. For $\eta = 2$, the objects Hill radii increase faster

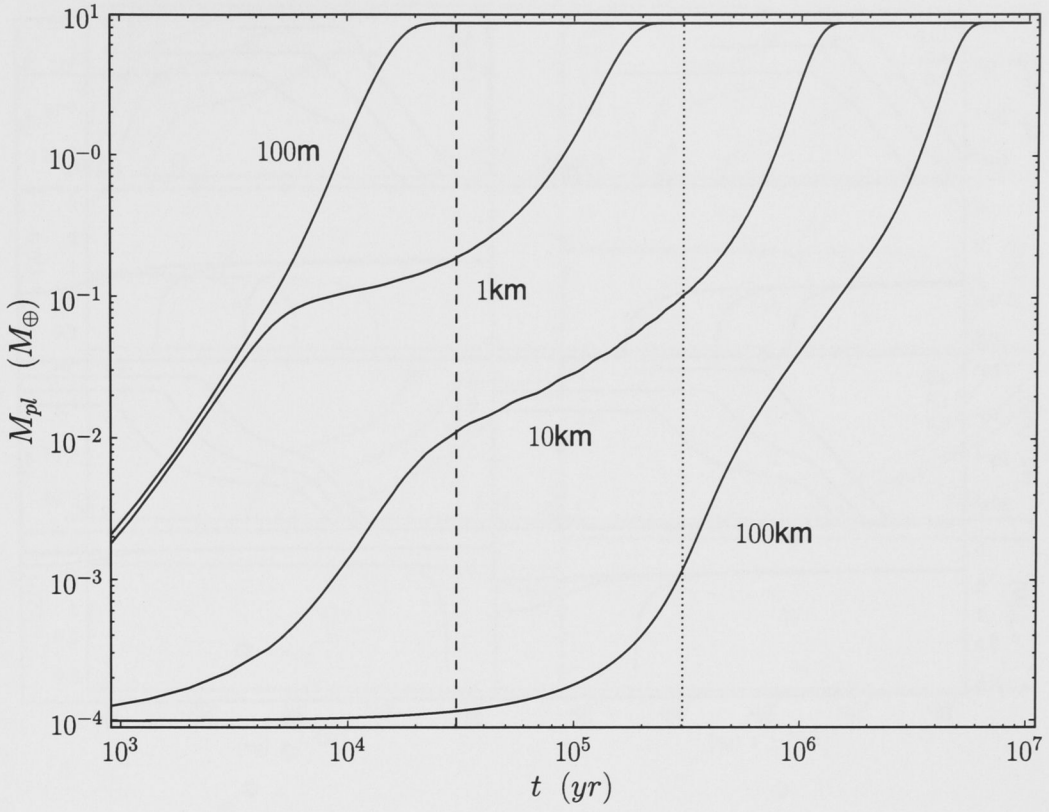

Figure 4.4 Growth to isolation of a protoplanet at 5 AU around a solar-mass star. Isolation times are in good agreement with Figure 1 of Chambers (2006b). Both models have $\sigma_0 = 10\,\mathrm{g\ cm^{-2}}$ and $\sigma_g = 900\,\mathrm{g\ cm^{-2}}$. Our model includes explicit calculation of planetesimal eccentricities and inclinations, which accounts for differences. Lines are for $r = 100\,\mathrm{m}$, 1 km, 10 km, and 100 km from left to right. The dashed (dotted) lines show the type I migration timescale for $f_{\mathrm{mig}} = 1$ (10).

than small bodies are stirred; thus growth remains shear dominated ($\tilde{e}, \tilde{i} \lesssim 1$). The protoplanet successfully migrates to the inner edge of the disk. For lower η, stirring overcomes damping at several $\times 10^3$ yr and growth slows. Higher η results in faster growth of larger objects, which migrate early enough to avoid stalling at intermediate radii. With $\eta = 1$, migration is somewhat significant and the $\sim 3\,M_\oplus$ planet stalls at ~1 AU due to dissipation of the gaseous disk. For $\eta = 0.5$, the Earth-mass planet migrates little and remains beyond the snow line. Final planet masses, and the degree of migration, are set by the initial surface density beyond the snow line.

We turn now to trends across a range of stellar masses. Because of smaller snow line distances, migration is easiest for planets in the 1–10 $M_\oplus$ range around lower mass stars. Low-mass stars are the most likely to form these planets, because the

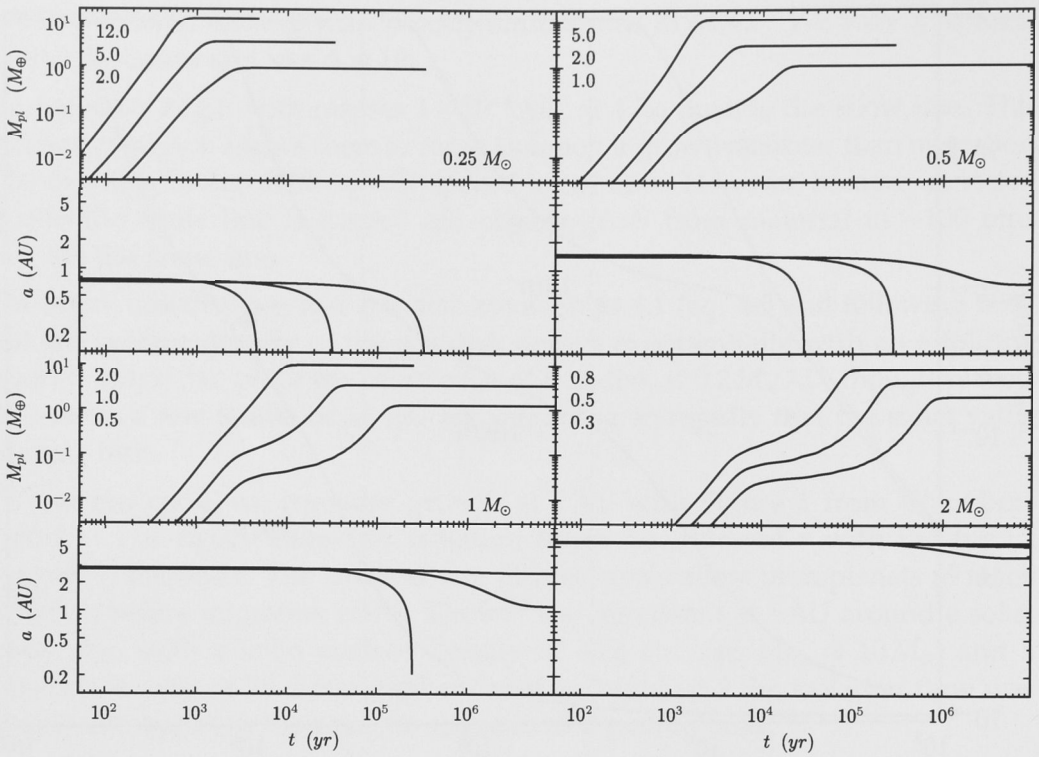

Figure 4.5 Results from the semi-analytic cold-finger disk model with $\Delta = 10$ and $r = 100\,\mathrm{m}$. Each vertical pair of panels shows mass and semi-major axis evolution for several relative disk masses. Higher disk masses (η in legends) form more massive planets that migrate earlier. All 1–10 $M_\oplus$ planets migrate to the inner disk edge for $0.25\,M_\odot$, while none do for $2\,M_\odot$.

range of disk masses that form them is much larger. For higher mass stars the more distant snow line makes migration unlikely for all but the most massive planets. Growth is driven out of the shear dominated regime more easily due to lower gas density at greater distances. This result confirms the maximum stellar mass $M_{\star,\mathrm{max}}$ described above. As in the analytic model, $M_{\star,\mathrm{max}}$ lies between 1–2 $M_\odot$ with $\Delta = 10$, because no planet with a mass $\lesssim 10\,M_\odot$ migrates significantly for $2\,M_\odot$. As stellar mass increases, the relative disk mass required to form 1–10 $M_\oplus$ planets decreases (eq. 4.7).

Figure 4.6 shows how growth changes if planetesimals are larger. Models again have $\Delta = 10$, but now the planetesimal radius $r = 10\,\mathrm{km}$. For larger planetesimals growth is easily stirred out of the shear dominated regime by the large objects for all stellar masses. The disk masses needed to reach the same range of planet masses are higher, because planets migrate out of the accretion region before they reach isolation. For $0.25\,M_\odot$ stars, the maximum $\eta = 30$ only just forms $10\,M_\oplus$ planets. Again, $M_{\star,\mathrm{max}}$ lies between 1–2 $M_\odot$, indicating that it is largely independent of planetesimal size. Though growth is slower, the results for

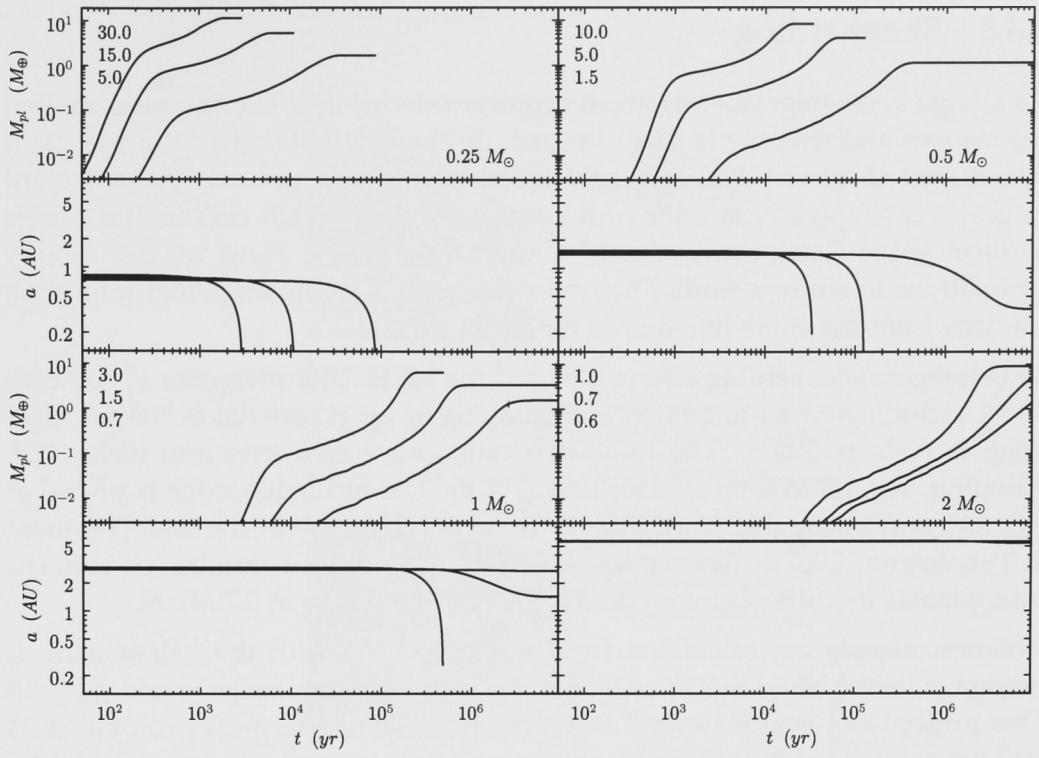

Figure 4.6 Same as Figure 4.5, but with r = 10 km. Protoplanets still reach 1–10 $M_\oplus$, but require much higher disk masses. Thus, results for protoplanets migrating to the inner disk edge are similar to the r = 100 m case.

r = 10 km are largely the same as 100 m, because the surface density can be increased to account for the slower growth.

Figure 4.2 also includes results from the semi-analytic model, showing the range of planet masses that reach short-period orbits for a range of stellar masses. Models were run for $\Delta = 10$, with r from 10 m to 10 km and $M_\star = 0.1$–$2M_\odot$. The upper limit decreases at 0.1 $M_\odot$ due to an upper limit on disk masses. Results from the analytic model are in good agreement. The difference in the lower limit arises because migration is faster at smaller radii, allowing smaller planets to reach the inner disk edge in the semi-analytic model.

In summary, using a more detailed migration model yields results similar to the simple analytic treatment in §4.4.1. The inclusion of growth rates due to different planetesimal sizes adds another dimension due to different relative timescales for migration and accretion. The model offers more insight into how growth proceeds and how the growth rate sets the required disk mass for forming short-period planets.

4.4.3 Shepherding

As a large body migrates inward, it captures interior objects onto mean motion resonances and shepherds them inward. In the original scenario, a gas giant forms near the snow line and subsequently migrates inward. As the giant migrates it shepherds interior protoplanets inward, which collide and merge to form super Earth-mass planets (Zhou et al., 2005). Here we use n-body simulations to study a similar scenario, but with a low-mass planet migrating inwards from the snow line due to type I migration.

To investigate shepherding effects, we used the MERCURY integrator (Chambers, 1999), including type I migration and damping forces (Cresswell & Nelson, 2006; Fogg & Nelson, 2007). The migration rate, and eccentricity and inclination damping, are reduced by a factor of $f_{\rm mig} = 10$. The inner disk edge is placed at 0.05 AU, and inside this point planets cease to interact with the disk (Terquem & Papaloizou, 2007). Simulations are initialised with a number of isolated protoplanets in a disk between 0.1 AU and the snow line at $2.7\,M_\star$ AU.

Isolation masses are calculated from Equation (4.7) with the half-spacing B randomly varied between 3.75 and 4.25. We assume solar metallicity and $f_{\rm ice} = 10$. One protoplanet begins beyond the snow line. This outermost protoplanet is $\approx$30 times more massive than the one immediately interior to it (eq. 4.2). Initial eccentricities (inclinations) are randomly distributed between 0 and 0.02 (0.5°) and the remaining orbital elements are randomly distributed. We set the mass of the outermost planet at the middle of the range shown for $M_\star = 0.25$, 0.5, and $1\,M_\odot$ in Figure 4.2; 2, 3.2, and $6\,M_\oplus$ respectively. Simulations are run for 10^8 yr with ~0.3 day time steps. Objects are allowed to collide and are assumed to merge into a single body with no fragmentation. These simulations do not include relativistic effects, or tidal interaction with the star. See Terquem & Papaloizou (2007) for a more detailed study of migration to small radii and how these effects affect final system dynamics.

Shepherding Results

Figure 4.7 shows the semi-major axis evolution resulting from these simulations. All show similar characteristics. Starting from the inner disk edge, a wave of chaotic growth moves outward (e.g. Chambers, 2001; Kenyon & Bromley, 2006), until the number of protoplanets is reduced such that their spacing is stable. This stability is set by a balance between mutual perturbations between protoplanets and damping by interaction with the gas disk.

When the outermost large protoplanet begins to migrate, it scatters the first objects it encounters into exterior orbits. When the interaction occurs, these objects are still undergoing eccentric chaotic growth and are less likely to be captured onto resonances and shepherded inward. Once scattered, the outer

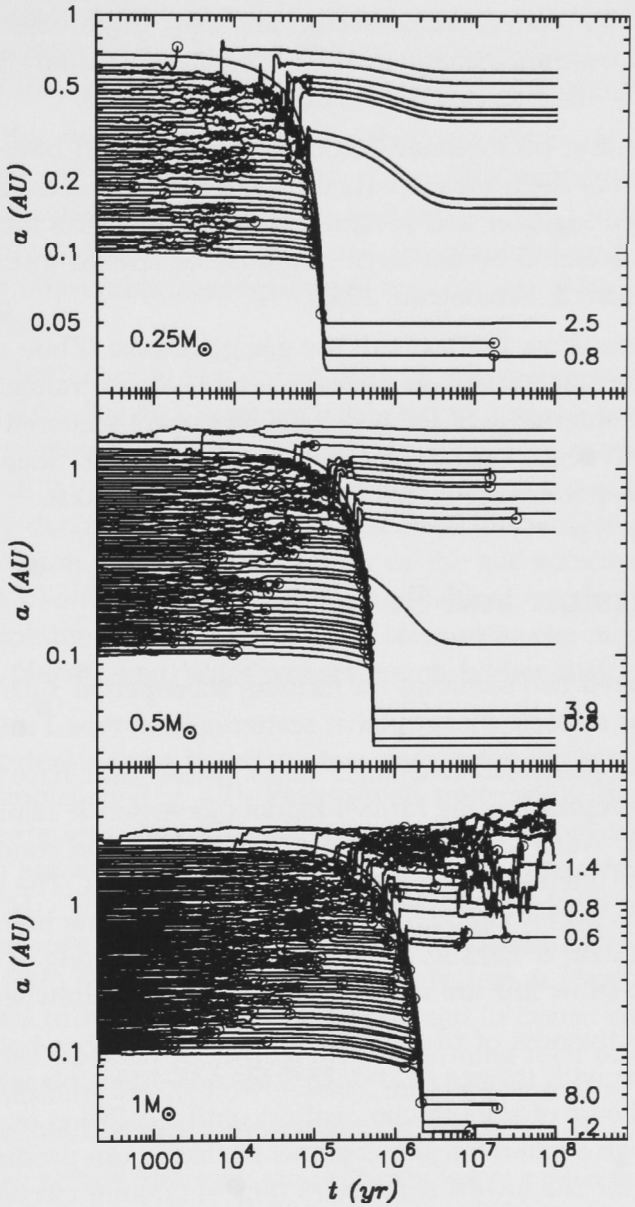

Figure 4.7 Migration of protoplanets in a cold-finger disk for 0.25, 0.5, and 1 $M_\odot$ (top to bottom). Initial outer planet masses are 2, 3.2, and 6 $M_\oplus$. Lines end in a ∘ when a collision occurs. Surviving planets more massive than 1 $M_\oplus$ are labelled by their final masses (in $M_\oplus$). Planets migrate earlier for lower stellar masses, because the snow line distance is closer. Objects scattered outward subsequently migrate and some resume chaotic growth. Shepherded objects merge as their orbits are pushed together by the larger migrating protoplanet.

objects slowly migrate inward. For 0.25 and $0.5\,M_\odot$ the scattered planets are still relatively close to the star and have time to set up chains of (mostly first order) resonant orbits. A few collisions occur. For $1\,M_\odot$ more objects are scattered outward, which continue chaotic growth. Despite the initial disruption by the migrating object, ~Earth-mass planets still form at ~1 AU.

When the migrating protoplanet encounters objects that have reached stable orbits, it shepherds them inward. These smaller objects accrete others as their orbits are pushed together and several $\sim 1\,M_\oplus$ rocky objects form. Shepherded objects may be accreted by the large migrator, or remain in interior resonant orbits (see Terquem & Papaloizou, 2007).

These simulations show that as with the gas giant case (Zhou et al., 2005), the effect of super-Earth migration on interior objects has observational consequences. Planets near the outer edge of the terrestrial region are scattered outward, while those in the inner region are shepherded to smaller radii. Shepherding results in multiple short-period planets with different compositions.

4.5 Discussion and Summary

We have considered two scenarios for forming short-period $\lesssim 10\,M_\oplus$ planets over a range of stellar masses: planet-planet scattering and type I migration.

Our models form planets in cold-finger disks. These disks have large snow line enhancements compared to the MMSN model (Stevenson & Lunine, 1988; Cuzzi & Zahnle, 2004). Water vapour from the terrestrial region condenses into ices outside the snow line as the gas disk diffuses and advects. The enhancement is increased by new water vapour delivered inside the snow line by drifting icy planetesimals (Cuzzi & Zahnle, 2004). Protoplanets forming in the cold-finger regions near the snow line are much larger than others elsewhere in the disk.

We test the effectiveness of planet-planet scattering with n-body simulations. We consider stars with masses $M_\star = 0.25$–$2\,M_\odot$ and $10\,M_\oplus$ planets. Planets with orbits near the limits of stability are evolved until a collision or ejection occurs, or 1 Gyr. Although equal mass planet-planet scattering can produce planets with small periastra for the lowest mass stars (Fig. 4.1), long circularisation times prevent them from achieving circular orbits on reasonable timescales. Thus, scattering is probably not a viable scenario for placing low-mass planets on short-period orbits for any stellar mass. For $0.25\,M_\odot$, planets have periastra ~0.05 AU and semi-major axes ~0.5 AU. Though transit durations are still several hours, orbital periods of several hundred days and maximum radial velocities of a few m s^{-1} make these planets hard to detect.

Migration of icy protoplanets from the snow line is a viable mechanism for forming short-period super-Earths. Planet masses set whether they migrate to the inner disk edge before the gas disk disperses. Some planets with insufficient

masses are stranded at intermediate radii as the gas disk disperses; a way to form "ocean planets" (Kuchner, 2003; Léger et al., 2004). The minimum protoplanet mass for migration to a close-in orbit increases as the snow line moves out with increasing stellar mass (Fig. 4.2). The maximum planet mass is $\sim 10\,M_{\oplus}$, because above this mass they instead accrete large atmospheres and form gas giants.

Above $\sim 1\,M_{\odot}$, the only protoplanets massive enough to migrate to close-in orbits are $\gtrsim 10\,M_{\oplus}$ and no hot super-Earths form. This maximum stellar mass is independent of the disk mass distribution and probes type I migration efficiency. Other uncertain parameters, such as snow line distance and disk profile do not have major observable consequences, but are not easily constrained by observations either.

For disks with similar snow line enhancements, the theory yields trends with metallicity (Fig. 4.3). For disk masses distributed as a power-law, the frequency of short-period planets increases with metallicity, because most disks have low masses. However, if disk masses are distributed around a relatively high mass, planet frequency decreases with increasing metallicity, because planets forming in the most common disks are pushed above the gas accretion mass at high metallicities. As planetesimal size increases, growth slows and becomes longer than the migration timescale. Simulations of concurrent accretion and migration with increased planetesimal sizes require much higher disk masses to yield similar results.

As icy planets migrate from the snow line, they interact dynamically with interior rocky protoplanets (Fig, 4.7). Protoplanets undergoing chaotic growth are scattered onto exterior orbits. Closer protoplanets on stable orbits damped by disk interaction are shepherded inward and coalesce into a few rocky objects with masses $\sim 1\,M_{\oplus}$. These objects may be accreted by the large migrating planet, or remain as separate planets on interior orbits. These orbits are likely near-commensurate with the icy migrators orbit (Terquem & Papaloizou, 2007). If planetary systems in such configurations are found in transit surveys, compositional models may discern differences, thus confirming their origins in rocky or icy regions (Valencia et al., 2007). However, different structural models may be degenerate if the planets have atmospheres (Adams et al., 2008).

Some planets may accrete hydrogen atmospheres due to a decreased planetesimal accretion rate following isolation (Ikoma et al., 2000; Rafikov, 2006). To be observed as hot super-Earths requires subsequent photoevaporation (e.g. Baraffe et al., 2005). Significant photoevaporation of planets with massive atmospheres is unlikely unless the planet mass is in the $\lesssim 70\,M_{\oplus}$ type I migration regime (Raymond et al., 2008). Thus, planets with remnant hydrogen atmospheres may form by the same migration mechanism we present here. Scattering is also a possibility for these planets to reach short-period orbits, because they have higher initial masses.

For planets originating in icy regions, their largely volatile composition has

important implications for their evolution during and after formation. Icy grains may enhance growth if they stick together more easily, but also allows the possibility of large evaporation events in high energy collisions of larger objects. During the violent accretion process and with the possible outcome of short-period orbits, melting and evaporation of ices will affect these planets (e.g. Lunine & Stevenson, 1982; Kuchner, 2003; Selsis et al., 2007).

After migrating to close-in orbits, initially icy/watery planets may retain large super-critical steam atmospheres, or become rocky cores stripped of volatiles entirely. Kuchner (2003) considered the existence of volatile-rich planets in the solar habitable zone and suggested that planets around solar luminosity stars would be safe from evaporation at $\gtrsim$1 AU but not at closer distances. He also noted that lower EUV luminosities for M dwarfs makes these stars less likely to evaporate planetary atmospheres. More recently, Selsis et al. (2007) revisited the issue and concluded that planets $\gtrsim 6 M_{\oplus}$ will retain most of their water content at $\gtrsim$0.04 AU from a solar-type star. The results of both studies suggest the evaporation timescale is strongly dependent on semi-major axis. Therefore, a trend may be noticeable within the small semi-major axis range of transiting planets.

The picture that emerges is of systems with evaporated rocky planets inside ~0.04 AU and steam planets somewhat outside this distance. A few stalled ocean (Kuchner, 2003; Léger et al., 2004) and icy planets extend through and past the habitable zone. For these planets, microlensing provides sensitivity complementary to transit and radial velocity methods at ~AU distances (e.g. Beaulieu et al., 2006), which will help yield trends with semi-major axis, particularly for low-mass stars.

Surveys such as the MEarth Project (Nutzman & Charbonneau, 2008), CoRoT (Baglin, 2003), and Kepler (Borucki et al., 2003) hope to discover super-Earths by the transit method. Like those discovered by radial velocity, most planets will orbit close to their parent stars. Because they are unlikely to form *in situ*, these planets necessarily require some form of migration or scattering from their formation regions. Observed systems will thus test and inform mechanisms that form and bring planets to visible orbits.

We acknowledge support from an Australian Postgraduate Award, a Smithsonian Astrophysical Observatory pre-doctoral fellowship (GK), and the *NASA Astrophysics Theory Program* through grant NAG5-13278 and the *TPF Foundation Science Program* though grant NNG06GH25G (SK). We thank the anonymous referee for a prompt report, which improved the content of the paper. *N*-body simulations were run on computers maintained by the RSAA Computer Section at Mt Stromlo Observatory.

CHAPTER 5

STELLAR MASS DEPENDENT DISK DISPERSAL

Kennedy & Kenyon (2008c)

Abstract

We use published optical spectral and IR excess data from nine young clusters and associations to study the stellar mass dependent dispersal of circumstellar disks. All clusters older than ~3 Myr show a decrease in disk fraction with increasing stellar mass for solar to higher mass stars. This result is significant at about the $1\,\sigma$ level in each cluster. For the complete set of clusters we reject the null hypothesis—that solar and intermediate-mass stars lose their disks at the same rate—with 97% confidence. To interpret this behaviour, we investigate the impact of grain growth, binary companions, and photoevaporation on the evolution of disk signatures. Changes in grain growth timescales at fixed disk temperature may explain why early-type stars with IR excesses appear to evolve faster than their later-type counterparts. Little evidence that binary companions affect disk evolution suggests that photoevaporation is the more likely mechanism for disk dispersal. A simple photoevaporation model provides an excellent fit to the observed disk fractions for solar and intermediate-mass stars. Although the current mass-dependent disk dispersal signal is not strong, larger and more complete samples of clusters with ages of 3–5 Myr can improve the significance and provide better tests of theoretical models. In addition, the orbits of extra-solar planets can constrain models of disk dispersal and migration. We suggest that the signature of stellar mass dependent disk dispersal due to photoevaporation may be present in the orbits of observed extra solar planets. Planets orbiting hosts more massive than $\sim 1.6\,M_{\odot}$ may have larger orbits because the disks in which they formed were dispersed before they could migrate.

5.1 Introduction

Most known extra-solar planets orbit roughly solar-mass stars; the result of observational biases towards these stars in planet hunting surveys. Recently, planets orbiting both low and intermediate mass stars have been discovered (e.g. Rivera et al., 2005; Johnson et al., 2007b), thus increasing the diversity of planet host stars. In parallel, there have been various models proposed that attempt to explain and predict the frequency and properties of these planets as a function of stellar mass (Ida & Lin, 2005; Kornet et al., 2006; Burkert & Ida, 2007; Kennedy & Kenyon, 2008b).

These models need observational constraints, which are provided in two ways. The observed properties of the planets yields one set of constraints, setting the final distributions that models must reproduce. These distributions contain trends such as an increasing planet frequency with increasing stellar metallicity (Fischer & Valenti, 2005). However, because planets are observed around main-sequence stars, these constraints provide no direct information about the circumstellar environment during the 1-100 Myr epoch of planet formation.

Planets form in circumstellar disks, and observations of these disks yield another set of constraints. These constraints are used as model parameters. For example, disks are made up of gas and dust, and in many cases have enough material to form planetary systems with planets as massive as our solar system (e.g. Natta et al., 2000; Andrews & Williams, 2005). Of these constraints, the strongest is the observed disk lifetime. The disk dispersal timescale sets the time taken for dust to grow into ~Earth-mass objects and accrete gas to form giant planets.

The timescale for disk dispersal is inferred from dust and/or gas signatures. The fraction of stars with disks in clusters of roughly coeval young stars decreases with increasing age, yielding the typical lifetime of circumstellar disks. The disk lifetime is usually derived from the dust signature (e.g. Haisch et al., 2001b), with the assumption that the gaseous component follows the same evolution. This assumption is probably well founded, based on a general agreement between dust and accretion signatures (e.g. Kenyon & Hartmann, 1995; Lada et al., 2006).

For gas giant formation, the disk lifetime is the strongest observational constraint, and therefore any stellar mass dependence on disk lifetime should be included in planet formation models. Burkert & Ida (2007) show this dependence is important, using it to reproduce a "valley" in the period distribution of planets orbiting stars $>1.2\,M_{\odot}$.

With new discoveries of planets orbiting M-dwarfs and K-(sub)giants, further trends with stellar mass are emerging. The frequency of giant planets appears to increase with stellar mass (Butler et al., 2006; Johnson et al., 2007a). Also, all planets around stars with masses $>1.6\,M_{\odot}$ have larger (~1 AU) orbits than solar-mass stars (Johnson et al., 2007b; Sato et al., 2008a,b). As with the valley

described by Burkert & Ida (2007), the larger orbits may be caused by changing disk dispersal timescale with stellar mass.

Recent Spitzer surveys of young clusters have started to reveal observational evidence of stellar mass dependent disk dispersal: stars with spectral types earlier than about mid-K appear to lose dust signatures earlier than their lower mass counterparts (Carpenter et al., 2006; Currie, 2008; Hernández et al., 2007; Dahm & Hillenbrand, 2007). This effect has also been demonstrated with higher mass Herbig Ae/Be objects in a number of OB associations (Hernández et al., 2005). Thus, there may be observational evidence for the stellar mass dependent disk dispersal used in the Burkert & Ida (2007) models.

In this paper, we look for evidence of mass dependent disk dispersal and its evolution using Hα equivalent widths (EW[Hα]) and infra-red (IR) excesses in nine ~1–10 Myr old clusters and regions. We also compare the disk lifetime inferred from the two signatures, which probe the different components of circumstellar disks. We find that disks around higher mass stars tend to disperse earlier than solar mass stars for all clusters older than ~3 Myr. Using all cluster data, we reject the null hypothesis—that disk dispersal is independent of stellar mass—with 97% confidence. The statistical significance of any mass dependence for individual clusters is not strong, at around the 1 σ level. Using a photoevaporation model, we show why the signal may be intrinsically weak. We suggest where future observations can make the most progress towards making our result more significant. Finally, we return to our motivation and study some possible effects that stellar mass dependent disk dispersal may have on giant planet formation. We suggest that mass dependent disk dispersal may have an observational signature in the semi-major axes of discovered planets.

5.2 Background

Nearly all stars begin their lives with circumstellar disks of gas and dust (e.g. Lada et al., 2000). The disks have typical radii of 10-1000 AU (e.g. McCaughrean & O'Dell, 1996) and masses ~0.01–0.1 $M_\star$ (e.g. Natta et al., 2000; Andrews & Williams, 2005). Assuming the typical interstellar gas/solids ratio of 100, many disks have material sufficient to build planetary systems like our solar system.

Observational probes of disk structure are very sensitive to physical conditions within the disk (e.g. Najita et al., 2007). The disk temperature decreases with distance from the central star, ranging from ~ 10^3 to 10^4 K close to the star, to 10–50 K at larger distances.

At large ($\gtrsim$10 AU) distances, beyond where planets form, cool gas and dust can be detected through IR and mm observations. Direct detection of the main gaseous component, H_2, is difficult, so gas disks are inferred from molecular components such as CO. At all radii, dust is generally inferred from thermal

emission, where detection at longer wavelengths corresponds to cooler dust at greater distances. For outer disks, the relevant wavelength for dust emission is in (sub)mm bands.

For inner disks ($\lesssim$10 AU), where planets probably form, temperatures and densities are much higher. Direct detection of H_2 is still difficult. Gas is usually inferred from evidence of accretion onto the central star. The most commonly used (and easiest to measure) accretion signatures are greater than expected UV flux or EW[Hα]. These signatures are caused by shocking/heating of the gas as it accretes onto the star (e.g. Calvet & Gullbring, 1998; Muzerolle et al., 2001).

The dusty component of the inner disk is detected by an excess of IR emission above the expected photospheric level. The IR excess is commonly characterised by colour-colour diagrams, where disks are inferred for objects with redder than photospheric colours. Alternatively, the shapes of spectral energy distributions (SEDs) may be used, where disks are inferred for objects with greater than photospheric SEDs.

Generally, dust and gas signatures are observed to agree for young stars. Models suggest that although grains may settle and grow beyond visible sizes, turbulence and fragmentation ensure the presence of small grains that remain well mixed with the gas (Dullemond & Dominik, 2005; Johansen et al., 2008). Therefore, though disk lifetimes are commonly inferred from dust signatures, there is observational and theoretical evidence that this method is valid.

There are, however, examples of objects where gas and dust signatures disagree. Many main-sequence stars show weak mid and far-IR excesses, but no sign of circumstellar gas. These "debris disks" are a separate class of objects, thought to arise from collisions in remaining planetesimal belts (e.g. Kenyon & Bromley, 2004a). Around 10% of stars in young clusters are seen to have little or no excess in the near-IR, but large excesses in mid-IR bands (e.g. Sicilia-Aguilar et al., 2006b; Lada et al., 2006). These objects are though to be currently in "transition" between the primordial and debris disk states, with an inner hole as the disk starts to clear.

Early studies of disk populations in young clusters found a disk dispersal timescale of ~4–5 Myr (Haisch et al., 2001b; Mamajek et al., 2004). These studies find somewhat longer disk lifetimes at longer wavelengths (i.e. greater distances). This result is unsurprising in the context of grain growth, because the growth timescale is proportional to the orbital period. Recent Spitzer surveys have confirmed these timescales with larger stellar samples.

Increased sample numbers have also allowed the study of how disk lifetime depends on stellar mass. Studies generally find that the fraction of stars with disks at a given age changes with the mass of the host star (Hernández et al., 2005; Carpenter et al., 2006; Lada et al., 2006; Hernández et al., 2007; Dahm & Hillenbrand, 2007; Luhman et al., 2008). While nearly all studies find evidence that higher mass stars lose their disks earlier than solar mass stars, these results

are not statistically compelling. In addition, Carpenter et al. (2006) and Currie (2008) find that of objects with IR excesses, earlier-type stars appear to be in a more evolved state, with smaller IR excesses relative to the stellar photosphere.

Differences in disk evolution with stellar mass are theoretically expected. For different stars, observations at fixed wavelength probe different parts of a circumstellar disk. Because the disk temperature decreases with distance from the star, thermal emission at longer wavelengths probes greater distances. for higher stellar luminosities, regions of fixed temperature (and wavelength) are at greater distances. Evolutionary timescales such as grain growth depend on properties such as orbital frequency and gas density, which decrease with radial distance from the star. Thus, the same wavelength will not necessarily find a disk in the same evolutionary state for different stars.

Aside from regions probed by wavebands, more obvious processes exist that may change the rate of disk evolution with stellar mass. Disks may experience accelerated photoevaporation due to the local environment (Adams et al., 2004; Balog et al., 2006) or the increased temperature and luminosity of higher mass host stars (Burkert & Ida, 2007). For low-mass stars, the effects of the local environment may be more important. These conditions are different for every star in every cluster and thus make the presence of global trends for low-mass stars unlikely. In the case of photoevaporation by the host star, the expected evolution should result in higher mass stars dispersing their disks earlier, leading to differences in disk fractions for different mass stars at fixed age. Transition objects can also be understood in terms of a photoevaporation model, where viscous evolution and ionising photons from the central star combine to remove the disk in an inside–out manner (e.g. Clarke et al., 2001).

To study how disk dispersal depends on stellar mass, we compile a sample of clusters from the literature in §5.3. To derive disk fractions, we use IR excesses and EW[Hα]. Though these signatures generally agree, we use both to look for any systematic changes with cluster age. We first compare the results for overall cluster fractions, comment on possible effects of stellar multiplicity in §5.3.1, and study the stellar mass and spectral type dependence in §5.3.2. Comparing solar and intermediate-mass stars, we find evidence for a stellar mass dependence; at about the $2\,\sigma$ level overall and about $1\,\sigma$ for individual clusters.

In §5.4, we consider different physical mechanisms that may cause the mass dependence. We first consider grain growth in different wavebands. Then, using a simple photoevaporation model we suggest why the mass dependence has low statistical significance. We argue that an alternative hypothesis, the increasing multiplicity fraction with stellar mass, is an unlikely cause for mass dependent disk dispersal.

Finally, we return to the initial motivation for studying disk evolution and consider some consequences of our results for giant planet formation in §5.5. We suggest that there may be a signature of stellar mass dependent disk dispersal

in the observed orbits of extra-solar planets. If the disk dispersal timescale decreases with increasing stellar mass and the migration timescale is constant or increases, then above some stellar mass planets will not have time to migrate before the disk disperses. This effect may cause the observed outward step in giant planet orbits to ~1 AU above $1.6\,M_{\odot}$.

5.3 Cluster Data

We select nine well studied clusters and regions from the literature. To cover a range of disk fractions, our aim is to have clusters with EW[Hα]from optical spectra, 3.6–8 μm photometry from the Spitzer Infra-Red Array Camera (IRAC), and ages spaced in log time between 1–10 Myr. Because we want a reasonable number of stars over a wide stellar mass range, many of our clusters are part of OB associations.

The clusters are: Taurus (Furlan et al., 2006), Chamaeleon I (Luhman, 2004; Luhman et al., 2008), IC 348 (Luhman et al., 2003; Lada et al., 2006), Tr 37 (Sicilia-Aguilar et al., 2005, 2006a,a), Upper Scorpius (Preibisch et al., 1998; Preibisch & Zinnecker, 1999; Preibisch et al., 2002; Walter et al., 1994; Carpenter et al., 2006), NGC 2362 (Dahm & Hillenbrand, 2007), Orion OB1bc and OB1a/25Ori (OB1b and OB1c members combined, and OB1a including 25 Ori objects, Briceño et al., 2005; Hernández et al., 2005; Briceño et al., 2007; Hernández et al., 2007), and NGC 7160 (Sicilia-Aguilar et al., 2005, 2006b). These clusters populate the 1–10 Myr age range fairly well when viewed logarithmically. There is a gap between 2–4 Myr, which is nicely occupied by NGC 2264 (Rebull et al., 2002). Though some data are available (Young et al., 2006), the bulk of Spitzer IRAC photometry for this cluster are unpublished.

To distinguish between stars with and without disks, we use two standard measures: EW[Hα] and IR excesses. When high resolution data are available, we use the spectral type independent criterion of 10% Hα width > 270 km s^{-1} to distinguish accreting (CTTS) and non-accreting (WTTS) stars. For the more common low resolution spectra, we use the spectral-type dependent accretion criterion of White & Basri (2003), which accounts for different chromospheric levels of Hα for different spectral types. We add a lower threshold of EW[Hα] > 0 for early-type stars <G9 (theirs is EW[Hα] > 3 $\dot{A}$ for all stars <K6), an approximate effective temperature where main-sequence dwarfs start to show Hα in absorption (e.g. Castelli & Kurucz, 2003; Hernández et al., 2005). We refer to objects with excess EW[Hα] as accretors. The disk fraction thus derived is the "accretion fraction."

To provide a measure of the IR excess from a dust disk, we use the slope of the SED, defined by $\alpha = \mathrm{d}\log \lambda F_{\lambda}/\mathrm{d}\log F_{\lambda}$ (e.g. Adams et al., 1987; Lada et al., 2006). Most young stars have relatively shallow or flat SEDs ($\alpha \gtrsim -2$) that

are easily distinguished from the steep SEDs of the typical stellar photosphere ($\alpha \lesssim -2.5$). Thus, the slope of the SED is a simple way to distinguish stars from disks. To take advantage of the large spatial coverage of most Spitzer surveys, we use IRAC data to derive α for stars with data in all four bands ([3.6], [4.5], [5.8], and [8]). Magnitudes are de-reddened using the relation derived by Indebetouw et al. (2005). For Upper Sco, we use the slope between [4.5] and [8] from Carpenter et al. (2006), which generally agrees with their 8 μm disk classification. For intermediate-mass HIP objects in Orion OB1bc, we use the JHK disk classification from Hernández et al. (2005).

Figure 5.1 shows de-reddened IRAC SED slopes for our cluster sample. There is a clear divide between objects with and without disks for the youngest clusters, Taurus and Cha I. The separation between objects with and without disks is least clear for IC 348: the IR fraction varies between 30% for $\alpha = -1.8$, to 57% for $\alpha = -2.6$. This variation results from a decreasing median SED slope with cluster age and/or the presence of transition objects (see below), which make the divide less clear for older clusters (e.g. Hernández et al., 2007). For a brief discussion of the limitations of using the SED slope, see Dahm & Hillenbrand (2007).

Based on Figure 5.1, we choose $\alpha > -2.2$ to distinguish between stars with and without disks. Our results do not vary significantly for reasonable range ($-2.6 < \alpha < -1.8$). We do not distinguish between stars with "weak" or "anaemic" disks (e.g. Lada et al., 2006) and those with photospheric SED slopes. The disk fractions thus derived are termed "IR fractions."

Requiring a star to have both accretion and dust indicators ensures a robust classification of objects with primordial disks. However, this constraint precludes any check on whether the dusty and gaseous components evolve together and reduces our sample numbers considerably. Thus, we consider accretion and IR indicators individually and compare the results to those for disks with both signatures.

Before analysing the cluster data in detail, we first consider overall disk fractions for each cluster. To provide data at 3 Myr, we include results from NGC 2264 for this figure only. The IR fraction for this cluster is derived from the I-K colour (Rebull et al., 2002). Though the I-K disk indicator is at shorter wavelengths, it gives a rough estimate of the disk fraction that we expect from Spitzer IRAC data.

Figure 5.2 shows disk fractions derived from the overall cluster data. Disk fractions decay from ~70% at 1 Myr to 5–10% by ~5–10 Myr. Tr 37 has a relatively high IR fraction (~50%) for its age; however, this fraction is not unreasonably high given the scatter observed for other clusters. Though the systematic uncertainty in ages is a few Myr, ranking the clusters by their disk fractions yields nearly the same order as ranking the clusters by their ages. Clusters lose most of their disks in ~5 Myr, with a small fraction retaining disks to ~10 Myr. Disk fractions from

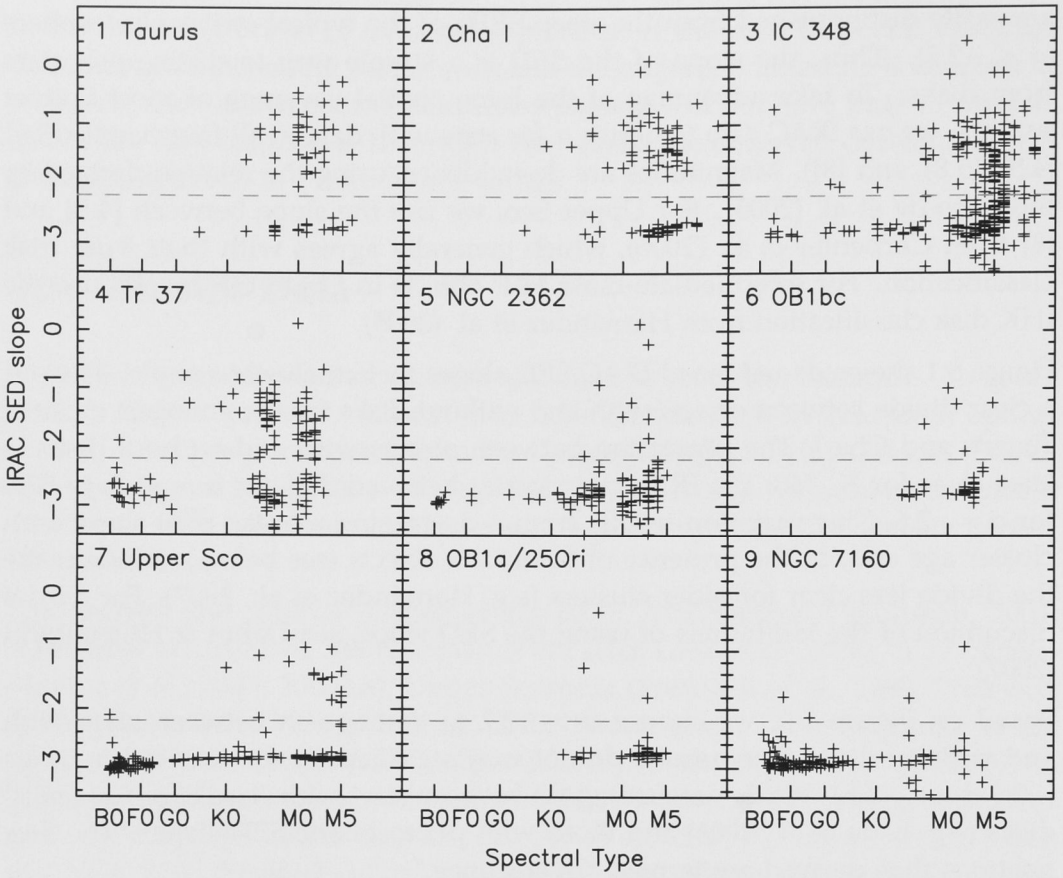

Figure 5.1 IRAC SED slopes for objects with spectral types. The x-axis is expanded toward later spectral types for clarity. Based on these data, we use a slope of $\alpha > -2.2$ (*dashed line*) to distinguish between stars with and without dust disks. Orion OB1bc lacks SED slopes for intermediate mass stars because their disk classification is based on JHK-excesses Hernández et al. (2005).

IR excesses and EW[Hα] generally agree (bottom panel of Fig. 5.2), showing that decay timescales for the gaseous and dusty components are similar.

5.3.1 Binary and Multiple Systems

The disks of stars in binary systems evolve differently from those around single stars. A companion star truncates the circumstellar disk, shortening the disk lifetime. The extent to which the disk is truncated depends on the separation and mass ratio (e.g. Papaloizou & Pringle, 1977; Armitage et al., 1999). Circumbinary disks may also be present. Therefore, the extent to which a binary companion dominates disk evolution is set by the parameters of each individual system.

Given the natural range of mass ratios and separations, disk dispersal in binary

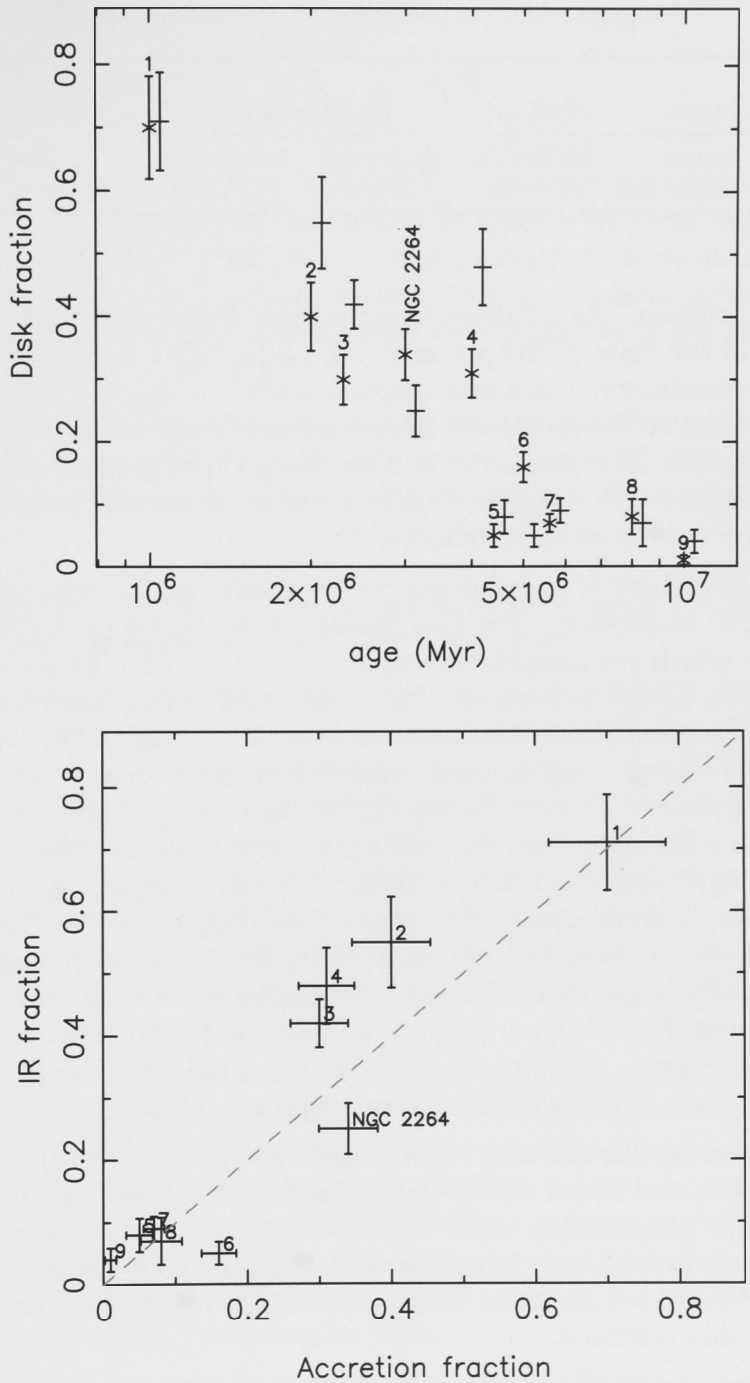

Figure 5.2 Overall cluster accretion (×) and IR-fractions (+), as a function of cluster age (*top*), and compared (*bottom*). For clarity, IR fractions are offset slightly right of adopted cluster ages, Upper Sco is offset right and NGC 2362 to the left of 5 Myr. In the bottom panel, equal fractions lie on the dotted line. Errors are Poisson ($\sqrt{N}$) estimates and the systematic error in age is a few Myr (e.g. Haisch et al., 2001b).

Table 5.1 Disk fractions for single and multiple stars.

	Single		Multiples	
Name	EW[Hα]	IR	EW[Hα]	IR
Taurus	40/55=72%	42/55=76%	33/50=66%	37/50=74%
Upper Sco	2/49= 4%	2/53= 3%	2/37= 5%	1/42= 2%

systems is complex. As a further complication, the occurrence of binaries is a function of the mass of the primary (e.g. Lada, 2006). Thus, for some fixed separation distribution, disks may disperse earlier on average for higher mass stars, depending on the prevalence of circumbinary disks for the closest systems. If enough systems have close orbits and the change in binary fraction with stellar mass is strong enough, this process may cause an observable difference in disk fractions over a range of stellar masses.

To look at the effects of companions, we construct two subsamples of objects with "known" multiplicity. The first consists of the Furlan et al. (2006) Taurus sample, for which we compare multiple systems with the balance of objects. Multiplicity in Upper Sco has also been well studied (e.g. Levato et al., 1987; Shatsky & Tokovinin, 2002; Kouwenhoven et al., 2005, 2007a). We collect binary and multiple objects observed and compiled by Kouwenhoven et al. (2007b), objects flagged as X, O, or G in the Hipparcos catalogue (see Kouwenhoven et al., 2007b), and objects from the Catalog of Components of Double & Multiple stars (CCDM) (Dommanget & Nys, 2002).[1] We then compare the disk fraction of systems to all other Upper Sco objects with Hipparcos identifiers. Due to the aforementioned bias, the real multiplicity fraction in both associations is almost certainly larger than observed. For higher mass stars, such as the BA-type Hipparcos stars in Upper Sco, the multiplicity fraction may be near unity (Kouwenhoven et al., 2007b). There are too few objects to make any useful comparison of the effect of different companion separations.

Table 5.1 shows the disk fractions of single and binary objects for our two samples. For both Taurus and Upper Sco there is no apparent difference in disk fractions between single and multiple stars. In other samples, binaries with separations $\gtrsim$20 AU appear to have little impact on disk lifetime and evolution (e.g. Monin et al., 2007; Pascucci et al., 2008). Thus, we conclude that binaries do not impact our derived disk fractions.

Exploring the possible impact of multiplicity on disk evolution merits further study. Samples with a large range in separation and primary mass are needed to study the possible implications for stellar mass dependent disk dispersal. However, based on the results of Table 5.1 and other observational studies (Furlan et al., 2006; Monin et al., 2007; Pascucci et al., 2008), we do not exclude

[1]Vizier catalogues: Hipparcos I/239/hip_main; CCDM I/274/ccdm

known multiple systems from our sample.

5.3.2 Stellar Mass Dependence

We now use our clusters to look for stellar mass dependent disk dispersal. In each cluster we split stars into bins defined by spectral type and stellar mass and examine the resulting disk fractions. We first qualitatively study the data and find that some stellar mass dependence appears for solar and intermediate-mass stars. We then focus on these stars and quantify the significance of the dependence in several independent ways.

To obtain the additional information required to analyse each object in our database, we obtain spectral types and extra photometry from Simbad[2] and Vizier.[3] Where needed, we calculate extinction using the dwarf colours of Kenyon & Hartmann (1995) and conversions from Bessell & Brett (1988) and Cardelli et al. (1989). We exclude objects with no spectral type. For all possible stars, we derive effective temperatures from the spectral type (Kenyon & Hartmann, 1995) and luminosity using de-reddened J or I magnitudes.

We begin by showing HR diagrams for the stars in our clusters in Figure 5.3. For most clusters, stars appear reasonably evenly distributed in mass. Orion OB1bc is a notable exception: the CIDA variability study of Orion (Briceño et al., 2005) was limited to lower mass stars, apparently due to CCD saturation for brighter objects. There is a marked gap between these objects and the higher mass Hipparcos objects studied by Hernández et al. (2005). Many of the higher mass stars in the Dahm & Hillenbrand (2007) NGC 2362 sample lack spectral types. Some deficiency of ~G-type objects is also expected due to stellar evolution, when ~solar-mass stars develop a radiative core and move to the main-sequence at roughly constant luminosity.

Figure 5.3 also identifies stars with IR excesses (grey dots). The decline in overall disk fraction with cluster age can be seen in the change from mostly grey to nearly all black (no disk) data points. For the youngest clusters, stars with and without disks appear evenly distributed. For older clusters, however, stars with disks have a marked spatial dependence on where stars lose their disk. Although many low mass stars in Tr 37 have disks, there are no stars with $\log T_{\rm eff} > 3.8$ (or $\log L_\star/L_\odot > 1$) with disks. Other clusters have a similar, but less obvious, lack of disk signatures among more massive stars.

To quantify how the disk fraction changes with stellar mass or spectral type, we bin the data. Some previous studies bin objects by their spectral type (e.g. Carpenter et al., 2006; Hernández et al., 2007). However, for the wide range of stellar masses we consider, pre–main-sequence (PMS) tracks have different loci

[2]http://simbad.u-strasbg.fr/simbad/
[3]http://webviz.u-strasbg.fr/viz-bin/VizieR

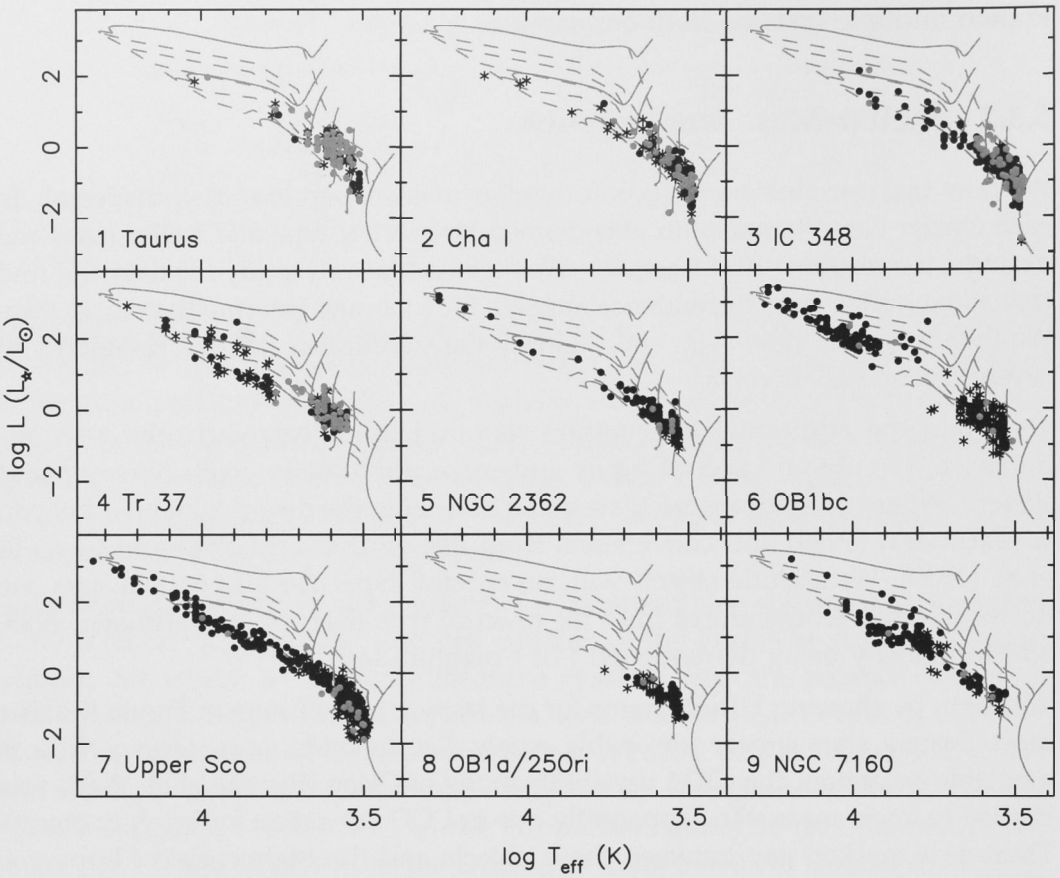

Figure 5.3 HR diagrams of objects with (*grey filled circles*), and without (*black filled circles*), IR excesses in our clusters. Objects without IR classification (which may be CTTS/WTTS) are marked by *'s. Grey lines show Siess et al. (2000) PMS tracks for 0.1, 0.3, 0.6, 1.5, 3, and 7 $M_{\odot}$ stars (*solid lines*) and isochrones for 0.1, 0.5, 1, 2, 5, and 10 Myr (*dashed lines*).

in the HR diagram. Convective low mass stars follow vertical Hayashi tracks at constant $T_{\rm eff}$. As they develop a radiative core, intermediate mass stars increase in $T_{\rm eff}$ at nearly constant luminosity. Thus, binning by spectral type is roughly a mass bin for low mass stars and an age bin for intermediate mass stars. The opposite is true for binning by luminosity. If a cluster contains stars with an apparent range of ages, earlier spectral types contain systematically older stars for a given stellar mass. This bias may result in an artificially high difference in disk fractions between bins.

Binned Data: Qualitative Results

We bin our clusters by spectral type (M, K, FG, and BA) and by mass (0.1–0.3, 0.3–0.6, 0.6–1.5, and 1.5–7 $M_{\odot}$) using the Siess et al. (2000) PMS tracks. We name the mass bins MB1, MB2, MB3, and MB4 respectively. Objects lying slightly

below the main sequence are included in the nearest mass bins by eye (e.g. Upper Sco intermediate mass stars). Bins MB1 and MB2 correspond well to M-type stars of all ages. As noted above, stellar evolution means that the correspondence for MB3 and MB4 changes with age. For young clusters, MB3 corresponds to K-type stars and MB4 to BAFG-types. By 10 Myr, MB3 contains GK-types and MB4 BAF-types.

The results of binning stars by mass and spectral type are summarised in Tables 5.2 and 5.3. Also shown are assumed ages and distances. Percentages next to each mass bin label in Table 5.3 show the fraction of stars expected for a standard IMF (Kroupa, 2001). The lowest mass and spectral type bins are incompletely covered for some clusters (Fig. 5.3), though this should not affect disk fractions. Though different PMS models differ significantly, our results do not differ much with other tracks (e.g. Palla & Stahler, 1999), because they have the same general form (i.e. stellar mass increases with $T_{\rm eff}$ and/or $L_\star$ and we are free to choose any mass binning).

Figure 5.4 shows accretion and IR fractions for our chosen bins. The binned data show a systematic decrease in disk fraction with increasing stellar mass and spectral type. Both accretion and IR fractions decrease from the K/MB3 to FG-BA/MB4 bins, for all clusters older than ~2 Myr old IC 348.

If the decrease in disk fraction with increasing stellar mass were only present in EW[Hα] measurements, it might be attributed to a detection bias against early-type stars, where excess Hα is harder to detect in low resolution spectra. However, it is present in both the accretion and IR fractions and based on the general agreement between the two signatures is probably real.

We observe, and expect, less stellar mass dependence on disk fraction for the youngest clusters. If stars of all spectral types have disks at early stages, then a difference in disk fractions between bins has had little time to develop for the youngest clusters. The results for these clusters will be somewhat influenced by the small numbers of intermediate-mass stars. The disk fraction in Cha I increases with increasing stellar mass (Luhman et al., 2008), which may be the result of initial variations in disk fraction with stellar mass. Only a few intermediate mass stars in the IC 348 sample of Luhman et al. (2003) have EW[Hα] measurements, so the high accretion fraction for these objects may simply be due to the small sample size. It is not clear why the IR fraction of IC 348 increases from MB3 to MB4. Given that the disk fraction is lower than for Tr 37, we expect it to show a similar trend. The difference may be a result of its younger age and perhaps an initially lower disk fraction.

Compared to solar and intermediate-mass stars, any trends for low-mass and late spectral type stars are less clear. There appears to be a consistent decrease in accretion fraction to the lowest mass/spectral type bins, but this trend does not appear in the IR-fractions as we bin them. Finer binning shows some clusters do decrease their IR-fractions toward low mass stars, though the uncertainties

Table 5.2 Cluster disk fractions binned by spectral type.

Name	Age (Myr)	M		K		FG		BA	
		EW[Hα]	IR	EW[Hα]	IR	EW[Hα]	IR	EW[Hα]	IR
1 Taurus	1	42/55=76%	50/67=75%	24/40=60%	24/40=60%	2/4=50%	1/2=50%	2/3=67%	2/2=100%
2 Cha I	2	37/107=35%	46/87=53%	13/23=57%	9/13=69%	2/2=100%	1/2=50%	1/2=50%	...
3 IC 348	2.3	46/173=27%	102/233=44%	7/12=58%	8/27=30%	3/3=100%	3/11=27%	...	2/7=29%
4 Tr 37	4	21/53=40%	28/48=58%	31/69=45%	30/59=51%	4/25=16%	3/9=33%	2/35=6%	1/13=8%
5 NGC 2362	5	4/86=5%	7/65=11%	2/35=6%	2/35=6%	0/4=0%	0/5=0%	0/7=0%	0/7=0%
6 OB1bc	5	13/85=15%	4/31=13%	21/68=31%	1/11=9%	0/10=0%	0/8=0%	6/103=6%	3/103=3%
7 Upper Sco	5	14/183=8%	13/92=14%	2/29=7%	5/25=20%	1/31=3%	0/35=0%	4/71=6%	3/78=4%
8 OB1a/25Ori	8	3/68=4%	1/38=3%	4/23=17%	2/8=25%	0/1=0%	...	...	...
9 NGC 7160	10	0/12=0%	1/8=12%	1/21=5%	1/17=6%	0/62=0%	1/47=2%	0/35=0%	1/34=3%

Table 5.3 Cluster disk fractions binned by mass.

Name	Dist (pc)	M		K		FG		BA	
		EW[Hα]	IR	EW[Hα]	IR	EW[Hα]	IR	EW[Hα]	IR
1 Taurus	140	2/2=100%	7/12=58%	31/42=74%	34/45=76%	27/41=66%	27/41=66%	5/10=50%	5/7=71%
2 Cha I	165	13/52=25%	21/47=45%	19/39=49%	14/22=64%	11/20=55%	7/11=64%	4/6=67%	2/3=67%
3 IC 348	320	21/96=22%	52/125=42%	12/41=29%	21/54=39%	6/16=38%	7/32=22%	4/4=100%	6/18=33%
4 Tr 37	900	...	...	17/38=45%	23/33=70%	34/89=38%	34/75=45%	7/50=14%	5/19=26%
5 NGC 2362	1500	1/7=14%	0/3=0%	2/67=3%	5/51=10%	3/43=7%	4/43=9%	0/14=0%	0/14=0%
6 OB1bc	440	0/4=0%	1/3=33%	11/72=15%	3/26=12%	21/77=27%	1/12=8%	7/93=8%	3/92=3%
7 Upper Sco	145	7/103=7%	9/50=18%	7/73=10%	5/43=12%	3/31=10%	3/28=11%	2/92=2%	3/96=3%
8 OB1a/25Ori	322	0/11=0%	0/7=0%	1/43=2%	1/29=3%	6/38=16%	2/10=20%	...	...
9 NGC 7160	900	...	...	0/12=0%	1/8=12%	1/38=3%	1/27=4%	0/80=0%	2/71=3%

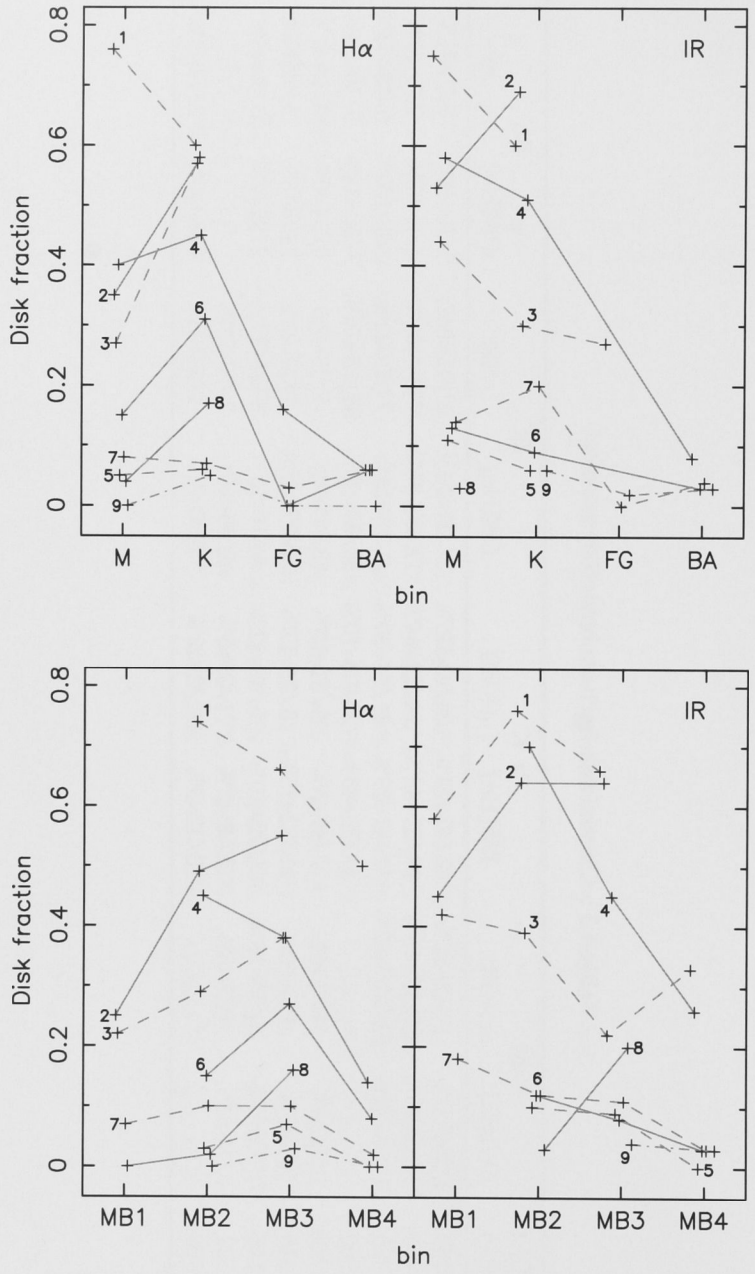

Figure 5.4 Accretion and IR disk fractions binned by spectral type (*top*) and mass (*bottom*). Grey solid, dashed, and dot-dashed lines (the same in each panel and Figure 5.6) link points from each cluster, which are numerically labeled in the same order as Table 5.2. Bins with less than 10 stars are omitted and for clarity, points are offset left and right from their bin locations slightly. Errors are omitted for clarity, but are included in Figure 5.5.

are large (e.g. Dahm & Hillenbrand, 2007; Hernández et al., 2007). External photoevaporation may affect low mass stars and could be the reason for lack of a clear trend. Given that external photoevaporation depends on the cluster environment and is therefore different for each star in each cluster, we now focus on trends for the higher mass stars.

Figure 5.5 again shows the binned results, this time comparing accretion and IR fractions. The error bars provide a measure of the significance of the differences seen in Figure 5.4 and show no major differences between IR and accretion fractions. The three young clusters Taurus, Cha I, and IC 348 have disk fractions that are largely consistent with one another. Of the older clusters, Tr 37, Orion OB1bc, and Upper Sco have somewhat significant differences between the K/MB3 and BA-FG/MB4 bins. Though the individual significance is not consistently high, of the older clusters with intermediate-mass stars, all five have lower disk fractions in their highest mass and spectral type bins.

To try a more robust primordial disk classification, we require a star to have both accretion and IR signatures to be classed as having a disk, because objects with only one disk signature may be some form of transition object. Figure 5.6 shows these "common" disk fractions. There are fewer objects overall, but the primary result is the same: the decrease in disk fraction for higher mass/later spectral type bins remains.

There are some differences between the results for binning by spectral type and mass. For mass binning, general trends are conserved, but the magnitude of the differences is similar or smaller. The difference in disk fraction between K and BA-stars in Tr 37 is ~40%, but only ~20% for the roughly comparable MB3 and MB4 stars. Carpenter et al. (2006) find that the disk fraction of KM stars in Upper Sco is higher than FG and BA stars at 99.2% and 92% confidence respectively. For MB3 and MB4 stars, we find a similar result of 87–90% confidence (see Table 5.4 and discussion below). Because it has a physical basis, we proceed using the mass binned results.

Quantifying Results for Solar and Intermediate-Mass Stars

We now put the differences in disk fractions on a more quantitative footing. There are two aspects of the results we can quantify: the significance of differences between bins on a cluster by cluster basis, and the significance yielded by our sample of nine clusters.

Figure 5.7 shows a direct comparison of the MB3 and MB4 bin fractions (where both bins have >10 stars). The errors are calculated from a binomial distribution and represent $1\,\sigma$ limits on the intrinsic disk fraction, given the observed fraction (Burgasser et al., 2003). The most obvious result is that all clusters, with the exception of Cha I and IC 348, have lower disk fractions in the higher mass bin (Cha I and OB1a have insufficient MB4 stars to feature on this plot). Thus, all

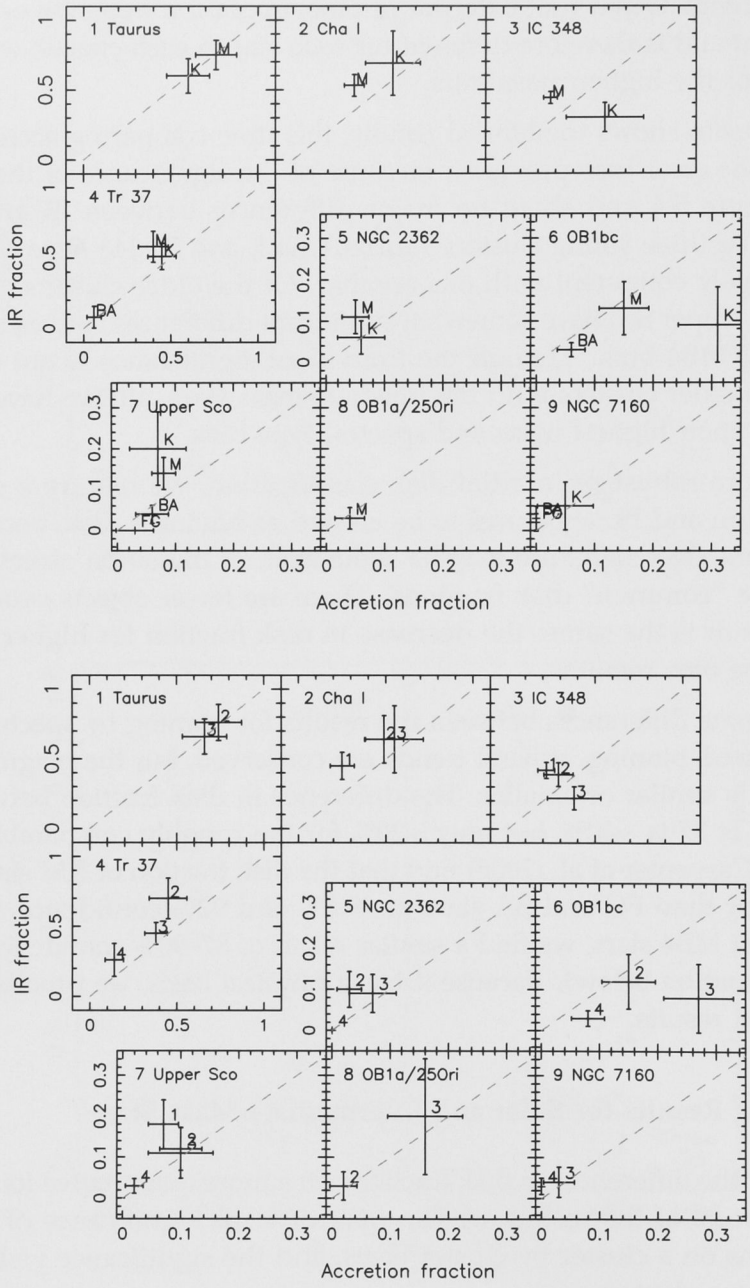

Figure 5.5 Accretion and IR disk fractions compared as in Fig. 5.2, but binned by spectral type (*top*) and mass (*bottom*). Errors are Poisson estimates and labels refer to the bin (1 = MB1 etc. for mass binned data). The lower right set of subpanels in each plot have zoomed axes for lower disk fractions in older clusters.

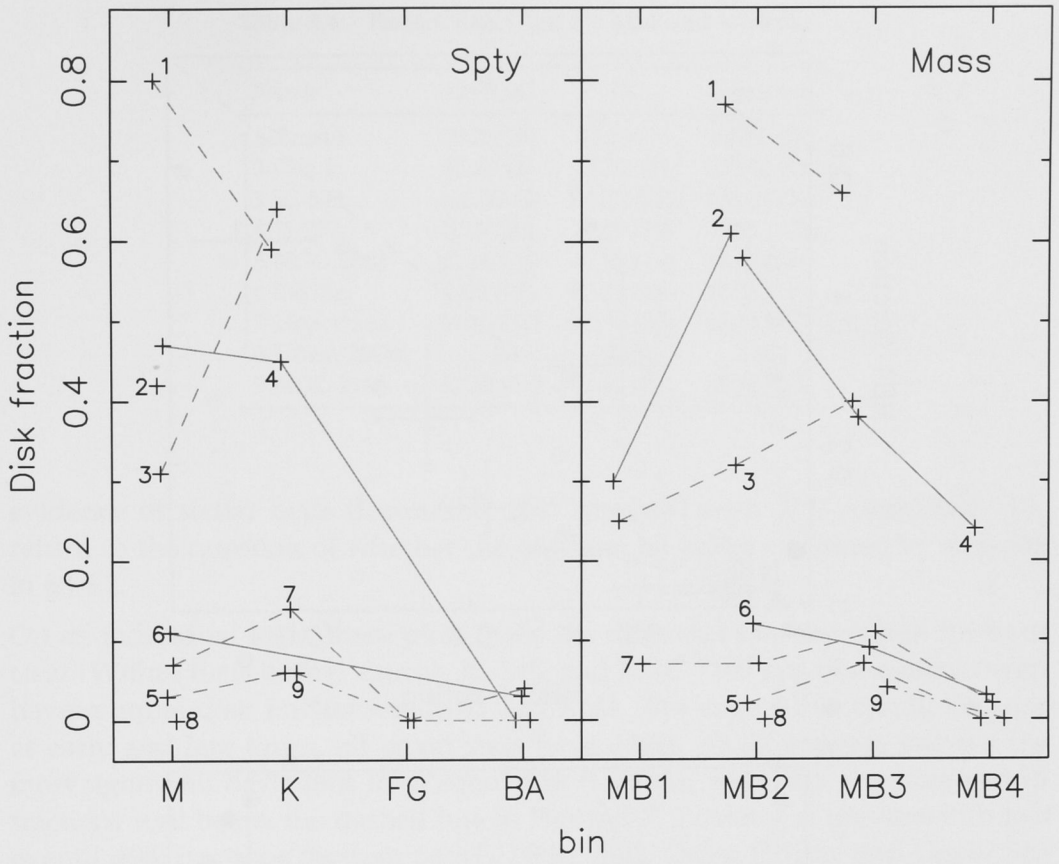

Figure 5.6 Same as Figure 5.4, but for stars showing both accretion and dust signatures. Errors are omitted for clarity, but are larger than in Figure 5.4 due to fewer objects.

clusters older than ~3 Myr have lower disk fractions in MB3 than MB4. There is a 1 in $2^5 = 32$, or 3% chance this configuration would occur if the difference between bins were random.

To test the significance of the trend for these 5 clusters, we compute the χ^2 value for the null hypothesis that MB3 and MB4 have equal disk fractions—that disk dispersal is independent of stellar mass. Using the ten data points with ≥10 stars and errors added in quadrature, we find $\chi^2 = 19$ for perpendicular deviations. We therefore reject the null hypothesis at 97% confidence. This relatively low confidence reflects the errors associated with each cluster.

Though the measurements of accretion and IR signatures are independent, they are correlated because stars with one signature tend to show the other. Thus there are fewer than the 9 degrees of freedom used above. If we combine the accretion and IR fractions of the clusters, by taking the average number of disks and stars for the two signatures, we find $\chi^2 = 10$. We again reject the null hypothesis with 97% confidence. Therefore we conclude that there is some

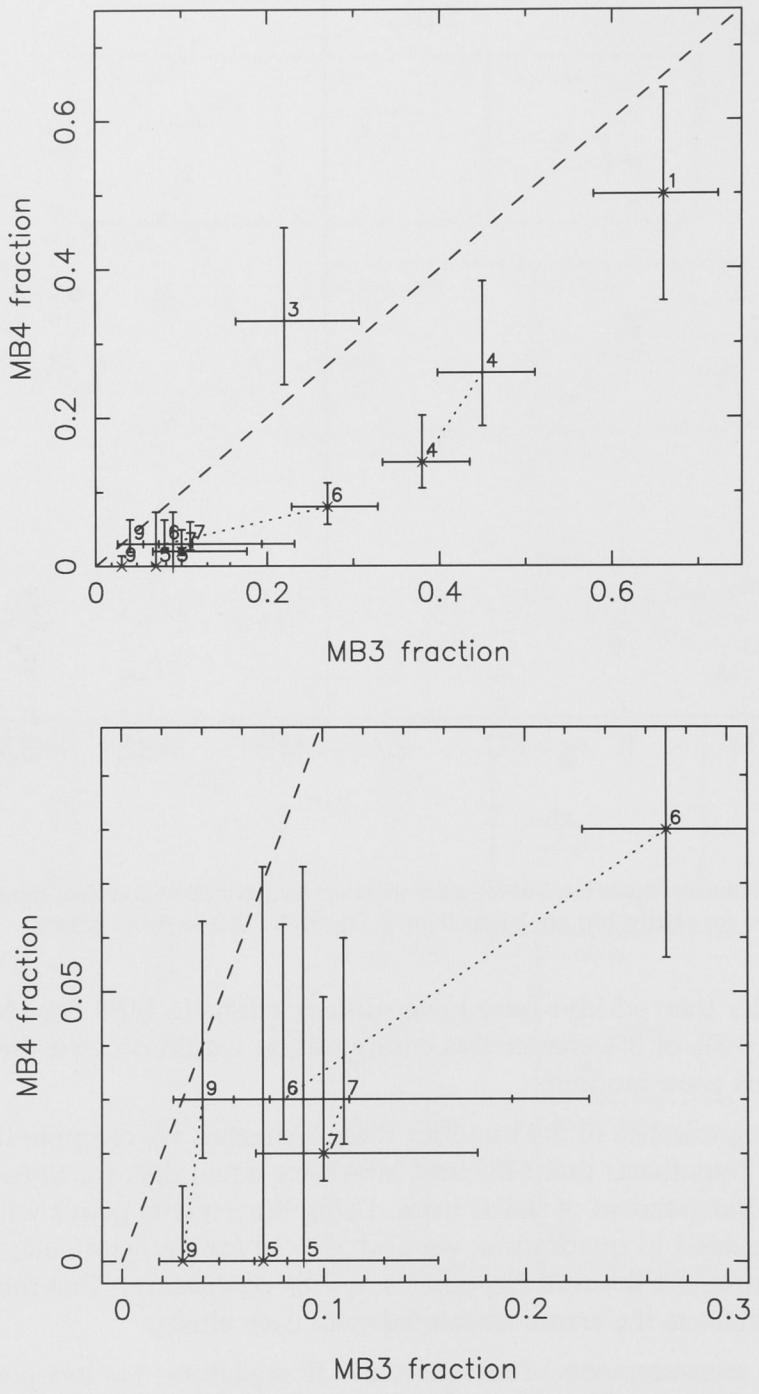

Figure 5.7 Accretion (×) and IR (+) disk fractions for stellar mass bins MB3 and MB4. Note the different scales in each plot. The bottom panel shows detail near the origin for >5 Myr clusters. Bins with equal fractions lie near the dashed line. The errors are $1\,\sigma$, as described in the text. Where a bin has no disks, the error with 1 disk is used for the upper error.

Table 5.4 Fishers Exact Test for MB3 and MB4 (%).

Name	EW[Hα]	IR	Common
1 Taurus	28.23(10)	75.74 (7)	68.04 (6)
2 Cha I	83.48 (6)	76.92 (3)	100.00 (1)
3 IC 348	100.00 (4)	88.83 (18)	100.00 (3)
4 Tr 37	0.19 (50)	10.58 (19)	20.50 (17)
5 NGC 2362	42.18 (14)	31.24 (14)	39.83 (14)
6 OB1bc	0.05 (77)	39.23 (12)	37.73 (11)
7 Upper Sco	10.13 (31)	12.79 (28)	14.41 (19)
8 OB1a/25Ori	...(0)	...(0)	...(0)
9 NGC 7160	32.20 (38)	62.42 (27)	28.13 (27)

evidence of stellar mass dependent disk dispersal with 97% confidence. We return to the question of whether the data can be better explained by a model in §5.4.2.

On an individual level, these plots make the differences between disk fractions clear. Within their errors, Taurus, IC 348, and NGC 7160 are all consistent with having equal disk fractions in MB3 and MB4. We expect this result, because at early and late times, all or no stars have disks. Tr 37 appears to have the most significant deviations from equal disk fractions, with both accretion and IR fractions well below the dashed line in Figure 5.7. Looking at clusters with low overall disk fractions (bottom panel), NGC 2362, Orion OB1bc, and Upper Sco also have somewhat significant deviations from equal fractions.

We test the significance of individual differences between MB3 and MB4 with Fisher's Exact Test (right-sided). This test finds the likelihood that a more extreme separation in disk fractions between the two bins should exist. In the right sided case, "more extreme separations" means a more positive difference in disk fractions MB3 – M*B*4. This test shows the significance of the difference in each cluster and highlights where future observations can make the most progress.

Table 5.4 shows the results of this test for accretion, IR, and common fractions, for objects in MB3 and MB4. The numbers in parentheses show the lower of the numbers of stars in MB3 and MB4, as measure of the minimum sample size each test result is based on. Thus, 0.19% (50) for Tr 37 is derived from comparing 34/89 (MB3) with 7/50 (MB4).

The accretion fractions of Tr 37 and OB1bc are by far the most significant, with less than 0.2% likelihood that a greater difference in disk fractions between MB3 and MB4 should occur. These clusters have the most significant results because of the large number of intermediate-mass stars with EW[Hα] measurements. By eye, this test agrees with the separations suggested by the errors in Figure 5.7. As noted above, we find a similar significance to Carpenter et al. (2006) for

Upper Sco. Thus, this test shows that the significance of differences in MB4 and MB4 disk fractions for the 4–5 Myr old clusters vary between 60–99%. It is this large range in significance that limits the confidence with which we reject the null hypothesis.

As can be intuitively seen in Figure 5.7, Fisher's Exact Test shows where the most progress can be made by future observations. The Spitzer observations of Orion OB1a/25Ori and OB1bc (Hernández et al., 2007) focus on low-mass stars Briceño et al. (2005). Many intermediate-mass stars have yet to be characterised, particularly in the Spitzer IRAC wavelength range we use here. NGC 2362 has a large population of intermediate-mass stars lacking published spectral types, which would increase the significance of the result for this cluster.

5.3.3 Summary

We find evidence of stellar mass dependent disk dispersal. All intermediate-mass stars in clusters older than ~3 Myr have lower disk fractions than solar-mass stars. Individually, the 4–5 Myr clusters Tr 37, NGC 2362, Orion OB1bc, and Upper Sco all have marginal significance, at around the $1\,\sigma$ level. The most significant results are for the accretion fraction of Tr 37 and Orion OB1bc. These results are generally in agreement with the results of the Fisher's Exact Test. We reject the null hypothesis—that the disk fractions in bins MB3 and MB4 are the same—at 97% confidence. This confidence is limited by the number of stars in each cluster.

5.4 Theoretical Mechanisms

The results in Figure 5.7 and Table 5.4 suggest that mass dependent disk dispersal is real. Though intermediate-mass stars in all clusters older than ~3 Myr have lower disk fractions than solar-mass stars, the results of Fisher's Exact Test show that most clusters have marginal (1 σ) individual significance. If the 4–5 Myr clusters represent the maximum possible difference, it may be hard to achieve 3σ significance for a single cluster with ~100 stars in the MB3 and MB4 bins. To consider how large we expect these differences to be, we look at disk evolution from a theoretical perspective.

To make an initial exploration of predictions for stellar mass dependent disk dispersal, we consider two plausible disk evolution models. To evaluate the observational signature of the evolution of solid material in the disk, we first consider the possibility that dust in the regions probed by the IRAC wavebands evolves more rapidly for more massive stars. To illustrate observational diagnostics derived from the global evolution of the disk, we then examine a photoevaporation model, where a larger ionising flux causes disks around more

massive stars to disperse earlier. Although we do not attempt to model the observational results in detail, we show that a simple photoevaporation model reproduces the evolution of MB3 and MB4 disk fractions much better than our null hypothesis.

5.4.1 Grain Growth

Dust signatures decline due to removal of small grains. These grains may be physically removed, or grow to unobservable sizes. The timescale for growth depends on the orbital period. With the simplifying assumption that a waveband traces dust at a single temperature and radial distance, observations at fixed wavelength probe different radial distances for different stellar luminosities. Therefore, dust around different stars will be in a earlier or later stage of growth. That is, for some stars there will have been little growth and the dust is still observable, and for others it may have grown to invisible sizes.

To show how different stars observed with the same instrument can have different grain growth timescales, we consider how the orbital period changes with stellar mass at fixed disk temperature. The distance a from a star of luminosity $L_\star$ to remain at a fixed temperature T is $a \propto L_\star^{-1/(4x)}$, where $T \propto a^{-x}$. For PMS stars $L_\star \propto M_\star^2$, so $a \propto M_\star^{-1/2x}$ (i.e. a waveband probes greater distances around lower mass stars). Because the period $P^2 \propto a^3/M_\star$ and $x \sim 3/4$ in the inner, less flared part of the disk (e.g. Adams et al., 1987; Kenyon & Hartmann, 1987), the relation for period with stellar mass is

$$P \propto M_\star^{\frac{3}{4x}-\frac{1}{2}} \sim \sqrt{M_\star} \tag{5.1}$$

That is, the greater luminosity of higher mass stars means the period at fixed temperature increases with stellar mass.

However, the growth timescale $\tau_{\rm grow}$ also depends on the surface density, which is generally thought to increase with stellar mass (based on mm observations, e.g. Natta et al., 2000; Andrews & Williams, 2005). Thus,

$$\tau_{\rm grow} \propto P/\sigma \propto \frac{1}{\sqrt{M_\star}} \tag{5.2}$$

indicates a decreasing growth timescale with increasing stellar mass: dust may disappear around higher mass stars more rapidly due to fast grain growth timescales. This theory provides a qualitative explanation for the much lower IR excesses found for early-type stars that have disks.

While faster growth may provide some of the observed differential evolution in disk fractions, it does not offer any explanation of why the accretion signature also drops earlier for higher mass stars. Indeed, if the presence of gas allows repeated fragmentation and hinders growth (Johansen et al., 2008), then removal of the

gas may be more important in setting observational signatures of both gas and dust. The leading theory for dispersal of the gaseous disk is photoevaporation, to which we now turn.

5.4.2 Photoevaporation

Viscous evolution and photoevaporation work together to provide a likely mechanism for removing the gaseous disks around young stars (e.g. Clarke et al., 2001). As the disk evolves and angular momentum moves outward, gas moves inward and is accreted onto the central star. At the same time, a wind of gas ionised by stellar radiation removes material from the outer disk, beyond the "critical radius" where the sound speed in the ionised gas is larger than the orbital velocity (e.g. Hollenbach et al., 2000). When the accretion rate through the inner disk onto the star drops below the wind loss rate, the inner disk becomes depleted and is rapidly accreted onto the star. With the inner disk removed, stellar radiation rapidly photoevaporates the remaining gas (Alexander et al., 2006).

A Simple Model

To explore how this process impacts the time variation of disk fractions in young clusters, we use a simple photoevaporation model. This model captures the important aspects of the process described above, with a prescription for the time evolution of the accretion rate. When the accretion rate drops below the (fixed) wind loss rate, the disk is considered dispersed (Alexander & Armitage, 2006).

For a viscous disk, the time dependent accretion rate is

$$\dot{M}_{\rm accr} = \frac{M_{\rm disk}(0)}{2t_\nu}\tau_\nu^{-3/2} \tag{5.3}$$

where $M_{\rm disk}(0)$ is the initial disk mass and $\tau_\nu = t/t_\nu + 1$ is a dimensionless time. The viscous timescale is defined at the scale radius R_0 by $t_\nu = R_0^2/(3\nu_0)$, where the viscosity is ν_0. Initially, $1/e$ of the disk mass lies outside R_0 (e.g. Lynden-Bell & Pringle, 1974; Hartmann et al., 1998; Alexander et al., 2006; Alexander & Armitage, 2006). Here we assume $\nu \propto R$.

The disk rapidly disperses when the accretion rate drops below the wind mass loss rate

$$\dot{M}_{\rm wind} \sim 1.6 \times 10^{-10} \left(\frac{\Phi}{10^{41}\ {\rm s}^{-1}}\right)^{1/2} M_\star^{1/2}\ \frac{M_\odot}{\rm yr} \tag{5.4}$$

where Φ is the number of ionising photons per second and $M_\star$ is in units of $M_\odot$ (Hollenbach et al., 1994).

Applying this model to a range of stellar masses requires specifying disk properties as a function of stellar mass. Specifically, this variation needs to be defined for the viscous timescale and wind loss rate. Assuming $t < t_\nu$, a typical disk temperature profile and $M_{\rm disk} \propto M_\star$, Alexander & Armitage (2006) suggest $t_\nu \propto M_\star^{-1}$ to match an apparent correlation of accretion with stellar mass $\dot{M}_{\rm accr} \propto M_\star^2$ (e.g. Muzerolle et al., 2005; Natta et al., 2006). Physically, their model implies that the disk scale radius decreases with increasing stellar mass. For the ionising flux, the Alexander & Armitage (2006) model uses $\dot{M}_{\rm wind} \propto M_\star$. Though they did not consider it significant, their model predicts a stellar mass dependent disk lifetime (their Fig. 2). Higher mass stars drive more powerful winds and have shorter accretion timescales; thus, photoevaporation shuts off accretion earlier for more massive stars.

Alternatively, Alexander et al. (2006) considered a linearly increasing scale radius with increasing stellar mass, but fixed Φ (thus $\dot{M}_{\rm wind} \propto \sqrt{M_\star}$). They fixed t_ν to scale with the orbital timescale at the disk scale radius and therefore $t_\nu \propto M_\star$. In this case the disk lifetimes increase nearly linearly with stellar mass.

Thus, there is little constraint on how the viscous timescale changes with stellar mass. Choosing $t_\nu \propto M_\star^{-1}$ based on the apparently strong positive correlation between accretion and stellar mass may be unfounded. Accretion measurements suffer a stellar mass dependent bias (Clarke & Pringle, 2006) and a linear relation ($\dot{M}_{\rm accr} \propto M_\star$) may be a better choice (t_ν independent of $M_\star$). Another parameter that has an impact is the disk scale radius. If the initial disk radius increases with stellar mass, then the viscous timescale increases with stellar mass. Observationally, how disk radius varies with stellar mass is poorly constrained. To explore the possibilities of the model, we adopt $t_\nu = 2 \times 10^{-4} M_\star^{P_\nu}$ yr (P_ν: viscous power-law index).

Some constraints on how the wind loss rate changes with stellar mass exist. As a rough upper limit, if the ionising flux scales with the bolometric stellar luminosity and $L_\star \propto M_\star^2$ for PMS stars, then $\dot{M}_{\rm wind} \propto M_\star^{1.5}$. If x-rays are important for photoevaporation (Ercolano et al., 2008), the ionising flux then scales with stellar mass $\Phi_{\rm x} \propto M_\star^{1.5}$ (Güdel et al., 2007), yielding $\dot{M}_{\rm wind} \propto M_\star^{1.25}$. In our model, we allow for variation of the wind loss rate by adopting $\dot{M}_{\rm wind} = 1.6{\times}10^{-10} M_\star^{P_{\rm w}} M_\odot$/yr ($P_{\rm w}$: wind power-law index).

The two cases outlined above then have $P_\nu = -1$ and $P_{\rm w} = 1$ (Alexander & Armitage, 2006), and $P_\nu = 1$ and $P_{\rm w} = 1/2$ (Alexander et al., 2006). For a typical disk mass, we follow Alexander & Armitage (2006) and set $M_{disk}(0) = 0.01\, M_\star$ (e.g. Natta et al., 2000; Andrews & Williams, 2005).

Figure 5.8 shows the two examples of disk evolution for a range of stellar masses using Equation (5.3). The disk is dispersed at the point where the accretion rate drops below the wind rate (where lines of the same type meet and terminate). The top panel shows the model with $P_\nu = -1$ and $P_{\rm w} = 1$; the disk lifetime decreases with increasing stellar mass. The bottom panel shows the other model,

with $P_\nu = 1$ and $P_w = 1/2$; the disk lifetime increases with stellar mass.

Of these two models, the top panel qualitatively explains the trend observed in our cluster data. The fact that all 5 clusters older than 3 Myr show a decreased disk fraction for higher mass stars argues that higher mass stars lose their disks earlier and that the model that reproduces this behaviour is more realistic. This qualitative agreement suggests that either the viscous timescale does not increase with stellar mass, or the wind loss rate increases relatively strongly with stellar mass.

To understand how the two models produce opposite trends in disk lifetime with stellar mass, we look at how the wind rate and viscous timescale change with stellar mass in more detail. Simplifying Equation (5.3) by assuming $t > \tau_\nu$, setting $\dot{M}_{accr} = \dot{M}_{wind}$, and solving for t (i.e. the epoch of disk dispersal) yields

$$\tau_{disk} \propto \frac{M_{disk}\sqrt{t_\nu}}{\dot{M}_{wind}} \propto M_\star^{1+P_\nu/2-P_w}. \tag{5.5}$$

This relation shows how disk lifetime varies with the viscous timescale and wind loss rate. Thus, the disk lifetime decreases with increasing stellar mass whenever $P_w > 1 + P_\nu/2$. The two models in Figure 5.8 thus have $\tau_{disk} \propto M_\star^{-1/2}$ and $\tau_{disk} \propto M_\star$.

For our purposes, Equation (5.5) shows that the difference between the scaling of viscous timescale and wind loss rate with stellar mass sets how the disk dispersal time varies with stellar mass. Though there are many uncertainties associated with the many model parameters, we proceed with two of our own "example" models to illustrate the implications of this model. These models also yield estimates to compare with our observational results.

The first model has $t_\nu \propto 1/M_\star$ and $\dot{M}_{wind} \propto M_\star$ ($P_\nu = -1$, $P_w = 1$). The disk lifetime is therefore $\tau_{disk} \propto M_\star^{-1/2}$, the same as the top panel of Figure 5.8. Other solutions to $P_w = 1.5 + P_\nu/2$ yield the same results, provided the disk lifetime is longer than the viscous timescale (true for the stellar mass bins MB3 and MB4). The second model has $P_\nu = 0$ and $P_w = 1.25$ ($\tau_{disk} \propto M_\star^{-1/4}$, the same as other solutions to $P_w = 1.25 + P_\nu/2$). This weaker dependence illustrates how strongly the results depend on changes to P_w and P_ν.

Application to Cluster Disk Fractions

To extend the model to a cluster of stars, we assume that a range of disk lifetimes at fixed stellar mass arises from the natural dispersion in initial disk masses within a cluster (e.g. Natta et al., 2000; Andrews & Williams, 2005). For fixed stellar mass (and $\dot{M}_{wind}$), more massive disks last longer than less massive ones due to higher accretion rates. We assume disk masses are normally distributed in log space about $M_{disk} = 0.01\,M_\star$ (used by Alexander & Armitage, 2006). A factor of 10 change in disk mass represents a $3\,\sigma$ variation. Therefore, at a given time,

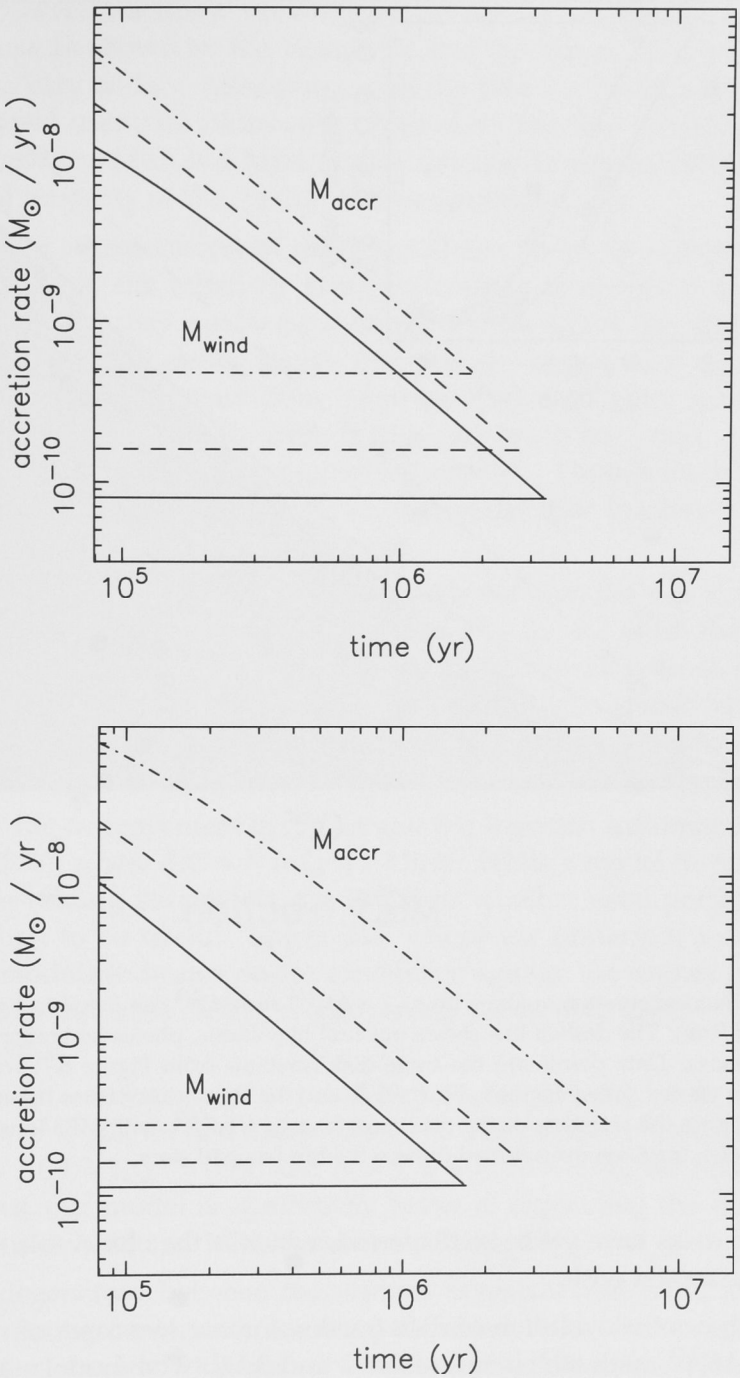

Figure 5.8 Evolution of accretion for different choices of viscous evolution timescale: $P_\nu = -1$, $P_w = 1$ (*top*), and $P_\nu = 1$, $P_w = 1/2$ (*bottom*). Diagonal lines show accretion rates for 0.5 (*solid*), 1 (*dashed*), and $3\,M_\odot$ (*dot-dashed*) and horizontal lines show the wind loss rate for the same stellar masses. Disks are dispersed (and lines terminate) when the accretion rate drops below the wind loss rate.

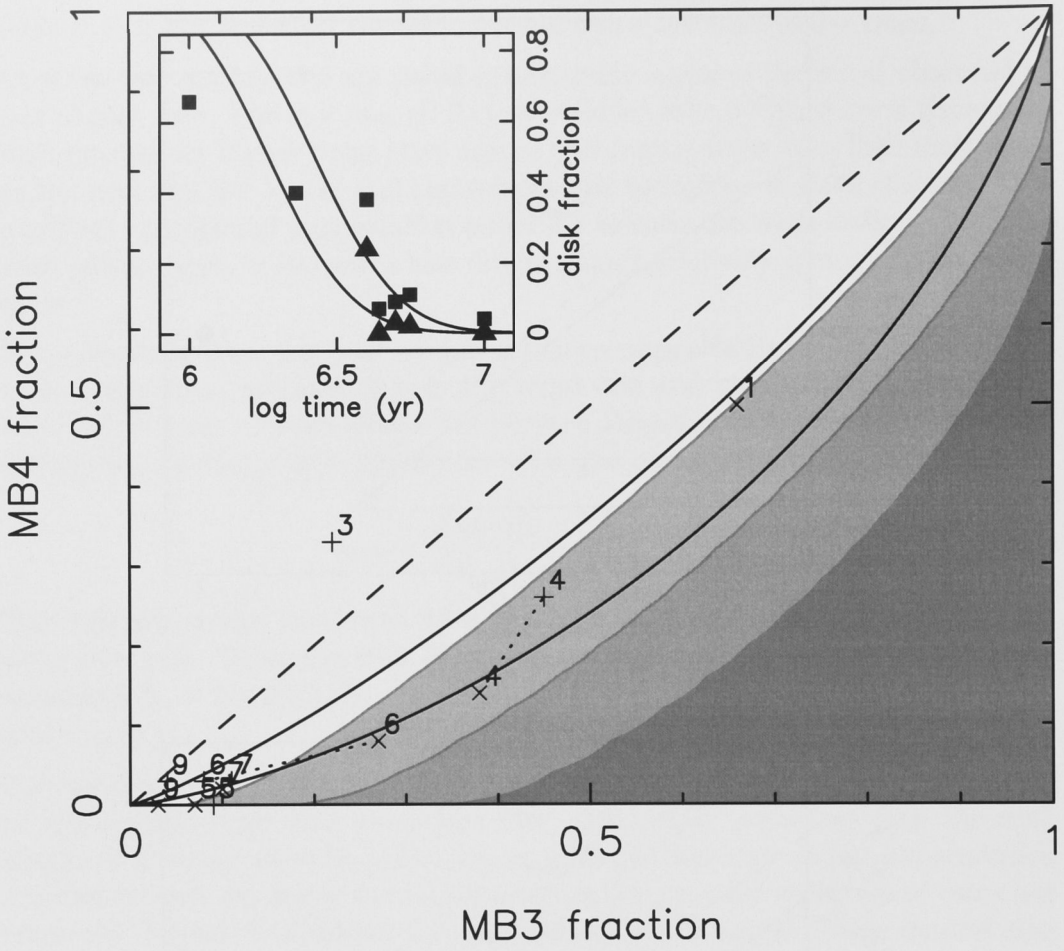

Figure 5.9 Photoevaporation model with $\tau_{\rm disk} \propto M_\star^{-1/4}$ and $M_\star^{-1/2}$ compared to significance contours (*solid lines*). The dashed line shows our null hypothesis, photoevaporation independent of stellar mass. Data points are the same disk fractions from Figure 5.7, with error bars omitted for clarity. Filled regions show >1, 2, and 3σ significance from lightest to darkest. The inset shows the accretion model over time for $\tau_{\rm disk} \propto M_\star^{-1/2}$, with MB3 (*squares*) and MB4 (*triangles*) disk fractions over-plotted (where the bin has ≥10 stars.

a fraction of disks have yet to be dispersed, which is the observable quantity we compare the model with.

Figure 5.9 shows the evolution of disk fraction for our two cases of $\tau_{\rm disk} \propto M_\star^{-1/4}$ and $\tau_{\rm disk} \propto M_\star^{-1/2}$, with stellar masses of 1 and $3\,M_\odot$. The model stellar masses represent the MB3 and MB4 mass bins in our cluster sample. The disk fraction loci start at the top right of the figure, when all stars have disks. They then move down and away from the line of equal disk fractions, as higher mass stars lose their disks at a faster rate than lower mass ones. Finally, the lines reach the lower left of the figure, when all stars have lost their disks.

Though we do not attempt to fit a model, it is clear that $\tau_{disk} \propto M_\star^{-1/2}$ is consistent

with our observed fractions. We compare the model and data in MB3 vs. MB4 space because as shown by the Figure 5.2 and the Figure 5.9 inset, individual bin fractions vary widely. Attempting to fit the time evolution of MB3 and MB4 would not yield useful or informative parameters. We thus consider the relative difference between MB3 and MB4 as disk fraction decreases, which appears to be a general property of the $\gtrsim$3 Myr clusters in our sample.

If our model is representative of the physical conditions in a photoevaporating circumstellar disk, the relatively small differences in observed disk fractions between mass bins may not be because there is no signal (i.e. disk fraction is actually *independent* of stellar mass). It is because the signal is naturally weak and most clusters have insufficient members for a significant result. Clusters that fall in the times where the bulk of disks are being dispersed, such as Tr 37, provide the best constraint how $\tau_{\rm disk}$ varies with $M_\star$. Though the 5 Myr clusters have differences as significant as Tr 37, the model disk fractions change little with P_v and $P_{\rm w}$ at these low disk fractions.

Calculating the perpendicular square residuals between the $\tau_{disk} \propto M_\star^{-1/2}$ model and our data yields an extremely good fit of χ^2 = 0.7–0.2 (with the method as described for testing our null hypothesis, §5.3.2). This result is much smaller than for the null hypothesis and than expected given the estimated errors. However, this comparison shows that a plausible model reproduces the data much better than the null hypothesis.

To quantify the improvement in χ^2, we use the Bayesian Information Criterion (Schwarz, 1978), where $BIC = N \ln(\chi^2) + k \ln N$. While a model fit can always be improved by adding parameters, the BIC tests whether extra parameters lower the χ^2 enough to be useful. Lower BIC values are preferred; a difference of 2 between models indicates positive evidence against the higher BIC value, a difference of 6 indicates strong evidence, and differences greater than 10 very strong evidence.

For the two χ^2 calculations of our null hypothesis (N = 10, k = 0, χ^2 = 19, and N = 5, k = 0, χ^2 = 10), we find BIC = 29 and 12. For the two χ^2 calculations of our model (N = 10, k = 1, χ^2 = 0.79, and N = 5, k = 1, χ^2 = 0.14), we find BIC = −0.1 and -8. Thus, our model is *significantly* better at explaining the differences in disk fractions in MB3 and MB4 than the null hypothesis.

Given the degeneracy between the viscous timescale and wind loss rate, we cannot put strong constraints on any parameters aside from $\tau_{\rm disk}$. The data do not support models with higher wind loss rates than observations of x-ray luminosity suggest, or stronger than inverse dependence of the viscous timescale on stellar mass.

To estimate the significance of the observed and model disk fractions in a more general way, we again use the binomial distribution. For every point in MB3 and MB4 space where MB3 > MB4 (i.e. below the dashed line in Figure 5.9), we estimate the likelihood of observing those fractions when the intrinsic fraction

lies somewhere in between. This calculation is slightly different than for finding individual errors. Instead of finding the upper and lower intrinsic fractions that the observed fraction is $1\,\sigma$ away from, we find the single intrinsic fraction with the highest chance of observing the fractions in MB3 and MB4 (which are different). Specifically, we use

$$\int_0^x B'(\epsilon;\, n_{\rm MB4},\, N_{\rm MB4})\, d\epsilon = \int_x^1 B'(\epsilon;\, n_{\rm MB3},\, N_{\rm MB3})\, d\epsilon \tag{5.6}$$

and solve for x. B' is the probability distribution for intrinsic fraction ϵ, with sample size N and observed number of disks n (see Burgasser et al., 2003). The integrated area gives the likelihood of measuring MB3 and MB4 from sampling stars with an intrinsic disk fraction x.

To make this significance estimate, we need to choose properties of a "typical" cluster. A standard IMF (e.g. Kroupa, 2001) suggests there should be roughly three times as many MB3 stars as MB4 stars. Table 5.3 shows a wide range in relative and overall numbers. Therefore we choose the expected IMF ratio and use 100 stars (75 lower mass, 25 higher mass) over the two mass bins. This "typical" cluster therefore has ~1000 stars between 0.1–7 $M_\odot$. With the caveat that only one of our cluster samples resembles this typical cluster by number and IMF in MB3 and MB4 (the IR fraction for Tr 37), this model allows us to roughly map out the entire disk fraction space MB3 and MB4 may occupy.

The contours in Figure 5.9 show the estimated significance of differences in the two bins. The regions are >1, 2, and $3\,\sigma$ from light to dark. Comparing the model to the contours, the $\tau_{\rm disk} \propto M_\star^{-1/4}$ model suggests nearly $1\,\sigma$ confidence is typical for samples with 100 stars in the MB3 and MB4 bins. For $\tau_{\rm disk} \propto M_\star^{-1/2}$, the difference in disk fractions generally sits within the $1\,\sigma$ region. Thus, the $t_{\rm disk} \propto M_\star^{-1/2}$ model is 1–$2\,\sigma$ significant for this assumed typical cluster.

Future Observations

To illustrate how the significance contours in Figure 5.9 change with cluster size, we repeat the calculation for one larger and one smaller cluster. Figure 5.10 shows the number of stars needed for a $3\,\sigma$ result over the possible range of disk fractions, with 48, 100, and 200 stars in MB3 and MB4. Over-plotted are evolutionary lines from the model. The Figure shows that $\gtrsim$200 stars are needed in the MB3 and MB4 bins for a $3\,\sigma$ result if $\tau_{\rm disk} \propto M_\star^{-1/2}$ and clusters show similar results to the data and our model. For clusters following a typical IMF, this requirement means a total of ~2000 stars between 0.1 and 7 $M_\odot$. However, it is important to remember that this is a general estimate based on a typical IMF. The accretion fraction of Tr 37 shows that doubling the number of stars in MB4, with a similar number in MB3 strongly increases the significance of the difference (Tables 5.3 and 5.4).

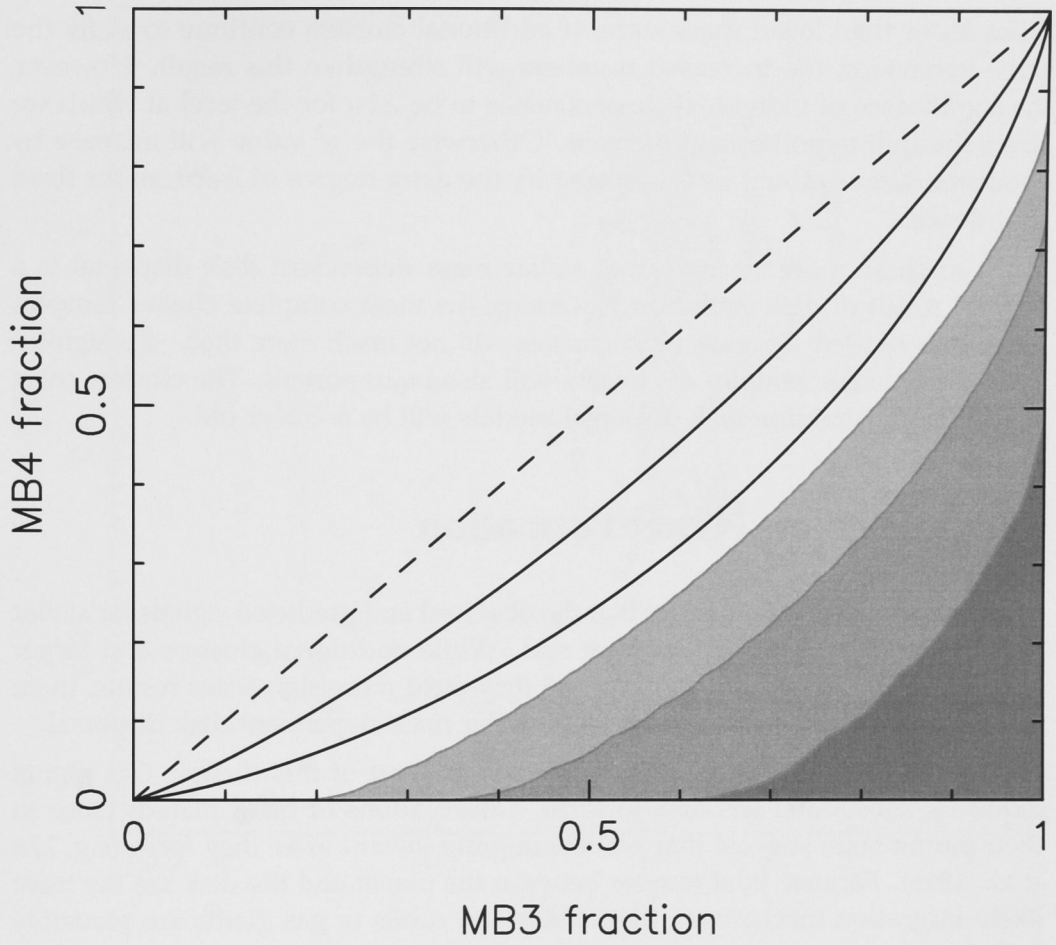

Figure 5.10 Same as Figure 5.9, but contours show the number of stars needed for a 3σ result: <48, 100, and 200 stars from darkest to lightest.

Though few young clusters with thousands of stars have been studied to date, multi-object spectrographs such as Hectospec on the Multiple Mirror Telescope (MMT) and 2df/AAOmega on the Anglo-Australian Telescope (AAT), make spectroscopy of this many objects possible. Clusters such as the Orion Nebula Cluster and h and χ Persei show that the desired numbers are obtainable. Despite being ~13 Myr old, h and χ Persei shows evidence for stellar mass dependent disk dispersal (Currie et al., 2007). A particularly promising cluster is NGC 2264, which may have as many as 1000 stars and at 3 Myr old is in a favourable age range for stellar mass dependent disk dispersal. For other regions, such as NGC 2362 and Orion OB1bc, additional work to obtain samples complete over the widest possible range of spectral types will be beneficial.

A complementary way forward is to increase the number of clusters studied. Here, we find higher mass stars in 5/5 clusters older than ~3 Myr lose their

disks faster than lower mass stars. If additional clusters continue to show the same behaviour, the increased numbers will strengthen this result. However, the significance of individual clusters needs to be $\gtrsim 1\,\sigma$ for the level at which we reject the null hypothesis to increase. Otherwise the χ^2 value will increase by about the same amount as is required by the extra degree of freedom for fixed confidence.

Thus, to show more strongly that stellar mass dependent disk dispersal is a general result of disk evolution, obtaining the most complete cluster samples possible is needed. Because most clusters will not reach more than $\sim 2\,\sigma$ significance, using larger samples of clusters will also be important. The clusters most useful for constraining disk dispersal models will be 3–5 Myr old.

5.5 Effects on Planet Formation

Our results in §3 and §4 suggest that the observed and predicted signals for stellar mass dependent disk dispersal are real. While additional clusters and larger samples of stars in 4–5 Myr old clusters may yield more significant results, there may be other observable signatures of stellar mass dependent disk dispersal.

The orbits of giant planets provide a plausible test of this theory. Gas giants require a substantial gas disk to form. Observations of giant planets close to their parent stars suggest that planets migrate inward after they form (e.g. Lin et al., 1996). Because tidal torques between the planet and the disk are the most likely migration mechanism, the masses and orbits of gas giants are plausibly linked to the mass and lifetime of the disk. If these correlate with stellar mass (§4), the mass and orbits of gas giant planets may correlate with the stellar mass.

Observations of gas giants are starting to provide the data to guide models. Figure 5.11 shows the semi-major axes of known extra-solar planets as a function of stellar mass. [4] Because the closest orbits are easiest to detect, the innermost orbits at each stellar mass are probably close to the real limits. These data suggest a small increase in the minimum separation a_{min} from $0.3\,M_{\odot}$ ($a_{min} \approx 0.02$ AU) to $1.6\,M_{\odot}$ ($a_{min} \approx 0.03$ AU) followed by a large jump to $a_{min} \approx 0.78$ AU at $\gtrsim 1.6\,M_{\odot}$ (see also Johnson et al., 2007b; Sato et al., 2008a,b). The trend in a_{min} with stellar mass is probably not a selection effect.

Post-main sequence stellar evolution probably does not cause the observed trend in a_{min} with stellar mass. Current radial velocity techniques are unable to achieve high accuracy for main sequence A-type stars. Thus, to discover planets around intermediate mass stars, radial surveys observe cooler, evolved objects. These stars have larger radii than on the main-sequence, $\sim 5\,R_{\odot}$ for a $2\,M_{\odot}$ sub-giant. If larger sub-giant stars engulf close planets or if tidal interactions cause close

[4] From http://exoplanet.eu , where a and $M_{\star}$ known.

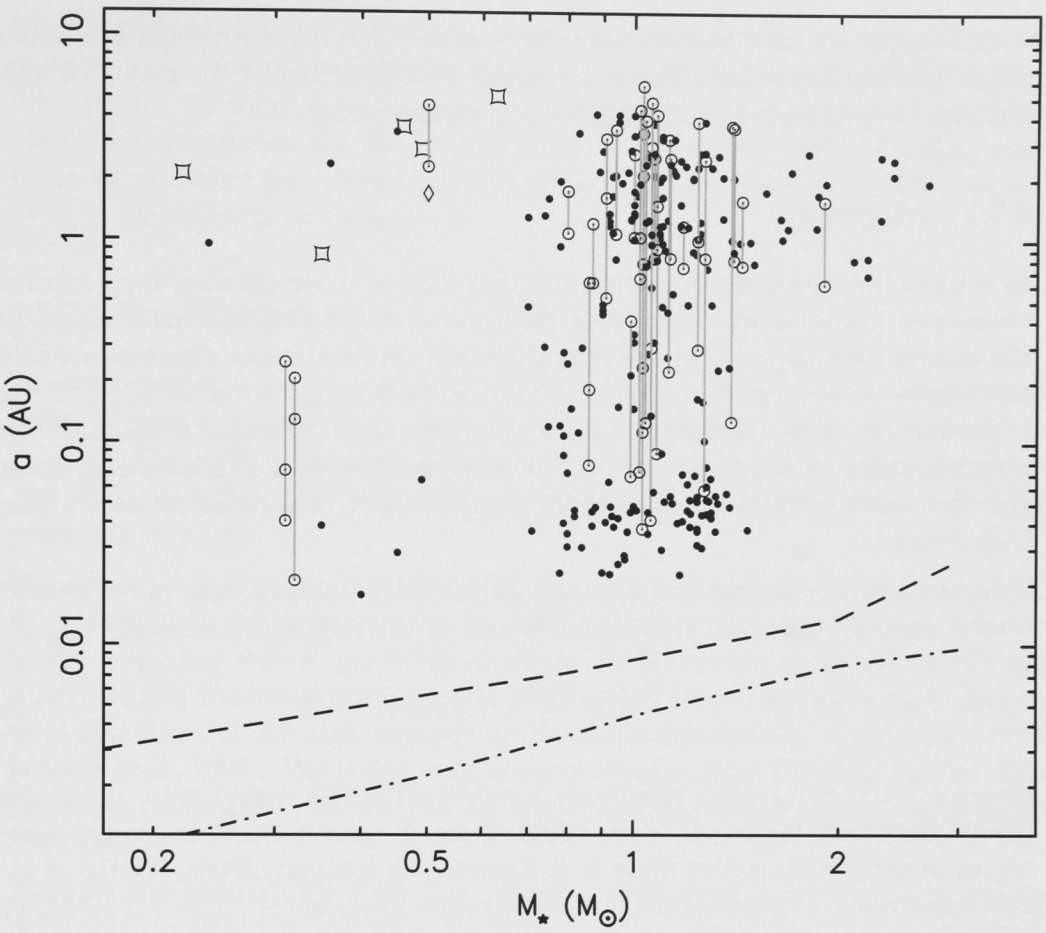

Figure 5.11 Observed semi-major axis distribution of extra-solar planets vs. host mass. Stellar radii from Siess et al. (2000) tracks at $3 \times 10^6 / M_\star$ (*dashed line*) and on the main-sequence (*dot-dashed line*) are also shown. There appears to be a real outward trend in semi-major axis for planets with host masses greater than $\sim 1\, M_\odot$.

planets to spiral into the star, massive sub-giants would have many fewer close-in giant planets (e.g. Rasio et al., 1996; Johnson et al., 2007b). However, Johnson et al. (2007b) suggest that (i) only post–helium-flash clump giants may have lost planets due to increased radii and (ii) engulfing very close planets is not solely responsible for the lack of short period planets around sub-giants and K giants. This conclusion is supported by numerical simulations (Sato et al., 2008a).

If the step in a_{min} at $1.6\, M_\odot$ is not due to post–main-sequence stellar evolution, then it is probably a signature of the planet formation process. Here, we consider two ways to link the orbits of gas giant planets with mechanisms of disk dispersal. In the photoevaporation model, more rapid disk dispersal for intermediate mass stars leads to a shorter time for gas giants to migrate closer to their host stars. Thus, gas giants around more massive stars may have larger orbits. In any model

of disk dispersal, intermediate (low) mass stars reach the main sequence before (after) the disk disperses. Thus, the radius of a PMS star at the epoch of disk dispersal may set the closest orbit for a gas giant planet.

5.5.1 Migration

To explore links between migration and disk dispersal, we consider their relative timescales (see also Ida & Lin, 2004b; Burkert & Ida, 2007). Our analysis of the cluster data shows that the disk dispersal timescale may decrease weakly with stellar mass. For the photoevaporation model, $\tau_{\rm disk} \sim 3 \times 10^6 / M_\star^{1/2}$. If the migration timescale increases with (or is independent of) stellar mass, then the migration timescale will exceed the disk dispersal timescale at some stellar mass. For stars more massive than this limit, planets will remain on orbits near where they formed.

Planets undergoing type II migration are locked to the disk and move inward on the viscous timescale. A typical estimate of the migration timescale $\tau_{\rm mig}$ is

$$\frac{1}{\tau_{\rm mig}} = \frac{1}{a}\frac{da}{dt} \sim 1.5\,\alpha\,h^2\,\Omega\,, \tag{5.7}$$

where $\alpha \sim 10^{-4}$ is a scaling parameter, $h \sim 0.05$ is the disk aspect ratio, and Ω the orbital frequency (D'Angelo et al., 2002). If the distance where planets originate varies linearly with stellar mass (e.g. Kennedy & Kenyon, 2008a; Kretke et al., 2008) and if α and h are constant, the migration timescale is $\tau_{\rm mig} \sim 1 \times 10^6 M_\star$ yr.

Setting $\tau_{\rm disk} = \tau_{\rm mig}$ yields $M_\star = 2$. Thus, with our adopted disk dispersal and migration timescales, planets around stars greater than $\sim 2\,M_\odot$ should have their migration halted by disk dispersal. Though this estimate is similar to the observed transition mass between close and more distant orbits, it is highly uncertain. For example, because type II migration is linked to the viscous evolution of the disk, how migration changes with stellar mass is uncertain (as discussed in §5.4.2). Exploring this picture in detail requires a detailed model that considers concurrent migration and disk dispersal as a giant planet grows.

This picture has two other implications for giant planet formation. In the core accretion model for gas giant planet formation, protoplanets grow more slowly at larger distances from their host star. Thus, the disk lifetime effectively sets an outer limit to where gas giants form (e.g. Kennedy & Kenyon, 2008b). If the disk lifetime depends on stellar mass, this outer limit is closer than predicted by models with a fixed disk lifetime (e.g. Ida & Lin, 2005; Kennedy & Kenyon, 2008b).

Differential disk dispersal rates may also affect giant planet frequency. Current observations suggest an increasing frequency of gas giants around more massive stars (Butler et al., 2006; Johnson et al., 2007a). In planet formation theory, this

frequency is set by two competing effects: (1) shorter disk lifetimes for more massive stars reduce the likelihood of forming giant planets, and (2) higher disk masses for more massive mass stars increase the probability of gas giant planet formation. As for the implications for migration, understanding how these effects affect gas giant formation requires more detailed models that are beyond the scope of this paper.

5.5.2 Pre–Main-Sequence Contraction

To conclude this section, we consider whether PMS stellar evolution can affect the orbits of close in giant planets. As young stars approach the main sequence, they contract. The PMS contraction, which is ongoing during giant planet formation and disk dispersal, may therefore affect the innermost orbits that migrating planets may reach.

The inner edge of a circumstellar disk (the truncation radius) is a function of the stellar radius (e.g. Bouvier et al., 2007). If planets cannot migrate interior to this edge (e.g. Lin et al., 1996), then the stellar radius at the epoch of disk dispersal sets the innermost possible orbit (aside from later movement due to tidal evolution, which also depends on stellar parameters e.g. Rasio et al., 1996; Jackson et al., 2008). The larger radii of more massive stars and their shorter disk dispersal timescales, prevent planets from reaching closer orbits during their PMS phase.

Because the radius of a PMS star changes with time, we can use our disk dispersal timescale to estimate the stellar radius when the disk is removed. Observationally, 5–10 stellar radii represents roughly the closest orbit a planet can reach by migration, which must occur while the disk is still present. The dashed line in Figure 5.11 shows how the stellar radius at $\tau_{\rm disk} = 3 \times 10^6 / M_\star^{1/2}$ yr varies with stellar mass using the Siess et al. (2000) PMS tracks. The PMS stellar radii shows a weak trend with stellar mass, similar to the innermost orbits. Thus, the innermost orbits of extra-solar planets may be set by the radius of their PMS host star, through the stars influence on the inner edge of the circumstellar disk.

This suggestion is uncertain for many reasons. For example, the disk inner radius may not be a linear function of the stellar radius and orbits evolve through tidal interaction with the host star after reaching close orbits. Future discoveries of extra-solar planets orbiting low-mass stars will fill in the left side of Figure 5.11, giving a better idea of how the innermost orbit changes with stellar mass.

5.5.3 Alternatives and Future Work

The diversity of planet formation models means there are alternative theories that may explain the observed orbits of intermediate mass stars. These theories

suggest the trend is either a formation signature, or a result of later stellar evolution. These theories make testable predictions, that will be judged based on future observations.

Kretke et al. (2008) suggest that the larger orbits may be a signature of the "dead zone" in a layered disk accretion model (Gammie, 1996). The inner edge of the dead zone (whose distance varies roughly linearly with stellar mass in their model) acts as a "trap" for both planets (e.g. Masset et al., 2006b) and their building blocks. However, if giant planet orbits were purely a result of the dead zone distance, one might expect a roughly linear dependence of planet semi-major axes on the mass of their hosts, rather than the step that appears in Figure 5.11.

One first step toward understanding the origin of the larger orbits for intermediate mass stars is to verify that the trend is real. Though difficult, if planets can be found orbiting intermediate mass stars before they leave the main-sequence, then the engulfment scenario may be ruled out. Further work using planet formation models (e.g. Burkert & Ida, 2007; Kennedy & Kenyon, 2008b) can study how changes in disk evolution affect the observable outcomes of planet formation. The continued discovery of planets around low and intermediate-mass stars will provide further constraints on the final outcomes these models must produce.

As we have shown, planet formation models provide a link between disk evolution and observed extra-solar planet distributions. Thus, the inclusion of differential disk lifetimes in these models can attempt to understand both how planets form, and how the disks they form in evolve.

5.6 Summary

Our results suggest a stellar mass dependent timescale for the dispersal of circumstellar disks around young stars. Intermediate-mass stars tend to lose their disks earlier than solar-mass stars. All clusters in our study older than ~3 Myr show this tend. We reject the null hypothesis—that solar and intermediate-mass stars lose their disks at the same rate—with 97% confidence. For each cluster, higher mass stars lose their disks earlier than their solar mass counterparts with a significance of roughly $1\,\sigma$. For low mass stars, there is a clear disagreement in disk dispersal timescales derived from accretion and dust signatures. For either signature among low mass stars, there is no clear trend in disk dispersal with stellar age.

By considering how the timescale for grain growth varies with stellar mass for a fixed disk temperature, we show that the dust around higher mass stars may appear to be more evolved than lower mass stars. This model provides an explanation for the lower IR excesses observed for early-type stars with disks, as compared to later-type stars.

Our analysis of a reasonable photoevaporation model demonstrates that the predicted signature of stellar mass dependent disk dispersal is subtle. In this model, the largest differences in disk fractions are expected when the bulk of cluster stars are dispersing their disks. Observations suggest that this dispersal occurs between 4–5 Myr. At earlier (later) times, we expect small differences because most (no) stars of all masses have disks.

Though it is hard to rule out the increasing multiplicity fraction with stellar mass as an alternative mechanism, the lack of any observed differences in disk evolution in multiple systems argues for photoevaporation as the likely mechanism. As noted in 5.3.1, the effects of binary companions are complex and largely unknown. Given that around half of stellar systems may be binaries or multiples in the primary mass range where planets are routinely discovered (e.g. Duquennoy & Mayor, 1991), and that planets are known to exist in binary systems (e.g. Hatzes et al., 2003), the effects of binaries merit further study. To make progress in this area requires larger samples of objects with known multiplicity. The most useful samples will contain objects with $\lesssim$10 AU separations, where the effects on disk evolution as observed by accretion and hot-dust signatures are thought to be strongest. Obtaining samples with a wide range of primary masses will be essential to understand the effects (if any) on stellar mass dependent disk dispersal.

Stellar mass dependent disk dispersal may have consequences for extra-solar planets observed around main-sequence and older stars. Current observations find a step in planet semi-major axes for stars more massive than $1.6\,M_{\odot}$. This feature may be caused by a shorter disk dispersal timescale for more massive stars. Giant planets forming around these stars have less time to migrate and remain on orbits near where they form. More planet detections over a range of stellar masses will test the reality of the apparent step in a_{min} at $1.6\,M_{\odot}$ and allow better tests of models for migration and disk dispersal. Studying tidal decay in more detail will also indicate the level at which stellar evolution affects these orbits.

The causes and effects of stellar mass dependent disk dispersal are many-fold and complex, and progress can be made in several directions. For young stars, high resolution spectroscopy and direct detection of the H_2 component of circumstellar disks will yield better knowledge of how the gaseous component evolves. For low-mass stars, consideration of the local environment may show that disk dispersal depends on proximity to luminous O stars. A greater knowledge of multiplicity on an individual level will allow further studies of how companions may affect disk evolution.

Testing our main result in more detail requires larger samples. To reject the null hypothesis with greater confidence requires both more clusters and a high level of completeness for new and known clusters. Because the error drops roughly as $1/\sqrt{N}$, large increases in significance for well studied clusters will

be difficult. However, clusters such as NGC 2362 and Orion OB1bc and OB1a have many more solar and intermediate-mass stars that need their circumstellar environments characterised, so will benefit from further study.

Additional clusters are also needed. Clusters with ages of ~ 4–5 Myr—where most stars lose their disks—provide the most sensitive measure of the dispersal time as a function of stellar mass. With many intermediate-mass stars and at ~3 Myr, NGC 2264 is probably the best example of a rich cluster with unpublished Spitzer IRAC data. It will be interesting to see whether this cluster shows results similar to the slightly older Tr 37, or the slightly younger IC 348. Obtaining spectroscopy of many objects in rich clusters and associations is made possible with multi-object spectrographs such as Hectospec and 2df/AAOmega.

Because there will be only a few clusters with the several thousand stars required for high significance, progress will come from increases in both cluster numbers and the best possible level of completeness for all clusters.

We thank Cathie Clarke and Charles Jenkins for helpful conversations. GK thanks Mark Wyatt and the Cambridge IoA, and the Harvard-CfA, where part of this study was carried out. This research was supported by an Australian Postgraduate Award and an ANU Vice-Chancellor's Travel Grant (GK), and the *NASA Astrophysics Theory Program* through grant NAG5-13278 and the *TPF Foundation Science Program* though grant NNG06GH25G (SK). This research has made use of the SIMBAD database and the VizieR catalogue access tool, both operated at CDS, Strasbourg, France.

CHAPTER 6

SUMMARY AND OUTLOOK

In this thesis I have explored some of the consequences of different host star masses for planet formation. Summarising individual results from each Chapter:

Chapter 2: The Moving Snow Line and Super-Earths

This Chapter (Kennedy et al., 2007) looks at the possible effect of PMS stellar evolution on planet formation around a low-mass star. This study was motivated by the general use of a static snow line in planet formation models.

Using a simple semi-analytic model, I consider how the decreasing luminosity of an M-dwarf causes the snow line to move as it contracts to the MS. The inward movement of the snow line as the PMS star contracts influences the mass of protoplanets. The increase in surface density caused by condensation of water ice increases protoplanet masses by a factor 3–5. The location of the snow line at isolation—when protoplanet formation is complete—sets where these large icy protoplanets are located. After an extended period of chaotic growth, these protoplanets go on to form super-Earth mass planets.

This study has consequences for the wider picture of planet formation. Because stellar evolution changes with stellar mass, the effects of the moving snow line will also change with stellar mass. With a more complex snow line model, I explored these consequences for gas giant formation in Chapter 3.

Chapter 3: The Snow Line and Giant Planet Frequency

This Chapter (Kennedy & Kenyon, 2008b) has two main aims: to develop a realistic snow line model for use over a range of stellar masses, and to apply this model to formation of gas giant cores. This study was motivated by the

oversimplified snow line treatment by Ida & Lin (2005) and the expansion of planet hunting surveys to a range of stellar masses.

I extend the model of Chapter 2, including the energy liberated by viscous disk evolution in calculating the snow line location. Using the concept of isolation to estimate protoplanet masses and formation times, the model suggests that giant planet frequency should increase with stellar mass, up to ~3 solar masses. This result differs from the Ida & Lin result because the improved snow line model results in a less extreme scaling with stellar mass—roughly $a_{\rm snow} \propto M_\star$, rather than $a_{\rm snow} \propto M_\star^2$. I find that the size of the region where gas giant cores form also increases with stellar mass, up to ~3 solar masses.

This study provides the first explanation of why gas giant frequency increases with stellar mass beyond solar-mass stars. It also suggests why intermediate-mass stars with planets tend not to have higher metallicity—increased disk masses provide ample material for planet formation and the boost from higher metallicities is not needed.

Chapter 4: Hot Super-Earths

This Chapter (Kennedy & Kenyon, 2008a) studies the results predicted for forming super Earth-mass planets over a range of stellar masses. It uses a static snow line, based on the scaling suggested by the previous two Chapters. The study was motivated by a number of different factors: the prospects for discovering super Earth-mass planets around low-mass stars by the transit method (Nutzman & Charbonneau, 2008), the introduction of models suggesting the inference of bulk composition from transit data (Valencia et al., 2007), and the preliminary result that these planets do not preferentially form around higher metallicity stars.

Using analytic and numerical models, I show that Type I migration leads to a higher frequency of super-Earths in short-period orbits for lower-mass stars. There is a maximum stellar mass above which these planets will reach close orbits due to farther formation distances for higher-mass stars. I show that the frequency of hot super-Earths may be independent of metallicity, or even increase with decreasing metallicity. This trend is caused by higher metallicity stars having sufficient mass to form gas giants instead of super-Earths.

Using scattering simulations, I show that only the lowest-mass stars are likely to have short-period super-Earths. Planet forming regions around these stars are closer, thus making scattering more effective.

This Chapter makes predictions for the frequency of short-period super-Earth mass planets as a function of stellar mass. These planets are subject to evaporation processes and may show compositional trends with orbital distance. With increases in RV and transit sensitivity, these predictions will be tested in coming years. The strongest tests will probably come from space based transit surveys

such as CoRoT and Kepler, which expect to find many low-mass, short-period planets. I show why there appears to be no preference for low-mass planets to form around metal-rich stars. This observational result is preliminary and will become clearer with further discoveries of low-mass planets.

Chapter 5: Stellar Mass Dependent Disk Dispersal

This Chapter (Kennedy & Kenyon, 2008, submitted to *The Astrophysical Journal*) looks for observational evidence of different disk lifetimes for different stellar masses. This study was motivated by a number of different Spitzer studies that generally find a decrease in disk fraction for intermediate-mass stars, when compared to solar-mass stars. If real, a stellar mass dependent disk lifetime has implications for gas giant formation models, such as that developed in Chapter 3.

Using accretion and dust signatures, I find some evidence for a stellar mass dependence for solar to intermediate-mass stars, though the statistical significance is limited by sample numbers. I take a simple photoevaporation model and extend it to a range of stellar masses. Results from this model match the observations well and suggest stronger significance can be attained with future observations. I consider possible consequences for planet formation, suggesting that the larger orbits of planets around intermediate-mass stars may be caused by a lack of migration due to shorter disk lifetimes.

This study represents a step forward for planet formation models. Only a few studies have considered the effects of different disk dispersal timescales for different stars, with little motivation for the dependence used. The results of this study provide an observationally backed dependence for use in future models. This study also highlights where the most progress can be made to make the stellar mass dependence on disk dispersal more robust.

6.1 Future Directions

The results of this thesis suggest many directions for future study, both theoretical and observational. The increasing diversity of planet host stars will provide ample observational data to motivate and test these studies.

Each Chapter might lead to more in-depth studies that extend the models considered in each. For example, a more comprehensive photoevaporation model would likely be beneficial for a detailed study of how disk dispersal changes with stellar mass.

However, given the strong links between Chapters 3 and 5—gas giant formation and disk dispersal—these studies are the most promising for future development

that directly relates to current observational results. Below I outline two possible studies that stem from these results.

6.1.1 Gas Giants Around Intermediate-Mass Stars

The increasing number of planets being discovered around intermediate-mass stars suggests these stars are a rich area for observational and theoretical study. The most obvious first step is a reconsideration of the model in Chapter 3, with the consideration of how disk lifetime changes with stellar mass. Shorter disk lifetimes will limit the size of the core forming regions, but should still allow gas giant frequency to increase with stellar mass.

The apparent trend towards larger orbits for planets orbiting intermediate-mass stars suggests that Type II migration would be a valuable component to add to an improved model. With a numerical model of growth like that developed in Chapter 4, or more complex models (e.g. Chambers, 2006a; Brunini & Benvenuto, 2008; Chambers, 2008), the concurrent growth and migration of planets over a range of stellar masses can highlight the effect of changing disk lifetimes on both planet frequency and individual planet orbits.

6.1.2 A Larger and More Complete Cluster Database

The cluster database used for the study of disk dispersal in Chapter 5 is not exhaustive. It was compiled with the intention of highlighting a possible dependence on stellar mass and the way towards a more robust result. We find that the samples can be improved in two key ways: an increased number of clusters, and the best possible completeness for existing clusters.

The path to a more comprehensive database therefore involves identifying clusters that can be included and/or improved with minimal additional effort. Many clusters are currently being studied by various groups (e.g. Orion and NGC 2264) and upcoming publications will provide the simplest additions to the database. Other clusters, such as IC 348 suffer from a lack of published optical spectroscopy for a relatively small number of objects, which can be remedied with new observations.

To obtain more and larger cluster samples requires looking to more distant regions. The membership and properties of some are currently being studied, (such as M17 and h & χ Persei; Hoffmeister et al., 2008; Currie et al., 2007), while others require further work. An example of a cluster that would benefit from further study is M16, a 2–3 Myr old cluster that shows promising signs of stellar mass dependent disk dispersal (Oliveira et al., 2008). This cluster would benefit from spectroscopy to find accretion signatures, spectral types, extinctions, and confirm membership for candidates. At a distance of ~2 kpc,

looking for stellar mass dependent disk dispersal would require sensitivity to ~19 in I band, for masses down to ~0.4 $M_{\odot}$ (Oliveira et al., 2005). The ~14 arcmin spatial extent of this cluster, with a higher concentration in the central 4 arcmin, makes study possible with multi-object spectroscopy on instruments such as IMACS (Magellan) or GMOS (Gemini). For example, optical spectroscopy near Hα of the inner 4 arcmin region with GMOS would take ~3 hours to achieve S/N ~ 30 for 19th magnitude objects. Similar observations for the 1.5 kpc cluster NGC 2362 have been proven by Dahm (2005).

Another way forward is to obtain higher resolution optical spectra for many known clusters, with an instrument such as Hectochelle on the MMT. This type of campaign would result in more accurate accretion measures and also an indication of the binary nature of many objects (e.g. Sicilia-Aguilar et al., 2006b).

6.2 Last Word

This thesis has looked at some aspects of planet formation that relate to the changing mass of host stars. Given that the best prospects for finding Earth-like planets—the ultimate goal of this field—do not necessarily lie with solar-type stars, this relatively new extension of a relatively old field deserves continued attention.

BIBLIOGRAPHY

Abe, Y., Ohtani, E., Okuchi, T., Righter, K., & Drake, M. Water in the Early Earth (Origin of the earth and moon, edited by R.M. Canup and K. Righter and 69 collaborating authors. Tucson: University of Arizona Press., p.413-433), 413–433

Adams, E. R., Seager, S., & Elkins-Tanton, L. 2008, ApJ, 673, 1160

Adams, F. C., Hollenbach, D., Laughlin, G., & Gorti, U. 2004, ApJ, 611, 360

Adams, F. C., Lada, C. J., & Shu, F. H. 1987, ApJ, 312, 788

Adams, F. C. & Shu, F. H. 1986, ApJ, 308, 836

Alexander, R. D. & Armitage, P. J. 2006, ApJ, 639, L83

Alexander, R. D., Clarke, C. J., & Pringle, J. E. 2006, MNRAS, 369, 229

Alibert, Y., Baraffe, I., Benz, W., Chabrier, G., Mordasini, C., Lovis, C., Mayor, M., Pepe, F., Bouchy, F., Queloz, D., & Udry, S. 2006, A&A, 455, L25

Andre, P., Ward-Thompson, D., & Barsony, M. 1993, ApJ, 406, 122

Andrews, S. M. & Williams, J. P. 2005, ApJ, 631, 1134

—. 2007, ApJ, 671, 1800

Armitage, P. J., Clarke, C. J., & Tout, C. A. 1999, MNRAS, 304, 425

Asplund, M., Grevesse, N., & Sauval, A. J. 2005, in Astronomical Society of the Pacific Conference Series, Vol. 336, Cosmic Abundances as Records of Stellar Evolution and Nucleosynthesis, ed. T. G. Barnes, III & F. N. Bash, 25–+

Backer, D. C., Foster, R. S., & Sallmen, S. 1993, Nature, 365, 817

Backman, D. E. & Paresce, F. 1993, in Protostars and Planets III, ed. E. H. Levy & J. I. Lunine, 1253–1304

Baglin, A. 2003, Advances in Space Research, 31, 345

Bailes, M., Lyne, A. G., & Shemar, S. L. 1991, Nature, 352, 311

Balbus, S. A. & Hawley, J. F. 1991, ApJ, 376, 214

Balog, Z., Rieke, G. H., Su, K. Y. L., Muzerolle, J., & Young, E. T. 2006, ApJ, 650, L83

Baraffe, I., Chabrier, G., Barman, T. S., Selsis, F., Allard, F., & Hauschildt, P. H. 2005, A&A, 436, L47

Barbieri, M., Alonso, R., Laughlin, G., Almenara, J. M., Bissinger, R., Davies, D., Gasparri, D., Guido, E., Lopresti, C., Manzini, F., & Sostero, G. 2007, A&A, 476, L13

Beaulieu, J.-P., Bennett, D. P., Fouqué, P., Williams, A., Dominik, M., Jørgensen, U. G., Kubas, D., Cassan, A., Coutures, C., Greenhill, J., Hill, K., Menzies, J., Sackett, P. D., Albrow, M., Brillant, S., Caldwell, J. A. R., Calitz, J. J., Cook, K. H., Corrales, E., Desort, M., Dieters, S., Dominis, D., Donatowicz, J., Hoffman, M., Kane, S., Marquette, J.-B., Martin, R., Meintjes, P., Pollard, K., Sahu, K., Vinter, C., Wambsganss, J., Woller, K., Horne, K., Steele, I., Bramich, D. M., Burgdorf, M., Snodgrass, C., Bode, M., Udalski, A., Szymański, M. K., Kubiak, M., Więckowski, T., Pietrzyński, G., Soszyński, I., Szewczyk, O., Wyrzykowski, Ł., Paczyński, B., Abe, F., Bond, I. A., Britton, T. R., Gilmore, A. C., Hearnshaw, J. B., Itow, Y., Kamiya, K., Kilmartin, P. M., Korpela, A. V., Masuda, K., Matsubara, Y., Motomura, M., Muraki, Y., Nakamura, S., Okada, C., Ohnishi, K., Rattenbury, N. J., Sako, T., Sato, S., Sasaki, M., Sekiguchi, T., Sullivan, D. J., Tristram, P. J., Yock, P. C. M., & Yoshioka, T. 2006, Nature, 439, 437

Beichman, C. A., Unwin, S. C., Shao, M., Tanner, A. M., Catanzarite, J. H., & Marcy, G. W. 2008, in IAU Symposium, Vol. 248, IAU Symposium, 238–243

Bell, K. R. & Lin, D. N. C. 1994, ApJ, 427, 987

Bennett, D. P., Anderson, J., & Gaudi, B. S. 2007, ApJ, 660, 781

Bessell, M. S. & Brett, J. M. 1988, PASP, 100, 1134

Bitner, M. A., Richter, M. J., Lacy, J. H., Greathouse, T. K., Jaffe, D. T., & Blake, G. A. 2007, ApJ, 661, L69

Bonfils, X., Forveille, T., Delfosse, X., Udry, S., Mayor, M., Perrier, C., Bouchy, F., Pepe, F., Queloz, D., & Bertaux, J.-L. 2005, A&A, 443, L15

Bonfils, X., Mayor, M., Delfosse, X., Forveille, T., Gillon, M., Perrier, C., Udry, S., Bouchy, F., Lovis, C., Pepe, F., Queloz, D., Santos, N. C., & Bertaux, J.-L. 2007, A&A, 474, 293

Borucki, W. J., Koch, D. G., Lissauer, J. J., Basri, G. B., Caldwell, J. F., Cochran, W. D., Dunham, E. W., Geary, J. C., Latham, D. W., Gilliland, R. L., Caldwell, D. A., Jenkins, J. M., & Kondo, Y. 2003, in Presented at the Society of Photo-Optical Instrumentation Engineers (SPIE) Conference, Vol. 4854, Society of Photo-Optical Instrumentation Engineers (SPIE) Conference Series, ed. J. C. Blades & O. H. W. Siegmund, 129–140

Boss, A. P. 2006a, ApJ, 643, 501

—. 2006b, ApJ, 644, L79

Bouvier, J., Alencar, S. H. P., Harries, T. J., Johns-Krull, C. M., & Romanova, M. M. 2007, in Protostars and Planets V, ed. B. Reipurth, D. Jewitt, & K. Keil, 479–494

Bower, G. C., Bolatto, A., Ford, E., Kalas, P., & Ulvestad, J. 2007, ArXiv e-prints, (0704.0238)

Briceño, C., Calvet, N., Hernández, J., Vivas, A. K., Hartmann, L., Downes, J. J., & Berlind, P. 2005, AJ, 129, 907

Briceño, C., Hartmann, L., Hernández, J., Calvet, N., Vivas, A. K., Furesz, G., & Szentgyorgyi, A. 2007, ApJ, 661, 1119

Brunini, A. & Benvenuto, O. G. 2008, Icarus, 194, 800

Brunini, A. & Cionco, R. G. 2005, Icarus, 177, 264

Burgasser, A. J., Kirkpatrick, J. D., Reid, I. N., Brown, M. E., Miskey, C. L., & Gizis, J. E. 2003, ApJ, 586, 512

Burkert, A. & Ida, S. 2007, ApJ, 660, 845

Butler, R. P., Johnson, J. A., Marcy, G. W., Wright, J. T., Vogt, S. S., & Fischer, D. A. 2006, PASP, 118, 1685

Calvet, N. & Gullbring, E. 1998, ApJ, 509, 802

Cardelli, J. A., Clayton, G. C., & Mathis, J. S. 1989, ApJ, 345, 245

Carpenter, J. M., Mamajek, E. E., Hillenbrand, L. A., & Meyer, M. R. 2006, ApJ, 651, L49

Castelli, F. & Kurucz, R. L. 2003, in IAU Symposium, Vol. 210, Modelling of Stellar Atmospheres, ed. N. Piskunov, W. W. Weiss, & D. F. Gray, 20P–+

Chambers, J. 2006a, Icarus, 180, 496

—. 2008, Icarus, 198, 256

Chambers, J. E. 1999, MNRAS, 304, 793

—. 2001, Icarus, 152, 205

—. 2006b, ApJ, 652, L133

Charbonneau, D., Brown, T. M., Burrows, A., & Laughlin, G. 2007, in Protostars and Planets V, ed. B. Reipurth, D. Jewitt, & K. Keil, 701–716

Charnoz, S., Morbidelli, A., Dones, L. H., & Salmon, J. 2008, ArXiv e-prints, (0809.5073)

Chauvin, G., Lagrange, A.-M., Dumas, C., Zuckerman, B., Mouillet, D., Song, I., Beuzit, J.-L., & Lowrance, P. 2004, A&A, 425, L29

Chauvin, G., Lagrange, A.-M., Zuckerman, B., Dumas, C., Mouillet, D., Song, I., Beuzit, J.-L., Lowrance, P., & Bessell, M. S. 2005, A&A, 438, L29

Chiang, E., Lithwick, Y., Murray-Clay, R., Buie, M., Grundy, W., & Holman, M. 2007, in Protostars and Planets V, ed. B. Reipurth, D. Jewitt, & K. Keil, 895–911

Chiang, E. I. & Goldreich, P. 1997, ApJ, 490, 368

Ciesla, F. J. & Cuzzi, J. N. 2006, Icarus, 181, 178

Clarke, C. J., Gendrin, A., & Sotomayor, M. 2001, MNRAS, 328, 485

Clarke, C. J. & Pringle, J. E. 2006, MNRAS, 370, L10

Cresswell, P. & Nelson, R. P. 2006, A&A, 450, 833

Cumming, A., Butler, R. P., Marcy, G. W., Vogt, S. S., Wright, J. T., & Fischer, D. A. 2008, PASP, 120, 531

Currie, T. 2008, ArXiv e-prints, (0801.1116)

Currie, T., Balog, Z., Kenyon, S. J., Rieke, G., Prato, L., Young, E. T., Muzerolle, J., Clemens, D. P., Buie, M., Sarcia, D., Grabu, A., Tollestrup, E. V., Taylor, B., Dunham, E., & Mace, G. 2007, ApJ, 659, 599

Cuzzi, J. N. & Zahnle, K. J. 2004, ApJ, 614, 490

Dahm, S. E. 2005, AJ, 130, 1805

Dahm, S. E. & Hillenbrand, L. A. 2007, AJ, 133, 2072

Daisaka, J. K., Tanaka, H., & Ida, S. 2006, Icarus, 185, 492

D'Angelo, G., Henning, T., & Kley, W. 2002, A&A, 385, 647

D'Angelo, G., Kley, W., & Henning, T. 2003, ApJ, 586, 540

D'Antona, F. & Mazzitelli, I. 1994, ApJS, 90, 467

Dohnanyi, J. W. 1969, J. Geophys. Res., 74, 2531

Dominik, C. & Decin, G. 2003, ApJ, 598, 626

Dommanget, J. & Nys, O. 2002, VizieR Online Data Catalog, 1274, 0

Dullemond, C. P. & Dominik, C. 2005, A&A, 434, 971

Duquennoy, A. & Mayor, M. 1991, A&A, 248, 485

Durisen, R. H., Boss, A. P., Mayer, L., Nelson, A. F., Quinn, T., & Rice, W. K. M. 2007, in Protostars and Planets V, ed. B. Reipurth, D. Jewitt, & K. Keil, 607–622

Eisner, J. A. & Carpenter, J. M. 2006, ApJ, 641, 1162

Ercolano, B., Drake, J. J., Raymond, J. C., & Clarke, C. C. 2008, ArXiv e-prints, (0805.4625)

Fischer, D. A. & Valenti, J. 2005, ApJ, 622, 1102

Fogg, M. J. & Nelson, R. P. 2007, A&A, 472, 1003

Ford, E. B. & Chiang, E. I. 2007, ApJ, 661, 602

Ford, E. B. & Rasio, F. A. 2008, ApJ, 686, 621

Fouchet, L. & Mayer, L. 2008, ArXiv e-prints, (0806.3975)

Frink, S., Mitchell, D. S., Quirrenbach, A., Fischer, D. A., Marcy, G. W., & Butler, R. P. 2002, ApJ, 576, 478

Furlan, E., Hartmann, L., Calvet, N., D'Alessio, P., Franco-Hernández, R., Forrest, W. J., Watson, D. M., Uchida, K. I., Sargent, B., Green, J. D., Keller, L. D., & Herter, T. L. 2006, ApJS, 165, 568

Gammie, C. F. 1996, ApJ, 457, 355

Garaud, P. & Lin, D. N. C. 2007, ApJ, 654, 606

Gillon, M., Pont, F., Demory, B.-O., Mallmann, F., Mayor, M., Mazeh, T., Queloz, D., Shporer, A., Udry, S., & Vuissoz, C. 2007, A&A, 472, L13

Gladman, B. 1993, Icarus, 106, 247

Goldreich, P., Lithwick, Y., & Sari, R. 2004, ApJ, 614, 497

Goldreich, P. & Soter, S. 1966, Icarus, 5, 375

Goldreich, P. & Tremaine, S. 1980, ApJ, 241, 425

Goldreich, P. & Ward, W. R. 1973, ApJ, 183, 1051

Gomes, R., Levison, H. F., Tsiganis, K., & Morbidelli, A. 2005, Nature, 435, 466

Gonzalez, G. 1997, MNRAS, 285, 403

Gould, A., Udalski, A., An, D., Bennett, D. P., Zhou, A.-Y., Dong, S., Rattenbury, N. J., Gaudi, B. S., Yock, P. C. M., Bond, I. A., Christie, G. W., Horne, K., Anderson, J., Stanek, K. Z., DePoy, D. L., Han, C., McCormick, J., Park, B.-G., Pogge, R. W., Poindexter, S. D., Soszyński, I., Szymański, M. K., Kubiak, M., Pietrzyński, G., Szewczyk, O., Wyrzykowski, Ł., Ulaczyk, K., Paczyński, B., Bramich, D. M., Snodgrass, C., Steele, I. A., Burgdorf, M. J., Bode, M. F., Botzler, C. S., Mao, S., & Swaving, S. C. 2006, ApJ, 644, L37

Greaves, J. S., Holland, W. S., Wyatt, M. C., Dent, W. R. F., Robson, E. I., Coulson, I. M., Jenness, T., Moriarty-Schieven, G. H., Davis, G. R., Butner, H. M., Gear, W. K., Dominik, C., & Walker, H. J. 2005, ApJ, 619, L187

Güdel, M., Briggs, K. R., Arzner, K., Audard, M., Bouvier, J., Feigelson, E. D., Franciosini, E., Glauser, A., Grosso, N., Micela, G., Monin, J.-L., Montmerle, T., Padgett, D. L., Palla, F., Pillitteri, I., Rebull, L., Scelsi, L., Silva, B., Skinner, S. L., Stelzer, B., & Telleschi, A. 2007, A&A, 468, 353

Guillot, T., Santos, N. C., Pont, F., Iro, N., Melo, C., & Ribas, I. 2006, A&A, 453, L21

Gullbring, E., Hartmann, L., Briceno, C., & Calvet, N. 1998, ApJ, 492, 323

Haisch, Jr., K. E., Lada, E. A., & Lada, C. J. 2000, AJ, 120, 1396

—. 2001a, AJ, 121, 2065

—. 2001b, ApJ, 553, L153

Hansen, B. M. S. & Barman, T. 2007, ApJ, 671, 861

Hartmann, L. 1998, Accretion Processes in Star Formation (Accretion processes in star formation / Lee Hartmann. Cambridge, UK ; New York : Cambridge University Press, 1998. (Cambridge astrophysics series ; 32) ISBN 0521435072.)

Hartmann, L., Calvet, N., Gullbring, E., & D'Alessio, P. 1998, ApJ, 495, 385

Hartmann, L., D'Alessio, P., Calvet, N., & Muzerolle, J. 2006, ApJ, 648, 484

Hatzes, A. P., Cochran, W. D., Endl, M., McArthur, B., Paulson, D. B., Walker, G. A. H., Campbell, B., & Yang, S. 2003, ApJ, 599, 1383

Hayashi, C. 1981, Progress of Theoretical Physics Supplement, 70, 35

Herbig, G. H. 1960, ApJS, 4, 337

Hernández, J., Calvet, N., Briceño, C., Hartmann, L., Vivas, A. K., Muzerolle, J., Downes, J., Allen, L., & Gutermuth, R. 2007, ApJ, 671, 1784

Hernández, J., Calvet, N., Hartmann, L., Briceño, C., Sicilia-Aguilar, A., & Berlind, P. 2005, AJ, 129, 856

Hind, J. R. 1853, Astronomische Nachrichten, 35, 371

Hoffmeister, V. H., Chini, R., Scheyda, C. M., Schulze, D., Watermann, R., Nürnberger, D., & Vogt, N. 2008, ApJ, 686, 310

Hollenbach, D., Johnstone, D., Lizano, S., & Shu, F. 1994, ApJ, 428, 654

Hollenbach, D. J., Yorke, H. W., & Johnstone, D. 2000, Protostars and Planets IV, 401

Hubeny, I. 1990, ApJ, 351, 632

Hubickyj, O., Bodenheimer, P., & Lissauer, J. J. 2005, Icarus, 179, 415

Ida, S. & Lin, D. N. C. 2004a, ApJ, 604, 388

—. 2004b, ApJ, 616, 567

—. 2005, ApJ, 626, 1045

—. 2008, ApJ, 673, 487

Ikoma, M., Nakazawa, K., & Emori, H. 2000, ApJ, 537, 1013

Inaba, S. & Ikoma, M. 2003, A&A, 410, 711

Inaba, S., Tanaka, H., Nakazawa, K., Wetherill, G. W., & Kokubo, E. 2001, Icarus, 149, 235

Inaba, S., Wetherill, G. W., & Ikoma, M. 2003, Icarus, 166, 46

Indebetouw, R., Mathis, J. S., Babler, B. L., Meade, M. R., Watson, C., Whitney, B. A., Wolff, M. J., Wolfire, M. G., Cohen, M., Bania, T. M., Benjamin, R. A., Clemens, D. P., Dickey, J. M., Jackson, J. M., Kobulnicky, H. A., Marston, A. P., Mercer, E. P., Stauffer, J. R., Stolovy, S. R., & Churchwell, E. 2005, ApJ, 619, 931

Jackson, B., Greenberg, R., & Barnes, R. 2008, ArXiv e-prints, (0801.0716)

Janson, M., Reffert, S., Brandner, W., Henning, T., Lenzen, R., & Hippler, S. 2008, A&A, 488, 771

Johansen, A., Brauer, F., Dullemond, C., Klahr, H., & Henning, T. 2008, A&A, 486, 597

Johnson, J. A., Butler, R. P., Marcy, G. W., Fischer, D. A., Vogt, S. S., Wright, J. T., & Peek, K. M. G. 2007a, ApJ, 670, 833

Johnson, J. A., Fischer, D. A., Marcy, G. W., Wright, J. T., Driscoll, P., Butler, R. P., Hekker, S., Reffert, S., & Vogt, S. S. 2007b, ApJ, 665, 785

Kant, I. 1755, Universal Natural History and Theory of the Heavens, ed. (translated) by Ian Johnston (Richer Resources Publications)

Kasper, M., Apai, D., Janson, M., & Brandner, W. 2007, A&A, 472, 321

Kasting, J. F., Whitmire, D. P., & Reynolds, R. T. 1993, Icarus, 101, 108

Kennedy, G. M. & Kenyon, S. J. 2008a, ApJ, 682, 1264

—. 2008b, ApJ, 673, 502

—. 2008c, ApJ, (submitted October 2008)

Kennedy, G. M., Kenyon, S. J., & Bromley, B. C. 2006, ApJ, 650, L139

—. 2007, Ap&SS, 311, 9

Kenyon, S. J. & Bromley, B. C. 2004a, AJ, 127, 513

—. 2004b, ApJ, 602, L133

—. 2006, AJ, 131, 1837

Kenyon, S. J. & Hartmann, L. 1987, ApJ, 323, 714

—. 1995, ApJS, 101, 117

Kirkwood, D. 1880, The Observatory, 3, 409

Kokubo, E. & Ida, S. 1996, Icarus, 123, 180

—. 1998, Icarus, 131, 171

Kornet, K., Wolf, S., & Różyczka, M. 2006, A&A, 458, 661

Kouwenhoven, M. B. N., Brown, A. G. A., & Kaper, L. 2007a, A&A, 464, 581

Kouwenhoven, M. B. N., Brown, A. G. A., Portegies Zwart, S. F., & Kaper, L. 2007b, A&A, 474, 77

Kouwenhoven, M. B. N., Brown, A. G. A., Zinnecker, H., Kaper, L., & Portegies Zwart, S. F. 2005, A&A, 430, 137

Kretke, K. A. & Lin, D. N. C. 2007, ApJ, 664, L55

Kretke, K. A., Lin, D. N. C., Garaud, P., & Turner, N. J. 2008, ArXiv e-prints, (0806.1521)

Kroupa, P. 2001, MNRAS, 322, 231

Kuchner, M. J. 2003, ApJ, 596, L105

Küppers, M., Bertini, I., Fornasier, S., Gutierrez, P. J., Hviid, S. F., Jorda, L., Keller, H. U., Knollenberg, J., Koschny, D., Kramm, R., Lara, L.-M., Sierks, H., Thomas, N., Barbieri, C., Lamy, P., Rickman, H., Rodrigo, R., & The Osiris Team. 2005, Nature, 437, 987

Lada, C. J. 1987, in IAU Symposium, Vol. 115, Star Forming Regions, ed. M. Peimbert & J. Jugaku, 1–17

Lada, C. J. 2006, ApJ, 640, L63

Lada, C. J., Muench, A. A., Haisch, Jr., K. E., Lada, E. A., Alves, J. F., Tollestrup, E. V., & Willner, S. P. 2000, AJ, 120, 3162

Lada, C. J., Muench, A. A., Luhman, K. L., Allen, L., Hartmann, L., Megeath, T., Myers, P., Fazio, G., Wood, K., Muzerolle, J., Rieke, G., Siegler, N., & Young, E. 2006, AJ, 131, 1574

Laplace, P. S. 1796, The System of the World: II, ed. (translated) by John Pond, Vol. II (Richard Phillips, Bridge Street, London)

Laughlin, G., Bodenheimer, P., & Adams, F. C. 2004, ApJ, 612, L73

Lecar, M., Podolak, M., Sasselov, D., & Chiang, E. 2006, ApJ, 640, 1115

Lee, M. H. & Peale, S. J. 2002, ApJ, 567, 596

Léger, A., Selsis, F., Sotin, C., Guillot, T., Despois, D., Mawet, D., Ollivier, M., Labèque, A., Valette, C., Brachet, F., Chazelas, B., & Lammer, H. 2004, Icarus, 169, 499

Levato, H., Malaroda, S., Morrell, N., & Solivella, G. 1987, ApJS, 64, 487

Levison, H. F. & Morbidelli, A. 2007, Icarus, 189, 196

Levison, H. F., Morbidelli, A., Gomes, R., & Backman, D. 2007, in Protostars and Planets V, ed. B. Reipurth, D. Jewitt, & K. Keil, 669–684

Levison, H. F., Morbidelli, A., Vanlaerhoven, C., Gomes, R., & Tsiganis, K. 2008, Icarus, 196, 258

Lilley, A. E. 1955, ApJ, 121, 559

Lin, D. N. C., Bodenheimer, P., & Richardson, D. C. 1996, Nature, 380, 606

Lin, D. N. C. & Papaloizou, J. 1985, in Protostars and Planets II, ed. D. C. Black & M. S. Matthews, 981–1072

Lissauer, J. J. 1987, Icarus, 69, 249

—. 1993, ARA&A, 31, 129

Lissauer, J. J. & Stevenson, D. J. 2007, in Protostars and Planets V, ed. B. Reipurth, D. Jewitt, & K. Keil, 591–606

Lisse, C. M., VanCleve, J., Adams, A. C., A'Hearn, M. F., Fernández, Y. R., Farnham, T. L., Armus, L., Grillmair, C. J., Ingalls, J., Belton, M. J. S., Groussin, O., McFadden, L. A., Meech, K. J., Schultz, P. H., Clark, B. C., Feaga, L. M., & Sunshine, J. M. 2006, Science, 313, 635

Luhman, K. L. 2004, ApJ, 602, 816

Luhman, K. L., Allen, L. E., Allen, P. R., Gutermuth, R. A., Hartmann, L., Mamajek, E. E., Megeath, S. T., Myers, P. C., & Fazio, G. G. 2008, ApJ, 675, 1375

Luhman, K. L. & Jayawardhana, R. 2002, ApJ, 566, 1132

Luhman, K. L., Stauffer, J. R., Muench, A. A., Rieke, G. H., Lada, E. A., Bouvier, J., & Lada, C. J. 2003, ApJ, 593, 1093

Lunine, J. I. & Stevenson, D. J. 1982, Icarus, 52, 14

Lynden-Bell, D. & Pringle, J. E. 1974, MNRAS, 168, 603

Lyne, A. G. & Bailes, M. 1992, Nature, 355, 213

Mamajek, E. E., Meyer, M. R., Hinz, P. M., Hoffmann, W. F., Cohen, M., & Hora, J. L. 2004, ApJ, 612, 496

Masset, F. S., D'Angelo, G., & Kley, W. 2006a, ApJ, 652, 730

Masset, F. S., Morbidelli, A., Crida, A., & Ferreira, J. 2006b, ApJ, 642, 478

Mayor, M. & Queloz, D. 1995, Nature, 378, 355

Mazeh, T., Zucker, S., & Pont, F. 2005, MNRAS, 356, 955

McCaughrean, M. J. & O'Dell, C. R. 1996, AJ, 111, 1977

McLaughlin, D. B. 1924, ApJ, 60, 22

Meyer, M. R., Backman, D. E., Weinberger, A. J., & Wyatt, M. C. 2007, in Protostars and Planets V, ed. B. Reipurth, D. Jewitt, & K. Keil, 573–588

Miguel, Y. & Brunini, A. 2008, MNRAS, 387, 463

Monin, J.-L., Clarke, C. J., Prato, L., & McCabe, C. 2007, in Protostars and Planets V, ed. B. Reipurth, D. Jewitt, & K. Keil, 395–409

Morbidelli, A., Levison, H. F., Tsiganis, K., & Gomes, R. 2005, Nature, 435, 462

Morbidelli, A., Tsiganis, K., Crida, A., Levison, H. F., & Gomes, R. 2007, AJ, 134, 1790

Muzerolle, J., Calvet, N., & Hartmann, L. 2001, ApJ, 550, 944

Muzerolle, J., Hillenbrand, L., Calvet, N., Briceño, C., & Hartmann, L. 2003, ApJ, 592, 266

Muzerolle, J., Luhman, K. L., Briceño, C., Hartmann, L., & Calvet, N. 2005, ApJ, 625, 906

Nagasawa, M., Thommes, E. W., Kenyon, S. J., Bromley, B. C., & Lin, D. N. C. 2007, in Protostars and Planets V, ed. B. Reipurth, D. Jewitt, & K. Keil, 639–654

Najita, J. R., Carr, J. S., Glassgold, A. E., & Valenti, J. A. 2007, in Protostars and Planets V, ed. B. Reipurth, D. Jewitt, & K. Keil, 507–522

Nakagawa, Y., Sekiya, M., & Hayashi, C. 1986, Icarus, 67, 375

Nakano, T. 1987, MNRAS, 224, 107

—. 1988a, MNRAS, 230, 551

—. 1988b, MNRAS, 235, 193

Natta, A., Grinin, V., & Mannings, V. 2000, Protostars and Planets IV, 559

Natta, A., Testi, L., Calvet, N., Henning, T., Waters, R., & Wilner, D. 2007, in Protostars and Planets V, ed. B. Reipurth, D. Jewitt, & K. Keil, 767–781

Natta, A., Testi, L., & Randich, S. 2006, A&A, 452, 245

Nelson, R. P. & Papaloizou, J. C. B. 2004, MNRAS, 350, 849

Neuhäuser, R., Guenther, E. W., Wuchterl, G., Mugrauer, M., Bedalov, A., & Hauschildt, P. H. 2005, A&A, 435, L13

Nutzman, P. & Charbonneau, D. 2008, PASP, 120, 317

Ohtsuki, K., Stewart, G. R., & Ida, S. 2002, Icarus, 155, 436

Oliveira, J. M., Jeffries, R. D., & van Loon, J. T. 2008, ArXiv e-prints, (0810.4444)

Oliveira, J. M., Jeffries, R. D., van Loon, J. T., Littlefair, S. P., & Naylor, T. 2005, MNRAS, 358, L21

Osterloh, M. & Beckwith, S. V. W. 1995, ApJ, 439, 288

Paardekooper, S.-J. & Mellema, G. 2006, A&A, 459, L17

—. 2008, A&A, 478, 245

Padoan, P., Kritsuk, A., Norman, M. L., & Nordlund, Å. 2005, ApJ, 622, L61

Palla, F. & Stahler, S. W. 1999, ApJ, 525, 772

Papaloizou, J. & Pringle, J. E. 1977, MNRAS, 181, 441

Papaloizou, J. C. B. & Larwood, J. D. 2000, MNRAS, 315, 823

Papaloizou, J. C. B., Nelson, R. P., Kley, W., Masset, F. S., & Artymowicz, P. 2007, in Protostars and Planets V, ed. B. Reipurth, D. Jewitt, & K. Keil, 655–668

Pascucci, I., Apai, D., Hardegree-Ullman, E. E., Kim, J. S., Meyer, M. R., & Bouwman, J. 2008, ApJ, 673, 477

Pascucci, I., Gorti, U., Hollenbach, D., Najita, J., Meyer, M. R., Carpenter, J. M., Hillenbrand, L. A., Herczeg, G. J., Padgett, D. L., Mamajek, E. E., Silverstone, M. D., Schlingman, W. M., Kim, J. S., Stobie, E. B., Bouwman, J., Wolf, S., Rodmann, J., Hines, D. C., Lunine, J., & Malhotra, R. 2006, ApJ, 651, 1177

Pasquini, L., Döllinger, M. P., Weiss, A., Girardi, L., Chavero, C., Hatzes, A. P., da Silva, L., & Setiawan, J. 2007, A&A, 473, 979

Plavchan, P., Jura, M., & Lipscy, S. J. 2005, ApJ, 631, 1161

Podolak, M. & Zucker, S. 2004, Meteoritics and Planetary Science, 39, 1859

Pollack, J. B., Hubickyj, O., Bodenheimer, P., Lissauer, J. J., Podolak, M., & Greenzweig, Y. 1996, Icarus, 124, 62

Preibisch, T., Brown, A. G. A., Bridges, T., Guenther, E., & Zinnecker, H. 2002, AJ, 124, 404

Preibisch, T., Guenther, E., Zinnecker, H., Sterzik, M., Frink, S., & Roeser, S. 1998, A&A, 333, 619

Preibisch, T. & Zinnecker, H. 1999, AJ, 117, 2381

Press, W. H., Teukolsky, S. A., Vetterling, W. T., & Flannery, B. P. 1992, Numerical recipes in C. The art of scientific computing (Cambridge: University Press, |c1992, 2nd ed.)

Rafikov, R. R. 2004, AJ, 128, 1348

—. 2006, ApJ, 648, 666

Rasio, F. A. & Ford, E. B. 1996, Science, 274, 954

Rasio, F. A., Tout, C. A., Lubow, S. H., & Livio, M. 1996, ApJ, 470, 1187

Raymond, S. N., Barnes, R., & Mandell, A. M. 2008, MNRAS, 384, 663

Raymond, S. N., Quinn, T., & Lunine, J. I. 2004, Icarus, 168, 1

Rebull, L. M., Makidon, R. B., Strom, S. E., Hillenbrand, L. A., Birmingham, A., Patten, B. M., Jones, B. F., Yagi, H., & Adams, M. T. 2002, AJ, 123, 1528

Rieke, G. H., Su, K. Y. L., Stansberry, J. A., Trilling, D., Bryden, G., Muzerolle, J., White, B., Gorlova, N., Young, E. T., Beichman, C. A., Stapelfeldt, K. R., & Hines, D. C. 2005, ApJ, 620, 1010

Rivera, E. J., Lissauer, J. J., Butler, R. P., Marcy, G. W., Vogt, S. S., Fischer, D. A., Brown, T. M., Laughlin, G., & Henry, G. W. 2005, ApJ, 634, 625

Rivkin, A. S., Howell, E. S., Vilas, F., & Lebofsky, L. A. 2002, Asteroids III, 235

Rossiter, R. A. 1924, ApJ, 60, 15

Russell, H. N. 1914, Nature, 93, 252

Sackett, P. D. 1999, in NATO ASIC Proc. 532: Planets Outside the Solar System: Theory and Observations, ed. J.-M. Mariotti & D. Alloin, 189–+

Safronov, V. S. 1969, Evoliutsiia doplanetnogo oblaka. (1969.)

Santos, N. C., Israelian, G., & Mayor, M. 2001, A&A, 373, 1019

Sasselov, D. D. & Lecar, M. 2000, ApJ, 528, 995

Sato, B., Izumiura, H., Toyota, E., Kambe, E., Ikoma, M., Omiya, M., Masuda, S., Takeda, Y., Murata, D., Itoh, Y., Ando, H., Yoshida, M., Kokubo, E., & Ida, S. 2008a, PASJ, 60, 539

Sato, B., Toyota, E., Omiya, M., Izumiura, H., Kambe, E., Masuda, S., Takeda, Y., Itoh, Y., Ando, H., Yoshida, M., Kokubo, E., & Ida, S. 2008b, ArXiv e-prints, (0807.0268)

Saumon, D. & Guillot, T. 2004, ApJ, 609, 1170

Scholz, A., Jayawardhana, R., & Wood, K. 2006, ApJ, 645, 1498

Schwarz, G. 1978, The Annals of Statistics, 6, 461

Selsis, F., Chazelas, B., Bordé, P., Ollivier, M., Brachet, F., Decaudin, M., Bouchy, F., Ehrenreich, D., Grießmeier, J.-M., Lammer, H., Sotin, C., Grasset, O., Moutou, C., Barge, P., Deleuil, M., Mawet, D., Despois, D., Kasting, J. F., & Léger, A. 2007, Icarus, 191, 453

Shakura, N. I. & Syunyaev, R. A. 1973, A&A, 24, 337

Shatsky, N. & Tokovinin, A. 2002, A&A, 382, 92

Shiraishi, M. & Ida, S. 2008, ApJ, 684, 1416

Sicilia-Aguilar, A., Hartmann, L., Calvet, N., Megeath, S. T., Muzerolle, J., Allen, L., D'Alessio, P., Merín, B., Stauffer, J., Young, E., & Lada, C. 2006a, ApJ, 638, 897

Sicilia-Aguilar, A., Hartmann, L. W., Fürész, G., Henning, T., Dullemond, C., & Brandner, W. 2006b, AJ, 132, 2135

Sicilia-Aguilar, A., Hartmann, L. W., Hernández, J., Briceño, C., & Calvet, N. 2005, AJ, 130, 188

Siess, L., Dufour, E., & Forestini, M. 2000, A&A, 358, 593

Skrutskie, M. F., Dutkevitch, D., Strom, S. E., Edwards, S., Strom, K. M., & Shure, M. A. 1990, AJ, 99, 1187

Stahler, S. W. 1983, ApJ, 274, 822

Stevenson, D. J. & Lunine, J. I. 1988, Icarus, 75, 146

Stewart, G. R. & Wetherill, G. W. 1988, Icarus, 74, 542

Strom, S. E., Edwards, S., & Skrutskie, M. F. 1993, in Protostars and Planets III, ed. E. H. Levy & J. I. Lunine, 837–866

Struve, O. 1952, The Observatory, 72, 199

Tanaka, H., Takeuchi, T., & Ward, W. R. 2002, ApJ, 565, 1257

Terquem, C. & Papaloizou, J. C. B. 2007, ApJ, 654, 1110

Thommes, E. W., Duncan, M. J., & Levison, H. F. 1999, Nature, 402, 635

—. 2003, Icarus, 161, 431

Throop, H. B. & Bally, J. 2008, AJ, 135, 2380

Torres, G., Winn, J. N., & Holman, M. J. 2008, ApJ, 677, 1324

Tremaine, S. & Zakamska, N. L. 2004, in American Institute of Physics Conference Series, Vol. 713, The Search for Other Worlds, ed. S. S. Holt & D. Deming, 243–252

Tsiganis, K., Gomes, R., Morbidelli, A., & Levison, H. F. 2005, Nature, 435, 459

Udry, S., Fischer, D., & Queloz, D. 2007, in Protostars and Planets V, ed. B. Reipurth, D. Jewitt, & K. Keil, 685–699

Valencia, D., Sasselov, D. D., & O'Connell, R. J. 2007, ApJ, 665, 1413

Walter, F. M., Vrba, F. J., Mathieu, R. D., Brown, A., & Myers, P. C. 1994, AJ, 107, 692

Ward, W. R. 1997, Icarus, 126, 261

Weidenschilling, S. J. 1977a, MNRAS, 180, 57

—. 1977b, Ap&SS, 51, 153

—. 1980, Icarus, 44, 172

—. 2000, Space Science Reviews, 92, 295

Wetherill, G. W. & Stewart, G. R. 1989, Icarus, 77, 330

White, R. J. & Basri, G. 2003, ApJ, 582, 1109

Wolszczan, A. & Frail, D. A. 1992, Nature, 355, 145

Wyatt, M. C. 2008, ARA&A, 46, 339

Wyatt, M. C., Smith, R., Su, K. Y. L., Rieke, G. H., Greaves, J. S., Beichman, C. A., & Bryden, G. 2007, ApJ, 663, 365

Youdin, A. N. & Shu, F. H. 2002, ApJ, 580, 494

Young, E. T., Teixeira, P. S., Lada, C. J., Muzerolle, J., Persson, S. E., Murphy, D. C., Siegler, N., Marengo, M., Krause, O., & Mainzer, A. K. 2006, ApJ, 642, 972

Zhou, J.-L., Aarseth, S. J., Lin, D. N. C., & Nagasawa, M. 2005, ApJ, 631, L85

Zinnecker, H., Correia, S., Brandner, W., Friedrich, S., & McCaughrean, M. 2006, in IAU Colloq. 200: Direct Imaging of Exoplanets: Science & Techniques, ed. C. Aime & F. Vakili, 19–24

Zuckerman, B., Forveille, T., & Kastner, J. H. 1995, Nature, 373, 494